



**NONLINEAR OPTICAL SPECTROSCOPY IN NOVEL ORGANIC COMPOUNDS
AND INORGANIC SYSTEMS**

Presented by

M. C. Rigoberto Castro Beltrán

Thesis submitted in partial fulfillment of the requirements for the degree of

DOCTOR OF SCIENCES (Optics)

At Centro de Investigaciones en Óptica

Dr. Gabriel Ramos Ortíz

Advisor

León Guanajuato, México 2011

*Y en la ingravidez del fondo
donde se cumplen los sueños
se juntan dos voluntades
para cumplir un deseo.*

*Ramón Sampedro
Mar adentro*

*To my parents, Maria Aida and Rigoberto,
who showed me the path of intellectual pursuits*

*To my sister and brother, Wendy and Aldo,
who maintain the balance in my thoughts*

*To my wife Anabel for the continuing guidance and
support along the way*

*To my sons Dana and Santiago,
for making the journey so enjoyable*

AKNOWLEDGEMENTS

I wish to express my gratitude to the researches and students of the GPOM (Grupo de Propiedades Ópticas de la Materia), who provided valuable support and understanding for this project, and also whom I benefited very much from their collaboration. My deepest thanks to Dr. Mario Rodríguez, Dr. José Luis Maldonado, Dr. Marco Antonio Meneses, Dr. Oracio Barbosa, Dr. Juan Luis Pichardo, Martín Olmos, Segio Servín, Diecencia Peralta, Laura Aparicio, Victor Manuel and Yenisey del Rocio Ponce.

I am particularly grateful to my advisor Dr. Gabriel Ramos Ortiz who gave me the opportunity to work at this project. His peerless experience and knowledge in nonlinear optical materials and techniques were very helpful in my PhD studies.

My special thanks to Prof. Isabelle Ledoux, Prof. Jean S. Lauret, Prof. Keitaro Nakatani, Prof. Ben Zhong Tang, Dr. Jorge Peón, Dr. Elder de la Rosa, Dr. Efraín Mejía, Dr. Norberto Farfán and Dra. Rosa Santillan, who also provided support for the performance of this dissertation.

I would also like to thank the Centro de Investigaciones en Óptica (CIO) and CONACYT for all the support provided throughout all my PhD studies.

Many thanks, to my friends Any, Ouicho, Alex, Ely, Tony, Uli, Marlenta, Angie, Memo, Pato, Mike, Kalin, Rafa, Berni, Jahir, Kamilo, Anu, el fofo, Mauricio and Oscar.

ABSTRACT

The optimization of the nonlinear (NL) optical response in NL materials is a key element in the development of future photonic and biophotonic applications. Nevertheless, the characteristics of the materials utilized so far do not meet all the stringent requirements imposed for their implementation into real systems. To understand better the NL optical behavior of new materials or to improve previous compounds, it is necessary to develop different studies of structure–property for several systems.

The main objective of this dissertation is to study the second and third–order NL optical properties in nonresonant and resonant regime of novel organic and inorganic materials, and to correlate the magnitude of such nonlinearities with the materials structure. A nonresonant electronic optical nonlinearity, by its nature, would have the fastest response time, limited only by the width of the driving laser pulse. In contrast, resonant optical nonlinearities have response times limited by the lifetime of the excitation and they also exhibit beam depletion due to absorption and thermal damage.

We studied the structure–property of different organic compounds such as, dipolar, octupolar, macromolecular and organometallic systems, because they are based on molecular units containing highly delocalized π –electrons a situation that increases their NL optical behavior. In particular, we studied the off–resonance nonlinearities of a hyperbranched (hb)–Polyyne. Due to the hb–Polyyne was composed by repeated units of octupolar moieties, we decided to study also the nonlinearities of a standard octupolar compound (Crystal Violet), in order to correlate its behavior with the responses of the hb–Polyyne. The hb–Polyyne presented high third–order NL optical results, probably associated with a cooperative effect. For instance, the hb–Polyyne presented third–order NL optical response of $\chi^{(3)} \sim 10^{-11} esu$ and a two photon absorption cross section $\sigma^{TPA} \sim 10^4 GM$. These nonlinearities were one order and 5 times higher than the values reported for Crystal Violet, respectively. The importance in these results is that, they are in the order of the required for photonic applications, i.e., optical power limiters and biomarkers, respectively.

We were also very interested in study the NL optical behavior of highly conjugated dipolar systems in presence of a metallic unit. We studied the NL optical properties of three organoboron compounds and compared their responses with respect to those of their corresponding ligands. Another significant feature in these organic and organometallic materials was that, these compounds were constituent by different electronic substituents groups, an additional parameter that allowed us to understand better their structure–property. We found that the N→B bond allowed more effective delocalization of the π -system and that the diethylamine and Nitro groups were the strongest donor and acceptor substituents, respectively. The maximum second–order NL value obtained was $\mu\beta = 26.1 \times 10^{-46} esu$, which was 5 times higher than that for its corresponding ligand. The magnitude of these nonlinearities were the order of the reported by optoelectronic applications.

With all the studies, we could understand better the limitations and advantages of the analyzed systems. For instance, the main advantage is that from modifying their molecular structure we can improve their NL optical properties, in order to obtain responses in the range of those required for photonic applications. On the other hand, from this dissertation and also taking into account data from the literature, the most significant limitations of organic compounds are: i) Due to many of their studies are carrying out in solutions, their nonlinearities are overestimated by thermo–optical contributions and ii) the thermal decomposition for organic materials is around 100–500 °C, which is a limitation for the design of photonic devices where the use of these compounds should be mainly in solid state formats.

Due to these mentioned details, we decided to study the NL optical properties of four photonic glasses. These glasses were composed by different network modifiers and intermediates and we could also correlate their NL optical behavior through them. It was found that these contributions increase as the ionic radius of both network modifiers and intermediates decreases. The magnitude of the NL refractive index was on the order of $n_{2elec} \sim 10^{-15} \text{ cm}^2/\text{W}$ and most importantly, this group of amorphous glasses did not show

NL thermo–optical contributions, something important for photonic applications where only electronic contributions are required.

Finally, the results presented in this dissertation open the door to future work in our research group, particularly in the development of new systems that contain the best properties of both materials, organic and inorganic compounds, as well as organic–inorganic ones. These hybrid materials could offer new perspectives for possible photonic applications and might be the basis for the development of new concepts, new structure–property relations and figures of merit, as well as for new projects on basic and applied science.

GENERAL OBJECTIVES

1. Study the mechanism of physical origin of the third–order NL optical response, in order to discriminate between the thermo–optical and electronic responses of the NL analyzed material.
2. Study the structure–property and the efficient NL optical phenomena that exhibit:
 - A highly conjugated polymer, conformed mostly by repeated octupolar units.
 - Dipolar systems where the insertion of a metal unit is present. Specially, study the N→B coordination bond in organoboron compounds.
 - A group of tellurite glasses, conformed by different network modifiers and intermediates.

INTRODUCTION

The field of the NL optics (NLO) has tremendously evolved since its beginnings in the early sixties. Its frontiers have been extended in many directions and its techniques have introduced upon many areas of both fundamental and practical interest, i.e., signal processing and more recently biomedical applications.

In signal processing and transmission, the advantages of optical over electronic techniques might change our lives in a major way by giving us access to larger bandwidth information, where photonic switches have responses on the femtosecond (fs) regime, which mean orders of magnitude over that of electronic switches. On the other hand, Biophotonics is now common in laboratories of spectroscopy and molecular biology for potential applications such as multiphoton microscopy, cancer detection and cancer treatments. The conception of these applications requires an intricate bold combination of facts and methods from most diverse fields, in order to perform functions and operations that fit into an overall technological ensemble. Furthermore, all these possible and future applications depend on the available of NL optical materials to achieve them.

Basically, all materials exhibit NL optical phenomena. The important NL optical materials from the device point of view are generally in solid formats and must meet a wide variety of requirements for practical use. In general, they will require stability with respect to ambient conditions and high-intensity light sources. They will have to meet many processing requirements for pattern or shape definition, and integration with additional dissimilar materials. The photonic device design can be carried out from the NL optical study of three types of materials: molecular materials, bulk materials (particularly inorganic compounds) and the third one and more recently type are the hybrid materials (a mixture of organic and inorganic compounds). For a better understanding of their NL optical behaviors is necessary study their NL optical properties separately and develop for each one of them different structure-property that allow us to visualize possible advantages and limitations regarding their immediate photonic applications. For this reason, we decided to study the NL optical properties of several organic compounds and

study also the properties of a special type of photonic glasses. We were interested in organic compounds because their nature combined with the versatility of synthetic chemistry can be used to modify and optimize their molecular structure to maximize the NL responses and other properties. In addition, organic materials combine exceptional characteristics such as easy processing, low cost, mechanical flexibility, and room temperature deposition on a variety of substrate materials. On the other hand, the study of nonlinearities of inorganics is also a very active field of research. For instance, the NL optical properties of glasses have attracted the attention of researchers for many years because of the practical importance of taking into account the NL properties of optical materials when designing specific optical elements. For instance, most of the photonic devices are available in solid state form.

Recently both materials (organic and glasses) have increased their expectations in photonic applications. There are, however, several restrictions which have to be considered upon using exclusively one type of these materials for optical applications. For instance, inorganic glasses are not universally suited for photonic and optoelectronic devices since they have low flexibility and many times their optical properties are inferior in comparison to their organic counterpart. In contrast, π -conjugated organic and polymer-based optical materials have advantages such as easy processability, high flexibility, good light emission and semiconducting properties as well as very high nonlinearities, nevertheless, they suffer in many cases of low photostability and fragility. Therefore, the possibility of combining organic and inorganic components in a unique composite (hybrid material) is a via to generate novel materials having optimized optical properties and to circumvent disadvantages that characterize to technologies based exclusively in organic or inorganic materials.

This dissertation is based on the study and characterization of the NL optical properties of two classes of organic compounds, i.e., macromolecular and organometallic structures

and the study of the NL properties of inorganic compounds, a special class of photonic glasses.

The NL optical characterization presented in this dissertation was conducted through the phenomena of NL refractive index modulation, harmonic generations, NL absorption, fluorescence and dynamics of excited states.

General aspects about the techniques used for the NL optical materials characterization are discussed as this dissertation unfolds. In addition, the main concepts and their applications will be presented as general outlines.

The general content is presented as follows:

Chapter I gives us an overview of the Z-scan, Thermally Managed (TM) Z-scan, Third Harmonic Generation (THG), Two Photon Excited Fluorescence (TPEF) and one photon excited fluorescence (OPEF) techniques. We begin with the NL optical study in solvents and an octupolar compounds through Z-scan, TM Z-scan and TM Z-scan with a “flow mechanism”. Through TM Z-scan with or without flow techniques we could discriminate between the electronic and thermal third-order NL optical contribution of the samples. Z-scan experiments show us information about the real and imaginary components of $\chi^{(3)}$. The study of the nonlinearities of hb-Polyne was conducted through TPEF, OPEF and THG experiments. Through TPEF and OPEF we have information about the TPA cross section and fluorescence quantum yield of the sample analyzed. Finally, with THG measurement, we know about the magnitude of $\chi^{(3)}$. With all these NL optical measurements we could appreciate the importance of the cooperative effect through repeating units of organic compounds in structures with high molar weight.

In chapter II the second and third-order NL optical properties of four borinates and their respective ligands were measured. Four organoboron compounds and their corresponding ligands were studied through Electric Field Induced Second Harmonic (EFISH) generation and THG techniques. Four-coordinative organoboron compounds are attractive because of their intrinsic high electron affinity, large capacity to perturb the electronic structure by

decreasing the LUMO level, etc. For all these characteristics, four-coordinate boron compound have emerged as very attractive materials for various optoelectronic applications. Through all the Chapter II we confirmed that the insertion of a metal unit in a conjugated structure significantly influences the π -electron behavior that can have important manifestations in the optical nonlinearity.

In chapter III we present studies of the third-order NL optical and photoluminescence properties in tellurite glasses through TM Z-scan and pump-probe techniques, respectively. We study the NL optical behavior in TeO_2 -MO- R_2O glasses with three different alkali metal oxides and two network intermediates. We observed a correlation between the n_{2elec} , the linear refractive index and the ionic radius of the samples. Photoluminescence studies showed two emission bands in the glasses after the photoexcitation.

Finally, chapter IV and V present the conclusions and the prospects of the work presented through of this dissertation, respectively.

TABLE OF CONTENT

INTRODUCTION	viii
LIST OF FIGURES	xv
LIST OF TABLES	xx
CHAPTER I	
THIRD-ORDER NL OPTICAL PROPERTIES OF OCTUPOLAR COMPUNDS	
I.1 BACKGROUND	1
I.2 DISCRIMINATION BETWEEN ELECTRONIC AND THERMO-OPTICAL NONLINEARITIES IN ORGANIC SOLUTIONS	6
I.2.1 TM Z-scan: GENERALITIES	7
I.3 EXPERIMENTAL RESULTS AND DISCUSSIONS	13
I.3.1 ELECTRONIC CONTRIBUTION (n_{2elec})	20
I.3.2 THERMAL CONTRIBUTION (n_{2ther})	25
I.3.3 THIRD-ORDER NL OPTICAL CONTRIBUTION IN A STANDARD OCTUPOLE	27
I.4 STUDY OF THE NONLINEAR OPTICAL PROPERTIES IN HYPERBRANCHED POLYYNE	32
I.4.1 GENERAL PROPERTIES OF THE hb-POLYYNE	35
I.4.2 LINEAR ABSORPTION	36
I.4.3 THG MEASUREMENTS	37
I.4.4 NL ABSORPTION CONTRIBUTIONS	43
I.4.4.1 OPEF AND TPEF MEASUREMENTS	48
I.5 REFERENCES	57

CHAPTER II

SECOND AND THIRD-ORDER NL OPTICAL EFFECTS IN NOVEL FOUR-COORDINATED ORGANOBORON DERIVATIVE AND THEIR BIDENTATE LIGANDS: THE EFFECT OF THE N→B BOND

II.1 BACKGROUND	60
II.2 FOUR-COORDINATED ORGANOBORON COMPOUNDS AND THEIR LIGANDS: GENERAL ASPECTS.	65
II.3 EXPERIMENTAL RESULTS AND DISCUSSIONS	
II.3.1 LINEAR ABSORPTION	70
II.3.2 NL ABSORPTION	71
II.3.3 EFISH MEASUREMENTS	80
II.3.4 THG MEASUREMENTS	88
II.4 REFERENCES	90

CHAPTER III

TELLURITE GLASSES AS NL OPTICAL MATERIALS

III.1 BACKGROUND	93
III.2 EXPERIMENTAL RESULTS AND DISCUSSIONS	
III.2.1 NL OPTICAL MATERIALS	96
III.2.2 ABSORPTION AND OPTICAL BANDGAP	97
III.2.3 NONLINEAR OPTICAL PROPERTIES	98
III.2.4 PHOTOLUMINESCENCE AND TRANSIENT ABSORPTION	104
III.3 REFERENCES	110

CHAPTER IV

IV.1 GENERAL CONCLUSIONS	112
IV.2 SCIENTIFIC PRODUCTION	115

CHAPTER V

GENERAL VIEWS

V.1 THE DESIGN OF BIOMARKERS IN THE GPOM: BEGINNINGS	117
V.2 FEASIBLE APPLICATION: THE CONTRAST CELLS THROUGH TPA EXCITATION AND HYBRID MATERIALS FOR OPTICAL POWER LIMITING	119
V.3 REFERENCES	124

LIST OF FIGURES

CHAPTER I

- Figure 1.1** Schematic representation of octupolar symmetries. 2
- Figure 1.2** Organization versus orientation of octupoles. b) may be derived retrosynthetically from a). 2
- Figure 1.3** a) monodisperse dendrimers and b) polydisperse hb-polymers. 3
- Figure 1.4** Experimental set up for Thermally-managed Z-scan. 7
- Figure 1.5** a) risetime for the chopped beam and b) the duty cycle for the modulation of the laser using a chopper wheel. 9
- Figure 1.6** a) Z-scan profiles for CS₂ at delays of 40 μs (continues line) and 600 μs (filled circles). b) Time evolution of the TM Z-scan signal at pre-focal (filled circles) and post-focal positions (filled squares). Continues lines are single exponential fitting to data. 13
- Figure 1.7** Flow mechanism incorporated in the TM Z-scan technique. 15
- Figure 1.8** a) Standard Z-scan traces taken at 600 μs of delay for toluene in static condition (continuous line), and dynamic condition with a flow of 0.8 ml/s (filled circles) and 3 ml/s (filled triangles). b) TM Z-scan signals showing the reduction (indicated by arrows) of thermal nonlinearities when toluene is flowing at 0.8 ml/s. 16
- Figure 1.9** Z-scan traces under different chopper frequencies. All measurements were taken for a time delay of 500 μs. 18
- Figure 1.10** TM Z-scan traces for THF, DCM and DW. The thermal responses are very pronounced respect the electronic responses. Because THF has the higher thermal conduction time, the thermal NLO response is largest compared with others. 19
- Figure 1.11** Ball configurations of the set of solvents, where the black entities are carbons. The design of the structures was carry out through CS Chem 3D ultra with an accessible surface of Wire Mesh and with a Map Property of Atom colors. 22
- Figure 1.12** Toluene Lewis configuration. Twelve possible $\sigma \rightarrow \sigma^*$ transitions and three $\pi \rightarrow \pi^*$ transitions can occur. 23

Figure 1.13 Summary of the electronic energy levels. Even when the energy changes are not shown to scale, is easily noticeable that the $n \rightarrow \pi^*$ and $n \rightarrow \sigma^*$ require less energy than the $\pi \rightarrow \pi^*$ or $\sigma \rightarrow \sigma^*$ transitions.	23
Figure 1.14 CS ₂ Lewis configuration. Only π bonds are present.	24
Figure 1.15 Left, Molecular structure of the octupolar compounds Crystal Violet, and right, ball configurations where the ends are Hydrogen and the blues are Nitrogen.	27
Figure 1.16 a) TM Z-scan traces of DW and CV dissolved in DW (1×10^{-4} M), b) TM Z-scan traces for different concentration of CV.	28
Figure 1.17 TM Z-scan traces for CV dissolved in DW for a) different solutions flows and with concentration of 1×10^{-3} M, b) static solution at concentration of 1×10^{-4} M and solution with flow of 0.8ml/s and concentration of 1×10^{-3} M.	29
Figure 1.18 Molecular structure of a) hb-Polyyne and b) Triphenylamine balls configuration. In a) configuration the dotted lines depict the extension of repeated units of the triphenylamine moiety.	33
Figure 1.19 Absorption spectra of hb-Polyyne in chloroform solution at concentration of 1×10^{-5} mol/L and in solid film deposited on glass substrate before correction of Fresnel losses at interfaces.	36
Figure 1.20 THG Maker-fringes experimental set up.	39
Figure 1.21 THG Maker-fringe patterns for (i) a 15-nm-thick hb-Polyyne film on glass substrate; (ii) a 1-mm-thick substrate without a film deposited on it. The fundamental wavelength is 1200 nm.	40
Figure 1.22 Wavelength dependence of the third order NL susceptibility for hb-Polyyne film. As a reference it is displayed the absorption spectra for hb-Polyyne (top and right axes).	41
Figure 1.23 Wavelength dependence of the third order NL susceptibility for a) MEH:PPV polymer film and b) CV film. As references, the absorption spectra for MEH:PPV and CV are included.	42
Figure 1.24 Schematic diagram of two-photon absorption (TPA).	44
Figure 1.25 TPEF experimental set up. The pump is focusing inside the sample contained in a cell of 1 cm. Fluorescence is collected at 90° .	46

- Figure 1.26** Experimental set up to measure the fluorescence quantum efficiency. 48
- Figure 1.27** OPEF and TPEF emissions spectra excited at 400 and 800 nm respectively. For 1×10^{-7} mol/L chloroform solutions of hb-Polyyne. Inset: picture of the hb-polyyne sample excited at 400 nm. 49
- Figure 1.28** Spectrum of TPEF as intensity function. 50
- Figure 1.29** TPEF emission spectra from solutions of hb-polyyne, Coumarin 480, Rhodamine 6G (R6G) and Rhodamine b (RB). Each solution is at the concentration of 10^{-5} mol/L. In all cases the pump was set to 180 mW. 51
- Figure 1.30** Wavelength dependence of the TPA cross section for hb-Polyyne. 52
- Figure 1.31** NL optical systems with large σ^{TPA} . **A** Crystal Violet, **B** Trialkynilamine, **C** Triphenylamine moiety with extended units of Octylsulfonylbenzene, **D** Triphenylamine moiety with extended units of ethylhexane – sulfonyl, **E** Triphenylamine moiety with extended units of fluorine; compound with butylamine and **F** second generation of a triphenylamine unit with four-arm; R= $\text{OC}_{10}\text{H}_{21}$. 53

CHAPTER II

- Figure 2.1** **A** Three-coordinate organoboron compound and **B** Four-coordinate organoboron compound. Yellow circle: Boron, Red circle: Oxygen and Blue circle: Nitrogen. 61
- Figure 2.2** **A** bidentate chelate compound, **B** donor-functionalized molecule and **C** N,N-chelate compounds. 62
- Figure 2.3** Electro-optic chromophore (2-(p-chlorophenyl)-(3' -nitrobenzo[d])- (4''-methoxybenzo[h])-1,3-dioxa-6-aza-2-boracyclonon-6-ene, a push-pull molecule. In inset, holographic image of an object transmitted through the PR sample. 63
- Figure 2.4** Novel boronates synthesized by the single step reaction of 2,4-pentanedione, aminophenol and phenylboronic acid. 63
- Figure 2.5** Molecular structures of ligands L1, L2 and L3 and borinates B1, B2 and B3. 66
- Figure 2.6** Schematic presentations of π -conjugated systems having the boryl group in **A**) in the chromophore chain, **B**) at the terminal position(s), and **C**) at the lateral positions. D=substituents groups, B=boryl group. 69

Figure 2.7 Linear absorption spectra of compounds L1, L2, L3, B1, B2 and B3 in DCM. 70

Figure 2.8 a) Normalized transmittance in open-aperture Z-scan experiments (fs excitation) for ligand L1 (filled circles) and borinate B1 (open squares) at irradiance of 53 GW/cm² and B1 at irradiance of 30 GW/cm² (open circles). **b)** closed-aperture (S=0.4) Z-scan curves for L1 (filled circles) and B1 (open squares) at irradiance of 53 GW/cm². Solutions of 10mM were employed. Continuous lines are theoretical fit to experimental data. 72

Figure 2.9 Structures reported in literature of boron-containing compounds. 74

Figure 2.10 Normalized transmittance in open-aperture Z-scan experiments (ns excitation) for L1 (filled circles) and boronate B (open squares) at irradiance of 88 MW/cm². Solutions of 100 and 25 μM were employed for L1 and B2, respectively. Continuous lines are theoretical fit to experimental data. 75

Figure 2.11 Schematic diagram of a five-level system. Absorption of an incident photon promotes an electron to the first excited singlet state. From this state, one to three things may happen: **i)** The electron can relax to the ground state by a radiative or by nonradiative transition. **ii)** The electron to undergo a spin-flip transition to a triplet state (intersystem crossing). **iii)** The molecule may absorb another photon, which promotes the electron to a higher-lying singlet state, from which it then relaxes back to the first excited singlet stat. 76

Figure 2.12 Main resonance forms for ligands and borinates. 78

Figure 2.13 Top view (above) and edge view (below) of a cell used for EFISH measurements. The glass is about 3mm thick and about 1 cm long. The gap in which the liquid is confined is 1-2 mm, and the electrodes extend about five times the gap spacing to avoid nonuniform electric field at the glass-liquid interface. The cell is translated in the x direction with respect to the beam to produce the fringes. 83

Figure 2.14 Example of an EFISH measurement for B3, L3 and DCM at 1.907 μm. 85

CHAPTER III

Figure 3.1 Dependence of $(\alpha \cdot hv)^{1/2}$ on the photon energy for tellurite glasses. Inset: absorption spectra of the tellurite glasses. 97

Figure 3.2 a) Normalized transmittance of standard Z-scan measurements for TeZnNa and TeZnK. The continuous lines are fittings to the experimental data. b) thermally managed Z-scan signals at valleys and peaks of traces shown in a). The traces of CS₂ are included as reference. 99

Figure 3.3 Normalized transmittance in standard Z-scan measurements for TeZnLi under excitation at 1 KHz pulse repetition rate and different intensities. The continuous lines are fittings to the experimental data. 103

Figure 3.4 Variation of n_2 as a function of intensities obtained under excitation at 1 KHz pulse repetition rate. For comparison, the values of n_2 obtained through TM Z-scan experiments are included. 103

Figure 3.5 Representative experimental setup for pump-probe measurements in transmission geometry. The chopper and lock-in amplifier pull out the change in the power of the transmitted probe induced by the presence of the pump. 105

Figure 3.6 Normalized photoluminescence spectra for sample TeZnLi after excitation with 244 nm and 355 nm laser light. 106

Figure 3.7 Schematic energy level diagrams for tellurite glasses. Dotted lines indicate nonradiative relaxations. 107

Figure 3.8 Transient changes of transmission of TeZnLi, TeZnNa and TeZnK samples for pump at 440 nm (2.8 eV) and probe at 516 nm (2.4 eV). 108

LIST OF TABLES

CHAPTER I

Table 1.1 Results of the n_{2elec} and n_{2therm} taken at $t = 0$ and $t = 500 \mu s$, respectively. The values of I_p and I_A were in range of $[1 - 10 \text{ GW/cm}^2]$ and $[400 - 600 \text{ W/cm}^2]$.	20
Table 1.2 Number of single and double bonds and possibilities of having $\sigma \rightarrow \sigma^*$, $n \rightarrow \sigma^*$, $\pi \rightarrow \pi^*$, $n \rightarrow \pi^*$ transitions for each solvent.	24
Table 1.3 Thermal characteristics of the set of solvents. For comparison, the thermal nonlinear refractive indices n_{2therm} of Table 1.2 are included here.	26
Table 1.4 n_{2elec} and n_{2therm} (measured for a delay of $500 \mu s$) values for CV at different concentrations. As the molar concentration increases, the values of transmittance have more uncertainty.	30
Table 1.5 Properties of hb – Polyynes.	36
Table 1.6 Comparison of the general properties of the set of molecules presented in Figure 1.32 respect our hb-Polyynes.	54

CHAPTER II

Table 2.1 Structural effects induced by boron complexation, with related BLA parameter (see text), in the polyenic fragment for molecules L1 – L3 and B1 – B2.	66
Table 2.2 Ranking of most common donors and acceptors strengths. R corresponds to any radical.	68
Table 2.3 Linear and NL absorption of L and B compounds.	77
Table 2.4 First Hyperpolarizabilities deduced from EFISH measurements at $1.907 \mu m$.	86
Table 2.5 Comparison of SH response in B3 respect to other boron complexes reported in our group.	87

CHAPTER III

Table 3.1 Code, glass composition (mol%) and refractive index for the tellurite glasses used in this study.	96
--	----

Table 3.2 Values of n_2 and third-order nonlinear susceptibility $\chi^{(3)}(-\omega;\omega,-\omega,\omega)$ measured through thermally-managed Z-scan technique. 100

CHAPTER I

THIRD-ORDER NL OPTICAL PROPERTIES OF OCTUPOLAR COMPOUNDS

Molecular structures with multidirectional charge transfer (CT), i.e., octupolar compounds, have gain considerable attention because they comprise larger nonlinearities in comparison to compounds with the traditional dipolar structure characterized by unidirectional CT. Octupolar compounds have various advantages: i) the absence of dipole moment often results in negligible solvatochromism so that they are inherently more transparent and ii) the coupling of excited states can lead to enhanced nonlinearities compared with one-dimensional chromophores.

This chapter is intended for the NL optical study of a standard octupolar and a macromolecular compound and for the phenomenological discrimination of their NL optical response through different optical techniques. In fact, this work was motivated for the need to get more information about the third-order NL optical properties of hyperbranched polymers conformed by repeated fragments of octupolar units.

I. 1 BACKGROUND

The interest in studying the NL optical properties of octupolar molecules is because the CT upon photoexcitation occurs along three different axes, in contrast to the unidirectional excitation that takes place in dipolar molecules. The advantages of using nondipolar chromophores include easier noncentrosymmetric arrangements and improved nonlinearities. Thus, an increasing number of octupolar organic structures have recently appeared in the literature¹⁻². The concept of octupolar nonlinearities was proposed in the nineties on the basis of group theory and quantum mechanical studies³. But the first demonstration of the potential of this system was reported by Zyss⁴. There are several studies that demonstrated that octupolar structures are attractive for cubic NL optical

effects⁵⁻⁶. Example of this is the great interest to know their two photon absorption (TPA) cross section for applications in optical power limiting⁷, two-photon fluorescence microscopy⁸, ultra-high-density optical data storage⁹, biological imaging¹⁰ and the controlled release of biologically relevant species¹¹. Basically, purely octupolar symmetries can be derived from a cubic structure either by projection along a C_3 axis giving rise to the D_{3h} symmetries or by fusion of one type of charge in the center leading to the D_{3h} , D_3 , T_d , or D_{2d} symmetries, see Figure 1.1.

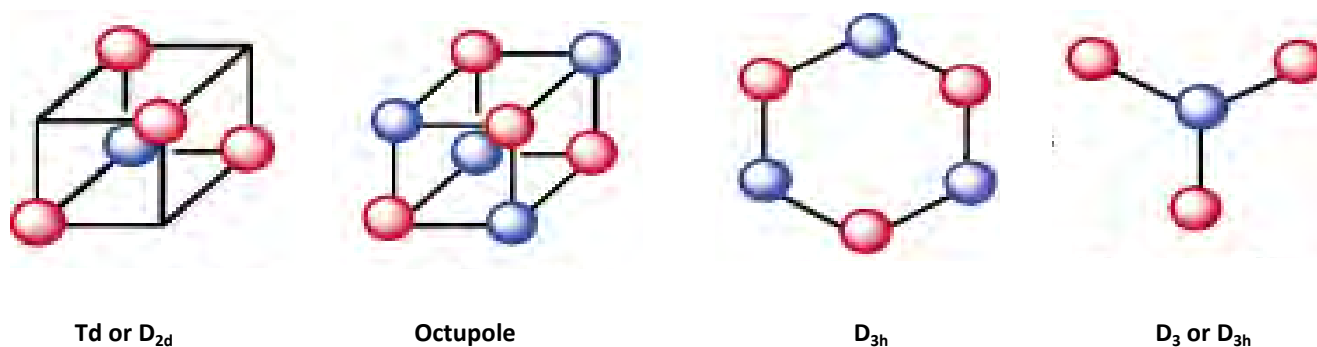


Figure 1.1. Schematic representation of octupolar symmetries.

A typical symmetry pattern that leads to crystalline octupolar nonlinearity is the trigonal network D_{3h} constituted with trigonal molecules. Through retrosynthetic analysis applied to D_3 or D_{3h} we can have synthons such as compound presented in Figure 1.2 a).

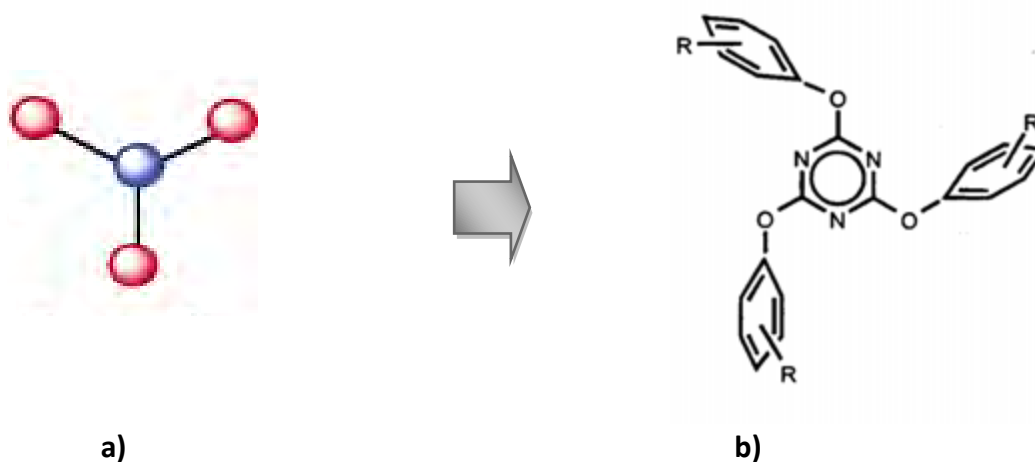


Figure 1.2 Organization versus orientation of octupoles. **b)** may be derived retrosynthetically from **a)**.

The construction of macroscopic assemblies featuring octupolar chromophores remains in its infancy, particularly as far as macro- and supramolecular architectures are concerned¹²⁻¹³. The design has been developed from the structures of dendrimers and highly delocalized polymers.

Conjugated polymers are of great interest because comprise highly polarizable π -electron fragments, which make possible the observation of efficient NL optical phenomena¹⁴. Furthermore, these materials are of low cost, easy integration, enormous design flexibility and present large and fast NL optical response. Many conjugated polymers with different linear chemical structures have been designed and synthesized for NL optical application¹⁵⁻¹⁸, but more recently the interest has extended to dendrimers¹⁹⁻²² and hb-polymers²³⁻²⁸. Dendrimers and hb-polymers belong to the same group of organic compounds with densely branched structures. They resemble each other because they are polymerized from monomers with mixed reactivities. However, dendrimers are defined as monodisperse, while hb-polymers are defined as polydisperse, Figure 1.3 shows both structures.

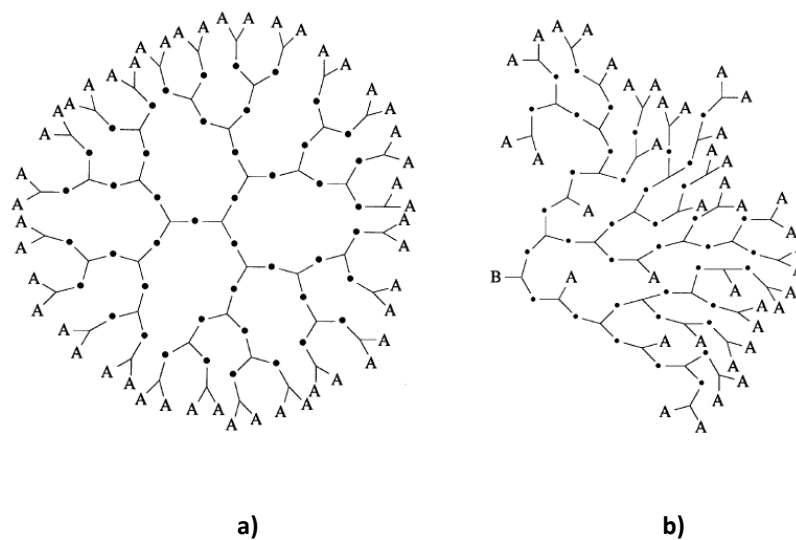


Figure 1.3 a) monodisperse dendrimers and b) polydisperse hb-polymers.

Hb-polymers have good solubility in common organic solvents, form good quality films, and possess an advantageous property in comparison with conventional linear polymers:

high density of NL optical chromophores can be used in their structures at the time that intermolecular electrostatic interactions are minimized because of the site isolation produced by the molecular topology²⁹⁻³⁰. Hb-polymers, on the other hand, are often easy to synthesize on a large scale and often at a reasonable cost, which makes them very interesting for large-scale industrial applications. The high density of extended π -conjugated systems in hb-polymers is advantageous for producing large NL effects. Good macroscopic electrooptic activity in these materials has been recently reported^{25, 27-28} as well as third-order NL effects such as optical limiting^{24,31-33}. In fact, some of these compounds have exhibited an optical limiting response larger than that of the fullerene C₆₀^{24,33}, the latter being one of the best materials for such applications.

This work was motivated for the need to get more information about the third-order NL optical properties of hb-polymers. As an example of this type of compounds, we chose for this dissertation a novel hyperbranched Polyynes (hb-Polyynes). As the hb-Polyynes of interest is principally conformed by repeated fragments of an octupolar moiety (triphenylamine units), we first carried out the NL optical study of a triphenylmethane derivative, named Crystal Violet (CV), which is considered as a prototype of octupolar system. The nonlinearities of CV will help to emphasize the importance of this octupolar units working cooperatively within macroscopic structures such in the case of hb-Polyynes.

This chapter is devoted to the NL study and characterization of both a molecule conformed with only one octupolar moiety (CV) and a molecule comprising a high density of octupolar units (hb-Polyynes). In the latter case the approximate numbers of octupolar units that form the molecular structure are 60. There are various techniques that can be employed for such NL characterization and it is necessary to evaluate the best option determined by the facilities available in the laboratory (laser sources, accessible wavelengths and regimes of laser pulse duration) and some limitation imposed by the samples (solubility, sample available, thermo-mechanical properties that can hamper their characterization through some type of techniques). In particular, many photonics

applications are based in the optimization of the third-order NL susceptibilities $\chi^{(3)}$ exhibited by materials, and Z-scan is commonly used as standard technique to measure such nonlinearities. However, although the implementation of this technique is simple, large amount of materials is required when they are tested in solutions and the interpretation of the experimental data is sometimes difficult when the nonlinearities arise from different physical processes. Z-scan measurements using fs pulses at high repetition (80 MHz) do not discriminate between thermo-optical effects and electronic effects present in the tested material. Taking this into account, we implemented two techniques able to discriminate between both effects: thermally managed (TM) Z-scan and TM Z-scan with flow, both are modifications to the standard Z-scan technique. The first technique, although recently published, is not widely discussed and the second (a novel modification of the TM Z-scan technique) arises from a fundamental problem of thermo-optical contributions in the characterization of liquids and solutions with TM Z-scan. Because both techniques were new in our laboratories, we needed first to demonstrate the effectiveness of the results and the discussion of the data. Firstly, we estimated the third-order nonlinearities of a standard third-order NL optical material and then we studied the nonlinearities of several solvents (most commonly used in the NL characterization of organic molecules including those with octupolar structure) with different capacities to diffuse heat. Diagrams and important aspects of the techniques are shown through the development of this chapter. Once this was concluded, we characterized both the thermo-optical and electronic third-order NL optical properties of solutions of CV. With this methodology, valuable information was obtained about the feasibility of using Z-scan in the study of the tensor element $\chi^{(3)}(-\omega; \omega, \omega, \omega)$ of pure electronic origin in solution of the hb-Polyne. Note that for an optimized photonic material the NL response of electronic origin, i.e., optical Kerr effect, must be large while the NL response due to thermo-optical effects must be negligible.

I. 2 DISCRIMINATION BETWEEN ELECTRONIC AND THERMO–OPTICAL NONLINEARITIES IN ORGANIC SOLUTIONS

The field of NLO has provided many techniques to characterize photonic materials, yielding direct information on the nonlinearities and its origin, which have been improved throughout the years³⁴⁻³⁵. One well established method, known as Z–scan, was introduced in 1989 by Sheik–Bahae and coworkers³⁶. Z–scan technique has been used extensively to measure the third–order susceptibility $\chi^{(3)}$ in various materials³⁴. Using this technique, one can measure both the signs and the magnitudes of the real and imaginary parts of $\chi^{(3)}$. However, the single–beam Z–scan technique cannot measure the dynamics of $\chi^{(3)}$ and hence cannot distinguish among the physical mechanisms that contribute to the optical nonlinearity. A variety of mechanisms can be related to the molecular NL susceptibilities. For instance, thermo–optical contribution are frequently present materials under excitation with cw or quasi–cw (high repetition rate, several MHz) light sources. At these operating regimes, the properties of the transmitted light are determined by both the linear and NL optical response of the materials, and by possible cumulative effects (thermal effects) caused by even very low single or multiple photon absorption of the laser energy. Therefore, the origin and strength of the NL responses in many situations could be incorrectly interpreted from Z–scan data. In fact, one finds in the literature many examples in which $\chi^{(3)}$ is overestimated since accumulative effects are ignored and the nonlinearities are not discussed. This, of course, had produced many reports that erroneously identify new materials comprising excellent photonic properties of the Kerr Type^{36,37-39}.

In order to discriminate between electronic and thermo–optical responses, one has to use experimental methods capable of separating the contribution of the purely electronic optical effect (Kerr effect) from that of the thermo–optical effects. A way to separate both contributions is conducting Z–scan measurements with different laser pulses and shorter repetition rates that give to the sample enough time to diffuse the absorbed heat. Another possibility is to perform all measurements with a technique that has the

possibility to detect simultaneously both contributions and discriminate one from the other. Due to the arrangement of lasers in our laboratory, we choose the second option. Following the proposal of A. Gnoli et al.⁴⁰, a modification in the standard Z-scan technique, called Thermally Managed (TM) Z-scan, allowed us to disentangle between the cumulative thermal lens effects from electronic contributions when femtosecond pulses of high repetition rate are used to characterize liquids and organic solutions.

I. 2. 1 TM Z-scan: generalities

The TM Z-scan technique is a combination of the standard Z-scan technique³⁶ with a special use of a detection system, where the detection consists in acquiring the temporal evolution of the transmittance from the sample. Through this method, we are able now to discriminate the contributions to the NLR index originated from cumulative thermal lens effect⁴¹ (slow response) and electronic polarization (fast response). In consequence, TM Z-scan gives the simultaneous measurements of the nonthermal and thermal nonlinearities. A schematic diagram of the experimental setup is shown in Figure 1.4.

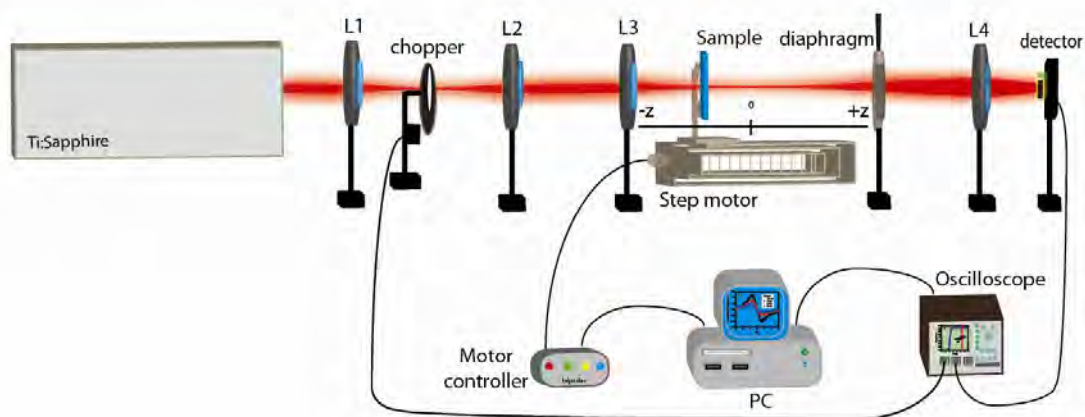


Figure 1.4 Experimental set up for Thermally-managed Z-scan.

The TM Z-scan technique, as well as the standard Z-scan technique, refers to the process of translating a sample under test along the axis of a focused beam (diffraction length or Rayleigh length) formed by L3, and measuring the transmittance through a diaphragm

located in the far field. Assume, for instance, a material with a thickness smaller than the diffraction length of the focused beam (a thin medium). This can be regarded as a thin lens of variable focal length. Starting the scan from a distance far away from the focus (negative Z), the beam irradiance is low and negligible NLR occurs; remains relatively constant. As the sample is brought closer to focus, the beam irradiance increases, leading to self-lensing in the sample. The Z-scan is completed as the sample is moved away from focus (positive Z) such that the transmittance becomes linear since the irradiance is again low. The transmitted signal is detected by a photodiode (Si photodiode with response time of 10 ns) and a digital oscilloscope. The thermal management involves the time evolution measurement of the normalized transmittance at the peak and valley positions of a standard Z-scan trace obtained using a fs laser with a high repetition (in our case, the laser source is a Ti:sapphire oscillator providing 100 fs pulses at repetition rate of 80 MHz). To do this, a laser beam is modulated by a mechanical chopper placed in the focus of a Keplerian telescope formed by the lens L1 and L2 in the scheme shown Fig. 1.4. The time resolution of the system is determined by the chopper opening risetime, which depends on the finite size of the beam waist in the keplerian telescope, the special modification implemented in the slots of the chopper wheel and the angular velocity of the chopper wheel. In our case the risetime was $\tau_0 = 10\mu s$. Figure 1.5 shows the risetime and the duty cycle of our experimental setup. Here the duty cycle of the system was 1.64%, which means the sample was exposed to the laser excitation for about 1.2 ms at intervals of 73 ms. The off-time window was chosen in order to allow the sample under test to release the accumulated heat absorbed during the excitation. The temporally resolved trace shown in Fig. 1.5 a) is hereafter named TM Z-scan signal.

The oscilloscope is triggered using the optical signal itself, instead of using the reference signal from the chopper controller, such that a value of transmission can be measured at any time of interest after the sample started to be excited. We named *delays* to the relative time at which transmission is measured with respect to the triggering point.

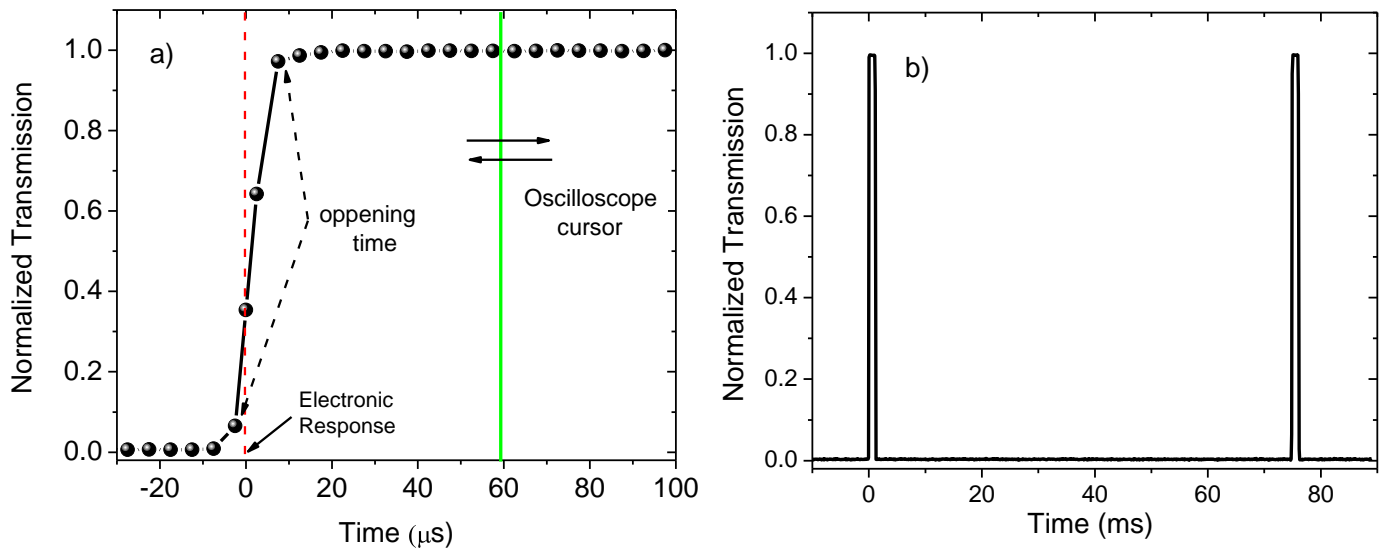


Figure 1.5 a) risetime for the chopped beam and b) the duty cycle for the modulation of the laser using a chopper wheel.

Notice that the opening time indicated in Fig 1.5 a) is not the actual $t = 0$ of the experiment. In principle, $t = 0$ should correspond to the time at which chopper wheel allow to pass the first fs pulses to excite the sample. Notice also that about 800 pulses (100 fs/pulse) excite the sample during the risetime so that the sample is electronically polarized even before the opening time depicted in Fig 1.5 a) is reached. Nevertheless, it results that due to limitations of temporal resolution of system we can only obtain actual data of transmission after the opening time. To calculate the transmission due to pure electronic polarization one extrapolates the time resolved Z-scan signals with a single exponential curve to the time $t = 0$. The determination of this point is very important since the NL electronic effects must appear at $t = 0$, while any other effect should be delayed with respect to that time.

The theory and formulas about the most important aspects to consider about the technique are shown briefly:

A critical parameter is the diffraction length, Z_0 , of the focused beam defined as $\pi\omega_0^2/\lambda$ for a Gaussian beam where ω_0 is the focal spot size. For “thin” (our case $L \leq n_0 Z_0$ where n_0 is the linear index), although all the information is theoretically contained within a scan range of $\pm Z_0$, it is preferable to scan the sample by at least $\pm 5Z_0$. The position of the aperture is rather arbitrary as long as its distance from the focus, $d \gg Z_0$. Typical values range from $20Z_0$ to $100Z_0$. The size of aperture is signified by its transmittance, S , in the linear regime, i.e., when the sample has been placed far away from the focus at low energy. In most reported experiments, $0.1 < S < 0.5$ has been used for determining NLR index. The $S = 1$ case corresponds to collecting all the transmitted light and therefore is insensitive to any NL beam distortion due to NL refraction. Such a scheme, referred to as an “open aperture” Z-scan, is suited for measuring NL absorption ($\Delta\alpha$) in the sample.

One of the attractive features of the Z-scan technique is the ease and simplicity by which the NL optical coefficients can be determined with a high degree of accuracy. However, as is the case with most NL optical measurement techniques, the measured quantities are the time-averaged nonlinearity induced $\langle\Delta n\rangle$ and/or $\langle\Delta\alpha\rangle$. Accurate determination of the NL coefficients such as n_2 or β depend on how precisely the laser source is characterized in terms of its temporal and spatial profiles, power or energy content and stability. Furthermore, because different mechanisms respond on different time scales, time-averaged experiments often measure several competing mechanisms so that the results can depend strongly on the temporal profile of the laser pulse.

Once a specific type of nonlinearity is assumed (i.e., and ultrafast $\chi^{(3)}$ response), a Z-scan can be rigorously modeled for any beam shape and sample thickness by solving the appropriate Maxwell's equations. However, a number of valid assumptions and approximations will lead to simple analytical expressions, making data analysis easy yet precise. Aside from the usual SVEA (slowly varying envelope approximation), a major simplification results when we assume the NL sample “thin” so that neither diffraction nor NLR cause any change of beam profile within the NL sample. This implies that

$L \ll n_0 Z_0$ and $L \ll Z_0 / \Delta\phi_0$, respectively, where $\Delta\phi_0$ is the maximum nonlinearly induced phase change.

The external self-action limit simplifies the problem considerably, and the amplitude \sqrt{I} and phase $\Delta\phi$ of the electric field E are now governed in the SVEA by the following pair of simple equations:

$$\frac{d\Delta\phi}{dz'} = \frac{2\pi}{\lambda} \Delta n(I) \quad 1.1$$

and

$$\frac{dI}{dz'} = -\alpha(I)I \quad 1.2$$

where z' is the propagation depth in the sample and $\alpha(I)$ in general includes linear and NL absorption terms.

For third-order nonlinearities we take:

$$\Delta n = \left\{ \frac{n_2}{2} |E|^2 \right\}_{Gaussian} = \{n_2 I\}_{MKS} \quad 1.3$$

and

$$\Delta\alpha = \beta I \quad 1.4$$

where n_2 is the NLR index, E is the peak electric field, and I denotes the intensity of the laser beam within the sample. Here, β denotes the third-order NL absorption coefficient, which for ultrafast NL absorption is equal to the two-photon absorption (TPA) coefficient. We defined the change in the transmittance between the peak and valley in a Z-scan as $\Delta T = T_p - T_v$, where T_p and T_v are the normalized peak and valley transmittances. The

empirically determined relationship between the induced phase distortion, $\Delta\phi_0$, and ΔT for a third-order NLR index process in the absence of NL absorption is:

$$\Delta T \cong 0.406(1 - S)^{0.27} |\Delta\phi_0|, \quad 1.5$$

where

$$\Delta\phi_0 = \frac{2\pi}{\lambda} n_2 I_0 L_{eff}, \quad 1.6$$

with, $L_{eff} = \frac{1 - e^{-\alpha L}}{\alpha}$, and S is the transmittance of the aperture in the absence of a sample. $\Delta\phi_0$ and I_0 the on-axis ($r = 0$), peak ($t = 0$) NL phase shift and the intensity with the sample at focus ($Z = 0$), respectively. The sign of $\Delta\phi_0$, and hence n_2 is determined from the relative positions of the peak and the valley. Use of $S = 0.4$ is a good compromise between having a large signal which averages possible beam non-uniformities, thus reducing background signals, and reasonably high level of sensitivity. We use values of peak intensity to know the electronic NLR index n_{2elec} , and average intensity to know the thermal NLR index n_{2therm} .

We are interested to obtain TM Z-scan signal at Z positions where transmission of the samples has a maximum and a minimum, corresponding to the peak and valley of a standard Z-scan trace, respectively. Then it is possible to calculate the change in normalized transmittance between peak and valley (ΔT) at early times before thermal effects appear (in principle at $t = 0$), and with that information the contribution from both cumulative and electronic nonlinearities can be inferred, provided no other mechanism besides the electronic nonlinearity is presented in the relatively short time of the chopper opening risetime.

I. 3 Experimental results and discussions

For the experiments explained in this chapter the typical peak intensities for excitation were in the range of $1 - 10 \text{ GW/cm}^2$ while the Rayleigh length for the excitation beam was 2.45 mm and the diaphragm (see Fig 1.1) transmittance at far field was $S = 0.4$.

We first performed measurements for Carbon Disulfide (CS_2) contained in a quartz cell of 1 mm. CS_2 is the most frequently used reference material for third-order NL measurements due to its large NL response. Figure 1.6 a) shows the normalized traces of the typical Z-scan curves recorded at delay times of $40 \mu\text{s}$ and $600 \mu\text{s}$ while Figure 1.6 b) displays the time evolution with the sample at pre-focal and post-focal positions.

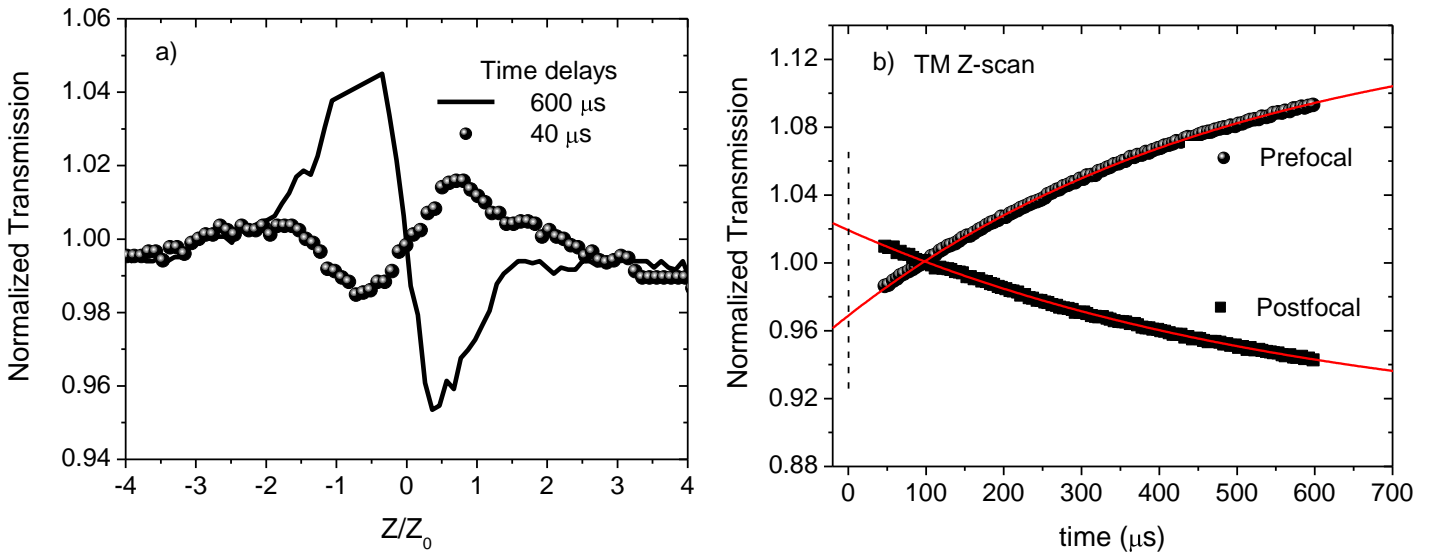


Figure 1.6. a) Z-scan profiles for CS_2 at delays of $40 \mu\text{s}$ (continues line) and $600 \mu\text{s}$ (filled circles). b) Time evolution of the TM Z-scan signal at pre-focal (filled circles) and post-focal positions (filled squares).

Continues lines are single exponential fitting to data.

It should be observed that in CS_2 there are involved two physical process that produce two nonlinearities, one fast (nonthermal) and the other of cumulative type (each one with n_2 values of opposite sign). Figure 1.6 a) show that CS_2 has two signs of NLR index, for instance, for the curve taken at $600 \mu\text{s}$, a negative self-lensing ($n_2 < 0$) prior to focus will

tend to collimate the beam, causing a beam narrowing at the aperture which results in an increase in the measured transmittance. As the scan in Z continues and the sample passes the focal plane to the right, the same self-defocusing increases the beam divergence, leading to beam broadening at the aperture, and thus a decrease in transmittance. On the other hand, we observe the opposite behavior for the curve taken at 40 μs , a peak is followed by a valley showing a positive signal of the NLR index ($n_2 > 0$).

There exist the possibilities that other type of samples could have the same sign for the thermal and nonthermal refractive indices; or also the possibility of samples with negligible electronic effect and strong thermal response; or cases having negligible thermal effects with strong electronic response. The latter correspond to materials which are attractive for photonic applications since they assure fast and large NL response combined with good heat dissipation. We will return to this issue in the final chapter of this dissertation. It is important to take into account that we can report the reconstruction of Z-scan profiles varying only the delays in the oscilloscope at each different time.

Figure 1.6 b) shows the time evolution, with the sample at positions corresponding to the minimum and maximum transmittance. By extrapolating the time evolution curves of CS₂ to $t = 0$ the change in normalized transmittance between pre-focal and post-focal position is $\Delta T = 0.0499$. The dashed line in Fig. 1.6 b) indicates the time $t = 0$ and the red lines defined the single exponential fitting to the TM Z-scan curves. Taking into account the equations presented above and the measurement of ΔT , performed at various times, the electronic NLR index (n_{2elec}) resulted to be $2.73 \pm 0.35 \times 10^{-15} \text{ cm}^2/W$. This value is the average of four measurements at different regions of the sample, and is in good agreement with values previously reported for fs excitation and low laser repetition rates^{40,42-43}. This confirms the good calibration of our experimental set-up.

Despite CS₂ has a large value of n_2 due to electronic polarization, the thermal contribution is much larger. For instance, $\Delta T = 0.16$ at the delay of 600 μs , the NL response of CS₂ due to cumulative effects is about three times larger than that due to pure electronic

polarization (taken at $t = 0$). Taking into account this result and the fact that the majority of solvents (frequently used in organic solutions tested in Z-scan experiments) have low capacity to diffuse heat, we introduce in the TM Z-scan technique a novel “flow mechanism” that provides further discrimination of thermo-optical and electronic responses, eliminating in most of the cases the thermal contribution up to a level of 50%. Figure 1.7 shows the novel “flow mechanism” as part of the TM Z-scan technique and the components that compose it, i.e., a special quartz cell for flow, a pump (clear pump drive, model 75211-22, 0.1 HP and 40-3600 rpm) and its controller.

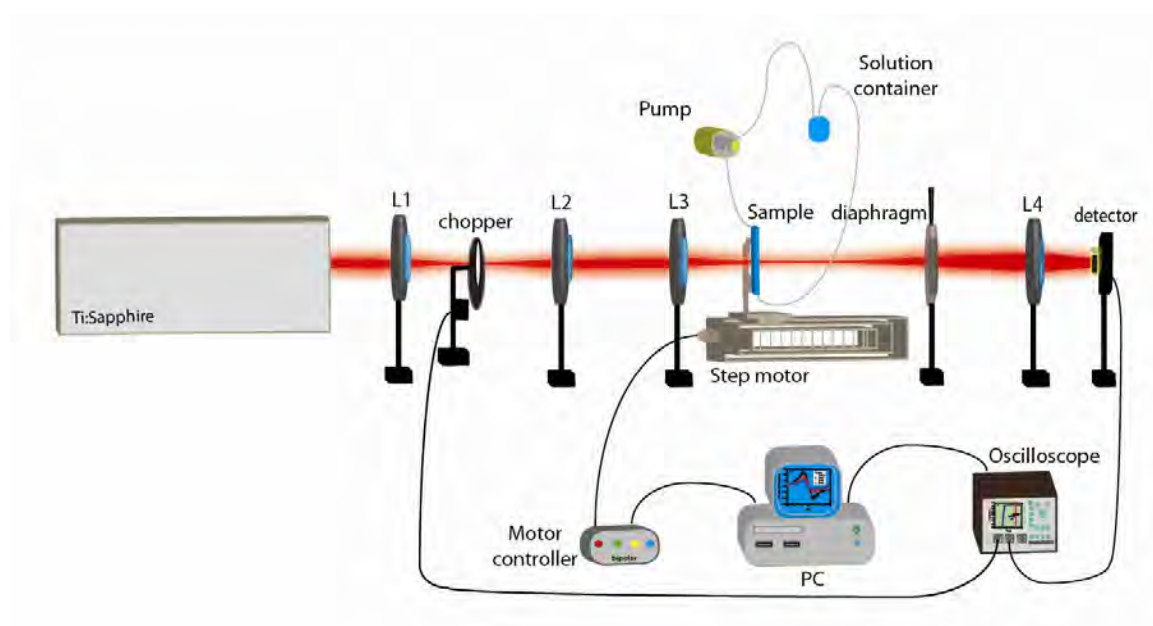


Figure 1.7 Flow mechanism incorporated in the TM Z-scan technique.

In this improved TM Z-scan configuration, we monitor the NL responses at the time that the flow of the solvent or solution can be varied. As the flow increases the thermal response vanishes at the region of optical excitation and with this, the electronic response prevails. Let us see the principle of operation. In terms of heat production, pumping a sample with fs pulses at high repetition rate is equivalent to pumping a sample with a continuous wave laser, therefore between each pulse the sample does not have enough time to dissipate heat and the effective n_2 is governed mostly by the thermal

contribution. However, when the solvent or solution is in motion, the n_2 due to thermal effects can be reduced or eliminated if the flow is faster than the rate at which the heat is produced in the region of excitation.

This new “flow mechanism” requires at least 20 ml of solution. We started the measurements with toluene solvent. Toluene is a solvent frequently used in the study of a large variety of organic molecules. Figures 1.8 a) and 1.8 b) show the traces of TM Z-scan with the “flow mechanism” incorporated. We observe that Toluene has an appreciable nonlinearity of electronic origin, but this is quickly canceled at $120 \mu\text{m}$ by a thermal nonlinearity of opposite sign. To study how the flow mechanism can help to reduce the thermal contributions, the flow volume was varied in a range of $[0.8 - 3] \text{ ml/s}$ while maintaining the acquisition time in the oscilloscope at a delay of $\sim 600 \mu\text{s}$. This delay was chosen because at that time the toluene exhibits exclusively thermal nonlinearities, as it is shown in Fig 1.8 b).

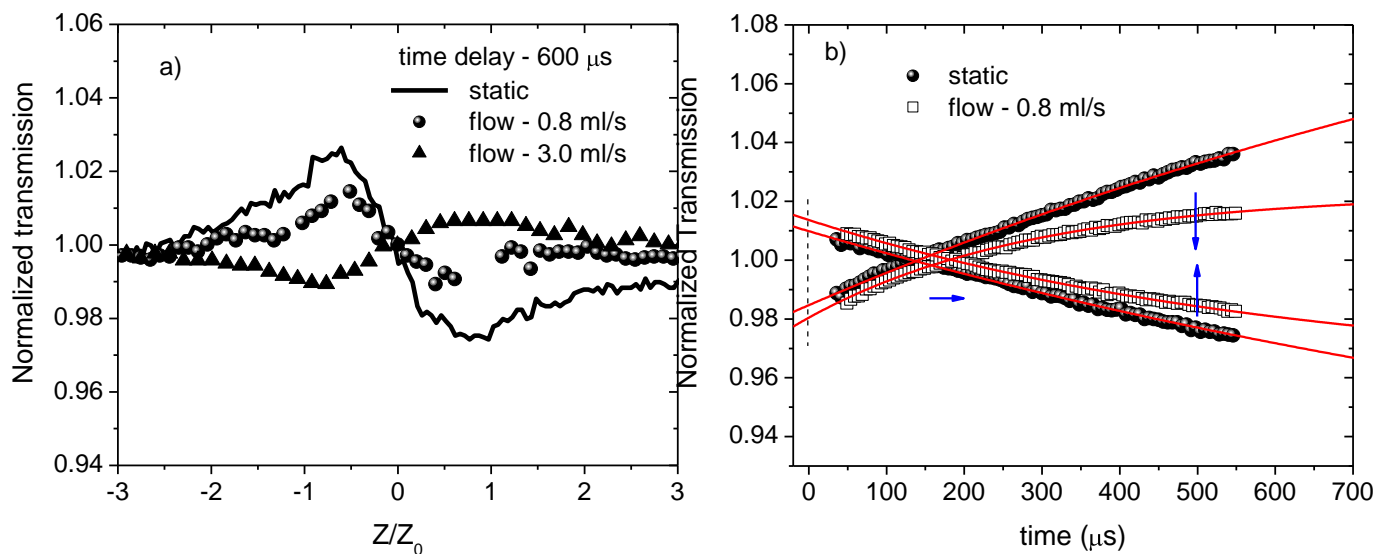


Figure 1.8 a) Standard Z-scan traces taken at $600 \mu\text{s}$ of delay for toluene in static condition (continuous line), and dynamic condition with a flow of 0.8 ml/s (filled circles) and 3 ml/s (filled triangles). b) TM Z-scan signals showing the reduction (indicated by arrows) of thermal nonlinearities when toluene is flowing at 0.8 ml/s .

In Figure 1.8 a), thermal contribution vanishes as the flow increases. This behavior is observed in the traces where the flow is presented at 0.8 and 3.0 ml/s, showing a decrease in their ΔT compared with the trace taken with a static solvent. As the solvent flows into the cell, the temperature gradient, which results in a variation of the sample density, decreases. Notoriously, these figures shows how the heat can be completely removed with a flow of 3 ml/s, and then the Z-scan trace consist of pure electronic contribution. This means that the “flow” removes the volume of solvent that had absorbed the heat at a rate faster than the time of cumulative effects. However, it must be pointed out that for flows above 1 ml/s it was necessary to average data due to fluctuations in the measurements. These fluctuations appeared as the flow was growing; bubbles began to appear in the solution. Nevertheless, the results for the case when the “flow mechanism” is used differs from conventional TM Z-scan results, where a stationary lens is formed constantly when a steady state is reached between rate of heat generation and heat diffusion.

Figure 1.8 b) shows a shift of $\sim 50 \mu s$ between the intersections of the curves and a reduction of 55% at $500 \mu s$ on the thermal amplitude evolution just with a flow of 0.8 ml/s. The subtle difference for ΔT values measured at the beginnings of the traces, at time $t = 0$, are mainly due to the weak amplitude variations caused by the flow. The $n_{zelec} = 2.15 \pm 0.041 \times 10^{-15} \text{ cm}^2/\text{W}$ that corresponds an average of three measurements at different sample regions is very close to that reported in the literature⁴⁴.

Through this new mechanism implemented in the TM Z-scan technique, we have the opportunity to performed three different curves, the first as a function of the position, the second as a function of the time and the third as a function of the flow. These curves allow us to have more information regarding the thermo-optical and electronic responses of our sample.

The frequency of the chopper is another parameter that can be optimized to reduce in some extent the thermal effects. Figure 1.9 shows Z-scan traces for toluene as a function of chopper frequencies taken at a delay of $500 \mu s$. In this case, the decrease in ΔT is due

to a decrease in the average power as the frequency of chopper modulation is increased. It should be observed that the electronic nonlinearities depend on the peak intensity of excitation whereas the cumulative nonlinearities (thermal effects) depend on the average power of excitation, therefore the variation of the chopper frequency in combination with the flow mechanism in a good strategy to keep the thermal as low as possible without modifying the sensitivity of the experimental set-up for the detection of electronic nonlinearities.

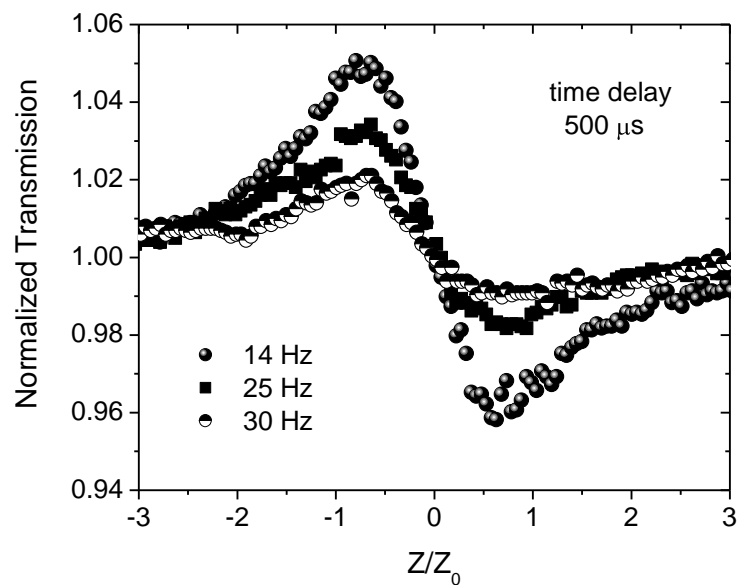


Figure 1.9 Z-scan traces under different chopper frequencies. All measurements were taken for a time delay of $500 \mu\text{s}$.

In our case the chopper frequency was set to a value where the thermal effect was reduced keeping at the same time an optimized duty cycle as shown in Fig 1.5 b) and the risetime shown in Fig 1.5 a).

Considering that the NL optical study of organic compounds occurs from solutions and that these are dissolved in standard organic solvents, we decided to study the NL optical magnitude and the dynamics of their NL optical contributions. The same procedure followed for the case of Toluene was implemented for other common solvents such as dichloromethane (DCM), chloroform, tetrahydrofuran (THF), acetone and distilled water (DW). Table 1 shows the n_{2elec} results for the set of solvents.

On the other hand, the TM Z-scan technique offers the possibility to analyze the thermal contribution of the set of solvents and this gives us the opportunities to explain the thermal phenomenon in our samples. For instance, Figure 1.10 shows the TM Z-scan traces without flow for three different solvents: tetrahydrofuran (THF), dichloromethane (DCM) and distilled water (DW).

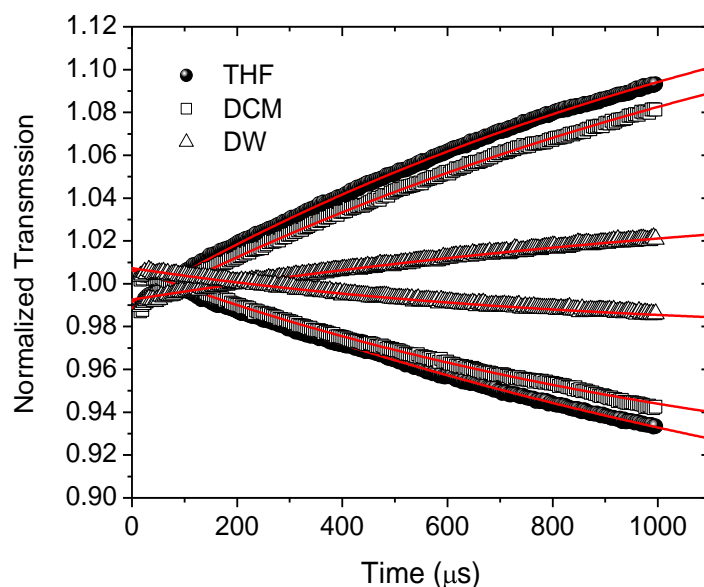


Figure 1.10 TM Z-scan traces for THF, DCM and DW. The thermal responses are very pronounced respect the electronic responses. Because THF has the higher thermal conduction time, the thermal NLO response is largest compared with others.

The Figure 1.10 shows that the solvents have different times for the heat dissipation, which can be associated with their grade of diffusivity. If we compare the DW and THF responses, we see that DW has a larger possibility to dissipate heat than THF, for instance, for a delay of 500 μs DW exhibits $\Delta T = 0.0161$ and THF $\Delta T = 0.0865$, which means a increment of 500% respect DW.

Table 1.1 shows the n_{2elec} the thermal NLR index (n_{2therm}) results for the set of solvents analyzed. For the n_{2elec} results, we took into account the peak intensity (I_p) and for n_{2therm} the average intensity (I_A). The explanation of both types of nonlinearities will be made in two sections: electronic and thermo–optical contributions.

Table 1.1 Results of the n_{2elec} and n_{2therm} taken at $t = 0$ and $t = 500 \mu s$, respectively. The values of I_p and I_A were in range of $[1 - 10 GW/cm^2]$ and $[400 - 600 W/cm^2]$, respectively.

Solvent	n	$n_{2elec}[\times 10^{-15}][cm^2/W]$	$n_{2therm}[\times 10^{-8}][cm^2/W]$
CS ₂	1.629	2.73 ± 0.35	3.20 ± 0.41
Toluene	1.497	2.15 ± 0.041	4.18 ± 0.12
DCM	1.424	2.05	5.72
Chloroform	1.445	1.78 ± 0.008	4.64 ± 0.004
THF	1.407	1.68 ± 0.12	6.73 ± 0.007
Acetone	1.359	1.59 ± 0.11	5.57 ± 0.008
DW	1.33	1.42 ± 0.007	1.75 ± 0.19

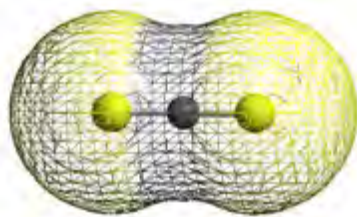
I. 3. 1 Electronic contribution (n_{2elec})

A first approach for the differences between the n_{2elec} values of the set of solvent is through their linear refractive indices (n)⁴⁵. Boling et al. predicted that the n_2 is related with the linear optical properties through the following equation:

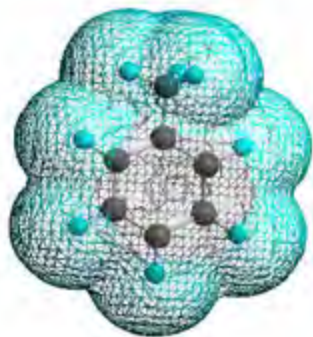
$$n_2 = \frac{(n^2+2)^2(n^2-1)^2(gf)}{6n^2\epsilon_0ch\omega_0(Nf)} \quad 1.7$$

This equation gives a prediction for n_2 in terms of the linear refractive index n , the quantities ω_0 and (Nf) can be deduced from the dispersion in n , and the combination (gf) , which is considered to be a constant quantity for a broad range of optical materials. The value $(gf) = 3$ is found to be in good agreement with measured values. We can see in Ref. [34] a comparison graph of certain materials that fit very well with this prediction (see page 261 Model of Boling, Glass and Owyong). Under this approximation, CS_2 has the largest n value and for this we expected that it must be the sample with most important NL optical contribution in comparison with DW that is the solvent with the smallest n value and with the lowest values of n_{2elec} . This approach fits very well for the rest of the solvents except for chloroform and DCM. We expected chloroform to be the solvent with higher n_{2elec} with respect DCM, but for the closeness in the values of their refractive indexes, the n_{2elec} values have a higher level of uncertainty between them.

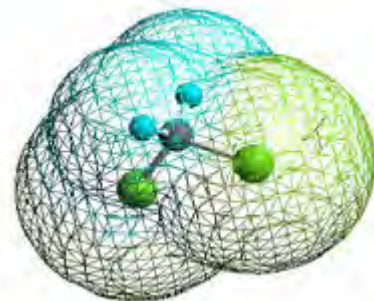
Another way to understand the results would be by linking the n_{2elec} values with the molecular interactions involving an electronically excited state⁴⁶. For this, we need to know about the electronic energy transfer from excited species (D^*) to an unexcited molecule (A). To start with the next explanation it is necessary to be familiar with the molecular structure of the set of solvents to study. Figure 1.11 shows the molecular structures of the set of solvents:



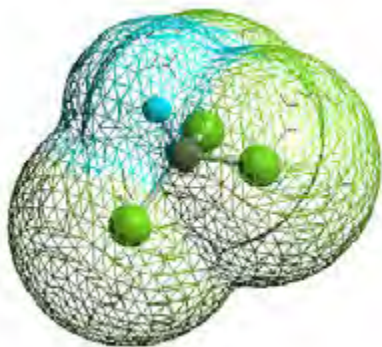
CS₂
Yellow ends: S



Toluene
Blue ends: H



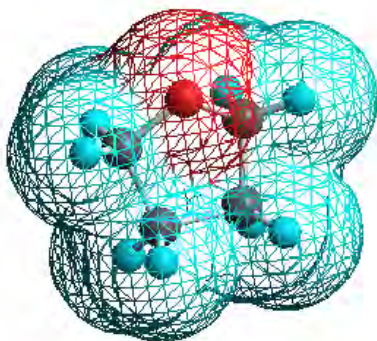
Dichlorometane
Blue ends: H
Green ends: Cl



Chloroform

Blue ends: H

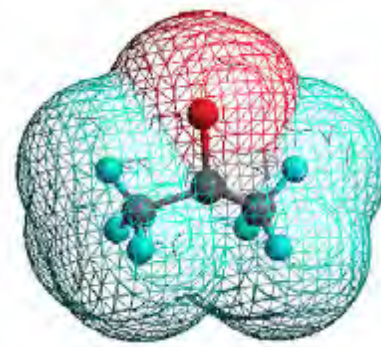
Green ends: Cl



THF

Blue ends: H

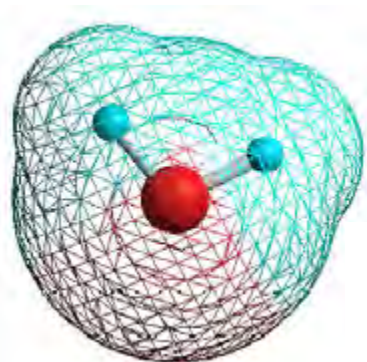
Red end: O



Acetone

Blue ends: H

Red end: O



Water

Blue ends: H

Red end: O

Figure 1.11 Ball configurations of the set of solvents, where the black entities are carbons. The design of the structures was carry out through CS Chem 3D ultra with an accessible surface of Wire Mesh and with a Map Property of Atom colors.

Briefly, because the NLR index is related with the electronic response of the material, is important to understand that the molecular bonds contribute largely to the Kerr response (electronic polarization). For example, toluene has twelve single bonds and three double bonds, see Figure 1.12. These bonds carry out energy transitions which reflect the state of polarization of the whole molecule.

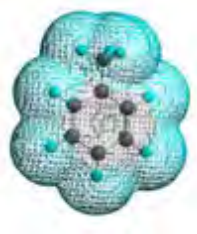
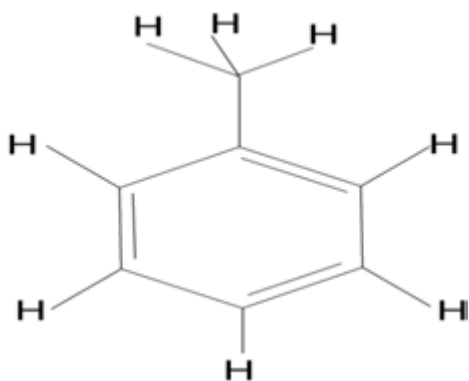


Figure 1.12 Toluene Lewis configuration. Twelve possible $\sigma \rightarrow \sigma^*$ transitions and three $\pi \rightarrow \pi^*$ transitions can occur.

In general terms, when the molecule is excited changes the electronic distribution. The transitions consists in the excitation of an electron from a filled molecular orbital (usually a π or σ orbitals) to the next higher energy orbital (antibonding orbitals, π^* or σ^*). The transitions are indicated in the form $\pi \rightarrow \pi^*$ or $\sigma \rightarrow \sigma^*$. Figure 1.13 summarizes the relationship of energy needed to carry out the different transitions. For instance, the electronic transition that requires less energy is $n \rightarrow \pi^*$ (where n is referred as pairs of electrons non-bonded in the molecule). On the other hand, the transitions that require more energy would be the $\sigma \rightarrow \sigma^*$ transitions.

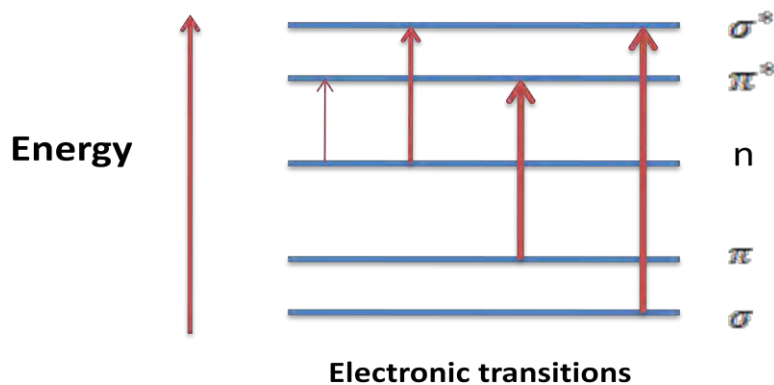


Figure 1.13 Summary of the electronic energy levels. Even when the energy changes are not shown to scale, is easily noticeable that the $n \rightarrow \pi^*$ and $n \rightarrow \sigma^*$ require less energy than the $\pi \rightarrow \pi^*$ or $\sigma \rightarrow \sigma^*$ transitions.

Consequently, we can understand the results obtained for n_{2elec} by correlating such values with the possible n, π or $\sigma \rightarrow (\pi^*, \sigma^*)$ transitions in the solvents when these are excited or rather, with the formation of possible excited complexes. Table 1.2 summarizes the number of single and double bonds and the possible $n \rightarrow (\sigma^* \text{ or } \pi^*)$ transitions in the set of solvents:

Table 1.2 Number of single and double bonds and possibilities of having $\sigma \rightarrow \sigma^*$, $n \rightarrow \sigma^*$, $\pi \rightarrow \pi^*$, $n \rightarrow \pi^*$ transitions for each solvent.

Sample	Number of single bonds	Number of double bonds	Number of possible transitions			
			$\sigma \rightarrow \sigma^*$	$n \rightarrow \sigma^*$	$\pi \rightarrow \pi^*$	$n \rightarrow \pi^*$
CS ₂	2	2	2		2	4
DW	2		2	1		
Toluene	12	3	12		3	
DCM	4		4	6		
Chloroform	4		4	9		
THF	13		13	2		
Acetone	9	1	9		1	2

Referring to CS₂, this has the solvent with more number of possible $n \rightarrow \pi^*$ transitions, see Figure 1.14.

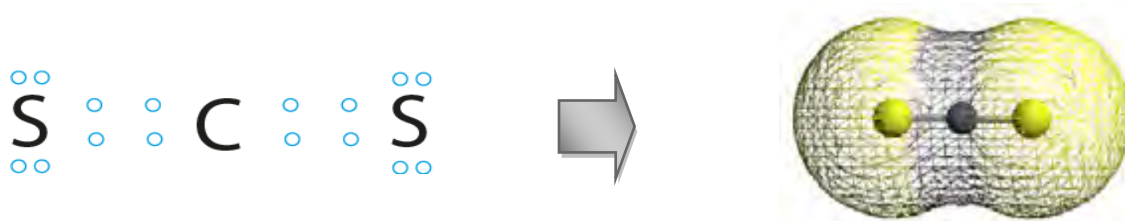


Figure 1.14 CS₂ Lewis configuration. Only π bonds are present.

The fact that makes CS₂ to have a large electronic contribution is principally due to the four possible $n \rightarrow \pi^*$ transitions and secondly to the $\pi \rightarrow \pi^*$ transitions. In these

transitions the electronic mobility is higher than in $n \rightarrow \sigma^*$ and $\sigma \rightarrow \sigma^*$ transitions, respectively. Referring to the Figure 1.13, we see that the $n \rightarrow \pi^*$ and $\pi \rightarrow \pi^*$ transitions are the transitions that require less energy to raise the bonding electrons to the next energy level, i.e., a π^* antibonding orbital. Figure 1.14 shows the orbitals occupied in the basic state and the excited state, where the shading volumes indicate regions of high electron density.

From this point of view, now we can analyze, from another perspective, the difference in the results of chloroform and DCM. Although DCM has higher n_{2elec} value than chloroform, the latter a larger numbers of probabilities to get a transition to a higher energy level, i.e., $n \rightarrow \sigma^*$. Chloroform has nine electron pairs unbond ready to be excited to an antibonding level (σ^*) of higher energy, in contrast DCM that only has six pairs of non-bonded electrons. Perhaps the explanation for this subtle difference focuses on the selective excitation and indirect excitation between each molecule. Details of intra- and inter-molecular energy transfer can be found in detail in Ref. [46].

I. 3. 2 Thermo-optical contribution (n_{2therm})

We followed the analysis made by M. Falconieri et al. in Ref [47], where they relate the thermal conduction effects, shown in the TM Z-scan traces, with the thermal conduction time t_c of each material. Here t_c is defined as $t_c = \omega_0^2 \rho C_p / 4k$, where ω_0 is the laser beam radius at the sample, ρ the density, C_p the specific heat and k the thermal conductivity, see Table 1.3.

In table 1.3 it is observed that the THF solvent has the largest value of t_c and DW the smallest. The “ t_c ” term is the inverse of the D (diffusivity): $t_c = \omega_0^2 / D$. D is the capacity of a solvent to diffuse the heat; therefore the larger is t_c less is the capacity of one solvent to spread the heat.

Table 1.3 Thermal characteristics of the set of solvents. For comparison, the thermal nonlinear refractive indices n_{2therm} of Table 1.2 are included here.

Sample	$C_p [Jg^{-1}K^{-1}]$	$\rho [gcm^{-3}]$	$k [Wcm^{-1}K^{-1}]$	$t_c [ms]$	$n_{2therm} [\times 10^{-8}]$ [cm^2/W]
CS ₂	1.045	1.263	0.00161	1.28	3.20
DW	4.61	0.997	0.00580	1.12	1.75
Acetone	2.150	0.7925	0.00160	1.66	5.57
DCM	1.000	1.325	0.00132	1.56	5.72
THF	1.765	0.888	0.00141	1.73	6.73
Toluene	1.669	0.866	0.00134	1.68	4.18
Chloroform	1.050	1.483	0.00115	1.64	4.64

These results explain very well the thermo–optical behavior of the solvents shown in Figure 1.10, where DW, with less NL thermo–optical contribution, is the solvent with high capacity to dissipate heat. For comparison purposes, the values of n_{2therm} from Table 1.1 are included in Table 1.3.

According to this table, there is a straightforward relationship between the characteristic diffusivity (the inverse of t_c) and the measured n_{2therm} . All these results present DW as an excellent solvent for the characterization of n_{2elec} (electronic polarization) in organic materials intended for photonic applications⁴⁸⁻⁵⁰.

In summary, the TM Z–scan technique applied in solvents showed us that they have large third–order NLO properties that need to be take it into account when we work with organic molecules dissolved into them. Another important aspect is that the TM Z–scan technique has the ability to distinguish between thermo–optical and electronic NL contribution but is not possible to remove the thermal contribution of the sample. With the incorporation of a “flow mechanism”, most of the thermal contribution decrease and with this now is feasible to have NL optical responses with a minimum of thermal contribution.

Table 1.1, 1.2 and 1.3 show important results, which are not present in a single document in the literature, of the electronic and thermo-optical NL optical contributions presented in the most common organic solvents.

Taking into account all the properties of the solvents and especially, the DW properties above mentioned, we decided to carry out the next NL optical characterization in an organic compound dissolved in DW. We conducted the following study through a nondipolar organic molecule. In this regards, we studied the NL optical contribution in a standard octupolar molecule (Crystal Violet). This molecule is of great interest because its NL optical response occurs with a charge transfer upon photoexcitation along three different axes, in contrast to the unidirectional excitation that takes place in dipolar molecules. We decided to study this molecule because we are very interested in their cooperative response. In the following section we study the NL optical properties in Crystal Violet (CV) compound (standard octupole) through TM Z-scan technique with the “flow mechanism”.

I. 3. 3 Third-order NL optical contribution in a standard octupole.

The next study begins with the NL optical study of an octupolar molecule, Crystal Violet (CV), under the same experimental conditions mentioned in previous sections. Figure 1.15 shows the CV structure.

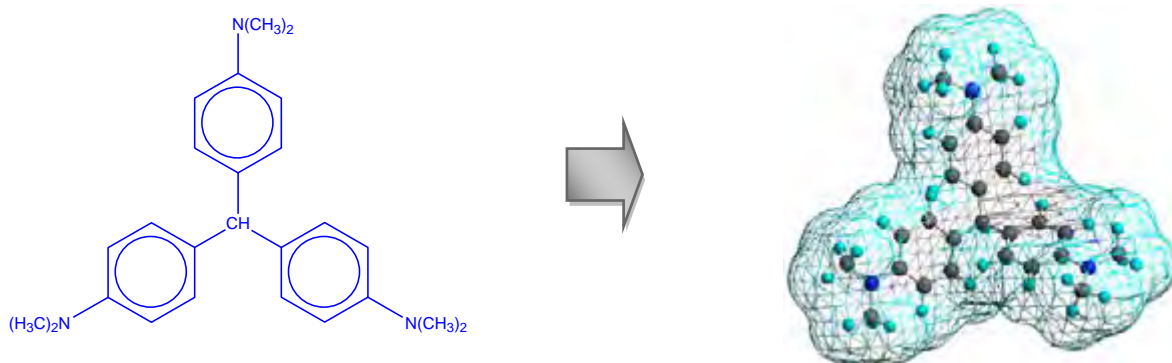


Figure 1.15 Left, Molecular structure of the octupolar compounds Crystal Violet, and right, ball configurations where the ends are Hydrogen and the blues are Nitrogen.

CV is an octupolar prototype molecule and has been used in recent years as a standard block in the construction of more complex molecules. The CV molecule was dissolved in DW at concentrations of [1×10^{-4} M, $(1 \text{ and } 5) \times 10^{-3}$ M].

Figures 1.16 a) and 1.16 b) show the TM Z-scan normalized traces of the transmittance for the DW and CV dissolved in DW (at different molar concentrations) at static solution. Figure 1.16 a) shows the comparison between DW and CV at 1×10^{-4} M concentration.

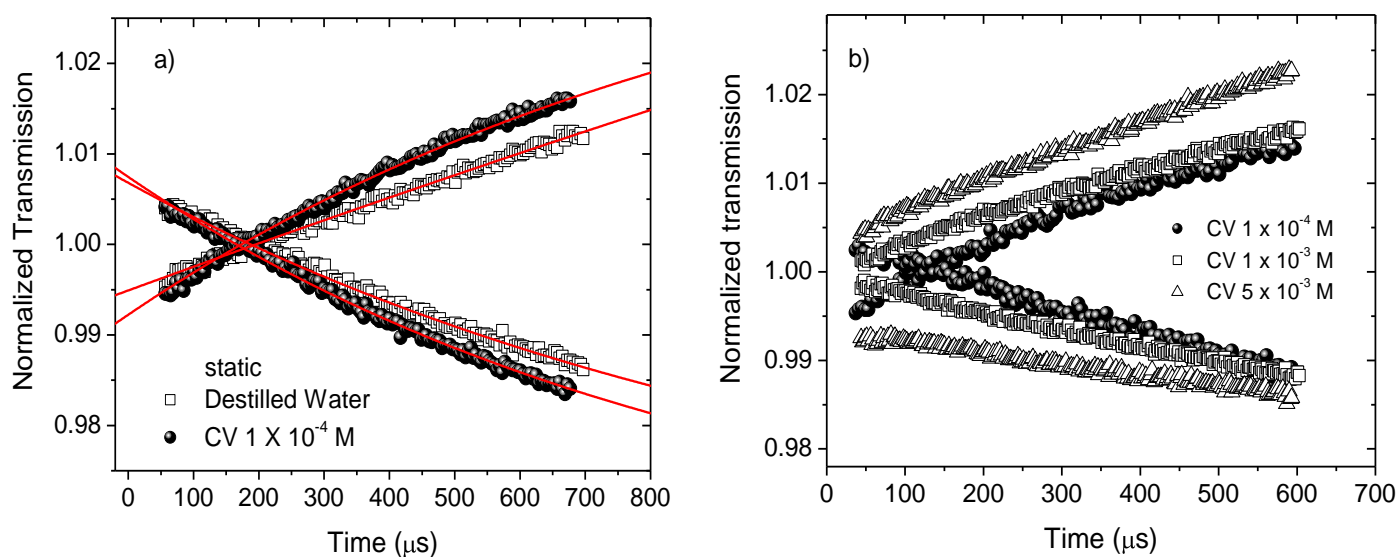


Figure 1.16 a) TM Z-scan traces of DW and CV dissolved in DW (1×10^{-4} M), b) TM Z-scan traces for different concentration of CV.

It is observed that at early times ($t = 0$), we cannot see differences between the electronic contributions of DW and CV dissolved in DW. However, around $500 \mu\text{s}$ we note a difference in the thermal evolution among them, which means that despite the low molar concentration (1×10^{-4} M), we observe a significant thermo-optical contribution. In this context, both DW and CV solution have a dominant thermal contribution and, both clearly have electronic and thermal NLR indexes of opposite signs. Figure 1.16 b) shows the TM Z-scan traces of CV solution at different concentrations. The thermal contribution

always prevails, and the electronic response is not appreciated because its contribution is weak and overwhelmed by the thermal one. Just with 1×10^{-3} M of concentration was enough to see how the thermal contribution is the only NL response that can be detected in the solution. Although TM Z-scan is sensitive to discriminate electronic effects of thermo-optical contributions, in this particular case the solution at high concentration produce mostly NL thermal contribution and the discrimination of both phenomena begins to fail. This is an important result obtained from TM Z-scan, because it demonstrated that the technique has shortcomings when we study organic solutions with a very outstanding thermo-optical coefficient.

To solve the problem of the thermal contribution, once again we propose that the CV solution circulate through the cell. The Figure 1.17 a) shows the TM Z-scan traces for different flows for CV solution at 1×10^{-3} M of concentration.

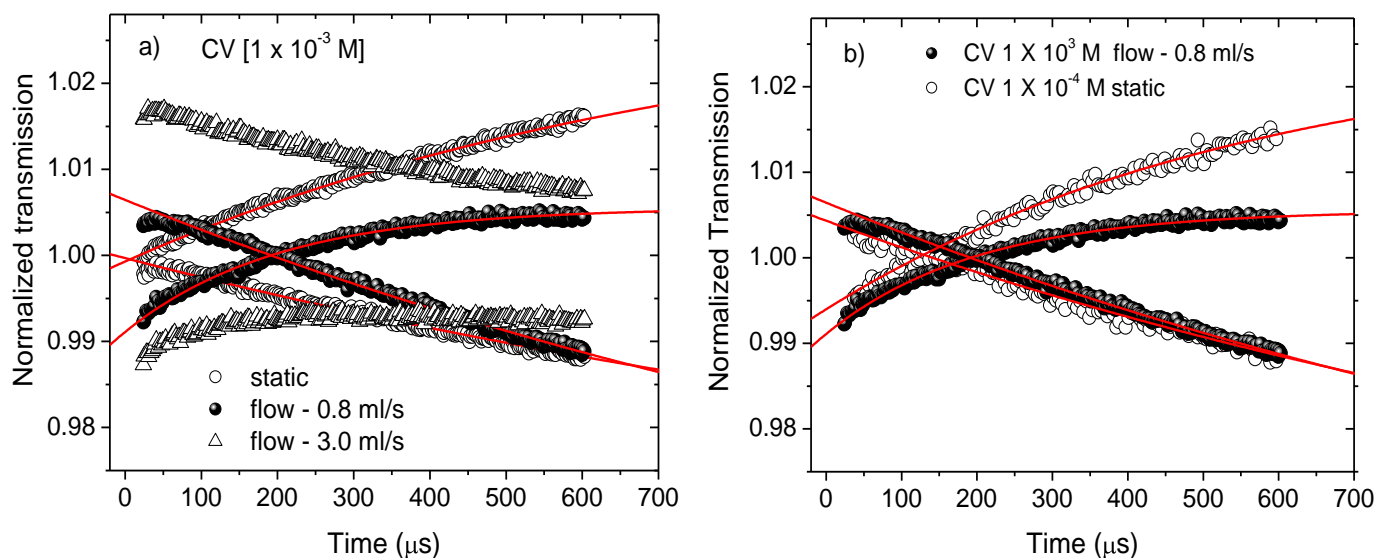


Figure 1.17 TM Z-scan traces for CV dissolved in DW for a) different solutions flows and with concentration of 1×10^{-3} M, b) static solution at concentration of 1×10^{-4} M and solution with flow of 0.8 ml/s and concentration of 1×10^{-3} M.

We observed a shift $\sim 180 \mu s$ between the intersections of the curves of CV at static solution and CV with solution flowing at 0.8 ml/s. Through this change, now it is possible to distinguish the electronic contribution of the CV molecule of the DW response.

With a flow of 3.0 ml/s, the thermal effect vanishes, although, the errors in signal due to turbulence are magnified. On the other hand, just a flow of ~ 0.8 ml/s is enough to remove most of the thermal contribution and in this special case, the difference between thermo–optical and electronic contributions becomes clear.

The figure 1.17 b) compares the traces at different molar concentrations (1×10^{-4} M – static solution and 1×10^{-3} M with a flow of 0.8 ml/s). They present differences of ΔT at $t = 0$ of $\Delta T = 0.0154$ (1×10^{-3} M) and $\Delta T = 0.0102$ (1×10^{-4} M). This reflects the electronic contribution of the molecule on the solvent by a difference of ~ 0.0052 . See Table 1.4 for the summary of the CV solutions results.

Table 1.4 n_{2elec} and n_{2therm} (measured for a delay of 500 μs) values for CV at different concentrations. As the molar concentration increases, the values of transmittance have more uncertainty.

Sample	Molar Concentration [M]	$n_{2elec}[cm^2/W]$	$n_{2therm}[cm^2/W]$ Static solutions
DW	-	$1.42 \pm 0.007 \times 10^{-15}$ [0 ml/s]	$1.75 \pm 0.019 \times 10^{-8}$
CV	1×10^{-4}	$1.49 \pm 0.002 \times 10^{-15}$ [0 ml/s]	$1.91 \pm 0.009 \times 10^{-8}$
CV	1×10^{-3}	$1.61 \pm 0.023 \times 10^{-15}$ [0.8 ml/s]	$2.39 \pm 0.021 \times 10^{-8}$
CV	5×10^{-3}	$1.74 \pm 0.04 \times 10^{-15}$ [1.5 ml/s]	$2.56 \pm 0.008 \times 10^{-8}$
CV	10×10^{-3}	No detected	6.92×10^{-8}

Table 1.4 shows the n_{2elec} and the n_{2therm} results of CV dissolved in DW at different molar concentration. The higher values of n_{2elec} corresponds to the solutions of CV. These results were expected since CV has higher linear refractive index than DW. Nevertheless, when the concentration of CV was so low i.e., 1×10^{-4} M, its electronic and thermo–optical NL contributions did not differ with respect those observed in DW. On the other hand, as the concentration increases i.e., 1×10^{-3} M, the NL contributions also increased. With the largest amount of molecules dissolved in the solution, greater is the probability

in which the molecules undergo de-excitation through non-radiative pathways, which often induces long transient thermal lensing in the samples. Due to the high thermal contributions that this concentration presented, it was necessary to have the solution in motion, in order to avoid or decrease the cumulative contributions. This mechanism allowed us to distinguish between both the real electronic contribution and the so reduced value of thermo-optical contribution. As the concentration in the solution of CV was increased, the uncertainty in the results of n_{2elec} increases, this was mainly because, at higher concentration, the thermal effects were more manifested and with them the problems to eliminate it. For instance, at 5×10^{-3} M, we needed to have a flow ~ 1.5 ml/s (at least) to distinguish between both contribution, nevertheless the variations in the measurements were very pronounced and with them the value of uncertainty.

In summary, the TM Z-scan technique applied in solvents showed us that they have large third-order NL optical properties that need to be take it into account when we work with organic molecules dissolved into them. TM Z-scan technique has the ability to distinguish between thermo-optical and electronic NL contribution but when the thermo-optical effects of a solution are prominent, the technique fails to discriminate between them. With the incorporation of the “flow mechanism”, most of the thermal contribution decrease and it makes feasible to have NL optical responses with a minimum of thermal contribution. The technical problems are notorious when the solution flow ceases to be laminar, i.e. when small bubbles appear. Another limitation is the amount of compound used; usually we needed 20 ml of solution which implied to spend a lot of material.

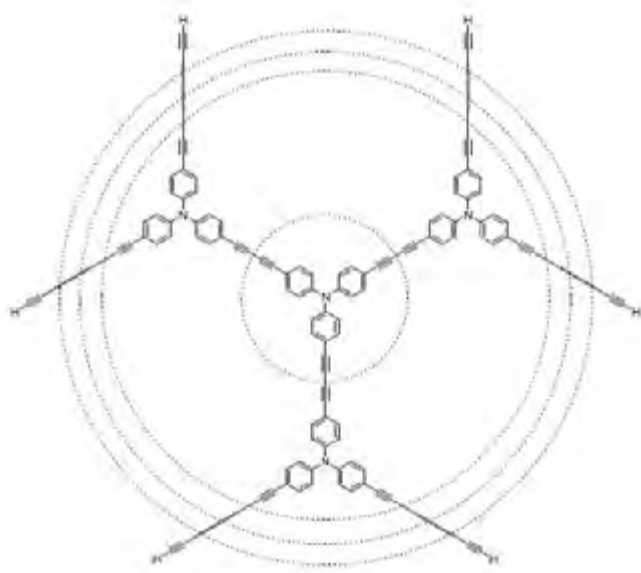
On the other hand, DW was the solvent with the lowest NL contribution compared with the other tested solvents. This makes it ideal to be applied as standard solvent in the characterization of organic compounds. Whereby, we decided to apply it in the characterization of the compound CV. The importance in the NL optical characterization of CV is due to the utility of such dyes as NL materials⁵¹. As a matter of fact, the dye CV has been used as a molecular prototype in some studies intended to recognize the basic NL

properties in octupolar structures. From the theoretical point of view, the multidirectional charge transfer that takes place in the three-fold symmetry structure of CV (octupolar dimensionality), has been correlated with its quadratic⁵² and cubic NL properties⁵³. In our group we have carried out studies about the third-order NL properties in CV⁵⁴ and reported the third-harmonic generation (THG) for fundamental wavelengths within the range 1100–1800 nm. That study demonstrated that the CV compound, with a multidirectional CT in its three-fold symmetry structure, exhibited efficient THG as a bulk effect with typical NL susceptibilities of the order of $\chi^{(3)} \sim 10^{-12}$ esu. These features make it attractive for photonic applications, i.e., ultra-fast optical correlators.

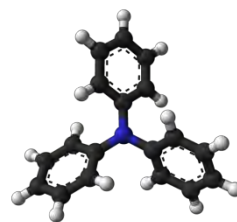
In the search for more efficient NL optical chromophores with strong polarization of the π -electronic cloud (with drift of the electron density from the core to the periphery or vice versa), we decide to extend our study through a macroscopic compound in which the multidimensional intramolecular CT takes place from a central unit (in our case, triphenylamine units) to the electron-withdrawing periphery. Based on the above information, we carry out NL optical measurements in a hyperbranched Polylyne (hb-Polylyne), which is a special case of hb-polymers. In the next sections we present the NL optical properties in an hb-Polylyne and the importance of this type of macroscopic structure as a compound with high density of extended π -conjugated systems based in octupolar moieties.

I. 4 STUDY OF THE NONLINEAR OPTICAL PROPERTIES IN HYPERBRANCHED POLYLYNE

The hb-Polylyne can be seen as repeated CV units. Taking into account the third-order NL optical results of CV, we decided to conduct third-order NL optical characterization in the hb-Polylyne (see molecular structure in Figure 1.18). This section is devoted to such NL studies.



a)



b)

WHITE ENDS: H

Central atom: N

Figure 1.18 Molecular structure of a) hb-Polyyne and b) Triphenylamine balls configuration. In a) configuration the dotted lines depict the extension of repeated units of the triphenylamine moiety.

For the study of the third-order NL optical properties of hb-Polyyne, we had restrictions to perform the measurements through the TM Z-scan technique because the high molecular weight of hb-Polyyne (24100 gr/mol) implied to use a large amount of compound to prepare few milliliters of solution. The measurement of electronic nonlinearities using TM Z-scan and Z-scan requires the use of solutions with concentrations of approximately 10^{-3} M, but solution at this level of concentrations can be prepared only with enough amount of material, but in our case, the amount of hb-Polyyne synthesized by our collaborators for these experiments was of just very few milligrams. Furthermore, in an attempt to prepare a solution of hb-Polyyne in a solvent of high thermal diffusivity, we found that such hb-polymer was not soluble in water. We found that hb-Polyyne was only soluble in THF, toluene and chloroform. In previous

experiments, we demonstrated that DW is the solvent with the lowest electronic and thermo-optical NL optical contributions and especially is the solvent with highest capacity to dissipate heat. In contrast, THF, toluene and chloroform are the solvents with less capacity to dissipate heat (see table 1.3). Solutions with these solvents meant a very serious restriction in the use of our Ti:sapphire of high repetition rate in TM Z-scan studies due to the large thermal nonlinearities that involve, and consequently the “flow mechanism” must be employed. However, this technique required at least 20 ml of solution to be implemented. This led to the conclusion that we did not have enough material to carry out third-order experiments with Z-scan, TM Z-scan or TM Z-scan with the novel “flow mechanism”.

In view of the restrictions mentioned above to perform the third-order NL optical studies of hb-Polyyne through Z-scan, we sought for another technique able to provide insight about its nonlinearities of electronic origin provided that no large amount of material is needed for the characterization. The option was to carry out the third-order NL optical characterization through third-harmonic generation (THG) measurements in thin solid films of hb-Polyyne. THG method is a quick screening for the evaluation of third-order nonlinearities and has the advantage that it probes purely electronic nonlinearity. Therefore, orientational and thermo-optical effects as well as other dynamic nonlinearities derived from excitations under resonance conditions are eliminated. This technique resulted very convenient since it combined with the property of hb-Polyyne to form solid films of excellent optical quality. Nevertheless, it is worth to mention that THG technique only provides an indirect insight into the tensor element responsible for nonlinearities of Kerr Type., i.e., $\chi^{(3)}(\omega; \omega, -\omega, \omega)$. In fact, the THG method does not provide any information on dynamics of nonlinearity and measures the tensor element of the type $\chi^{(3)}(-3\omega; \omega, \omega, \omega)$.

During the THG experiments it was found that not only the modulus of $\chi^{(3)}$ resulted to be significant, but also its imaginary part: the NL absorption (NLA) process in this material in solid state was notorious. For this reason we decided to study also the two-photon

absorption (TPA) contribution. TPA refers to the imaginary part of $\chi^{(3)}$ through which a molecule absorbs two photons simultaneously in the presence of an intense laser beam. The NL optical absorption experiments are usually carried out through Z-scan experiments in open aperture configuration, but such technique implied some the restrictions as it was mentioned above. Therefore, the NL optical study was then conducted through two-photon excited fluorescence (TPEF) experiments because the hb-Polyyne presented a high quantum efficiency of fluorescence.

This section presents the THG experiments in solid films of hb-Polyyne with ns laser pulses in the telecommunication wavelength range (1100–1600 nm) as well as the TPA characterization of very diluted solutions of hb-Polyyne through TPEF experiments with fs laser pulses (at high repetition rate) within the wavelength range of biomedical applications (740–860 nm).

I. 4. 1 General properties of the hb-Polyyne

The molecular structure of compound hb-Polyyne was introduced in Fig 1.18. This compound is mostly based on a set of repeated triphenylamine units. Basically, triphenylamine and CV have similar molecular configuration. Their main difference is that the central atom of the CV is a carbon atom and in the triphenylamine units are nitrogen atoms.

This hb-polymer is assembled by connecting the branches of triphenylamine moieties through polyynes chains, i.e., sp-hybridized carbon chains characterized by alternating single and triple bonds $-C \equiv C - C \equiv C -$. Details of its synthesis are reported in Ref. [55]. In this reference, hb-Polyyne was characterized by using absorption spectroscopy, IR and NMR analyses to corroborate the degree of branching, the signals and peaks of resonances that support the expected molecular structure. Table 1.5 shows the most important parameters of the hb-Polyyne.

Table 1.5 Properties of hb – Polyynes.

Compound	M_w	T_d	Refractive index 600 – 1700 nm
hb – Polyynes	24100 gr/mol	516 °C	1.816 – 1.770

In Table 1.5 we can see that the hb–polyynes shows very high refractivity ($n=1.770 - 1.861$) in the spectra region useful for optical communications, thanks to its polarizable aromatic rings and slender tripe–bonds rods. Therefore, we can expect strong NL optical contributions. We can see also that the hb–Polyynes is strongly resistant to thermal decomposition (thermolysis) with $T_d \sim 520$ °C.

I. 4. 2 Linear absorption

Figure 1.19 presents the absorption spectra of hb–Polyynes in solution (continuous line) and in spin–coated film (continuous line with open squares).

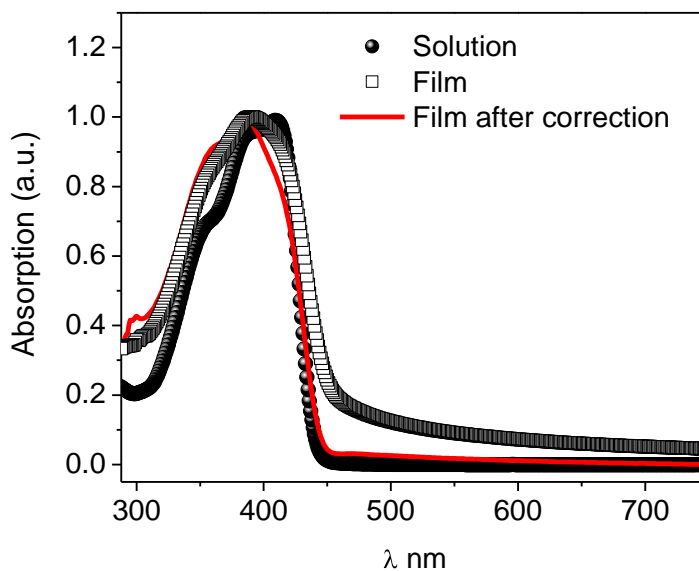


Figure 1.19 Absorption spectra of hb-Polyynes in chloroform solution at concentration of 1×10^{-5} mol/L and in solid film deposited on glass substrate before correction of Fresnel losses at interfaces.

In regard to the maximum absorption, the spectra have peaks at 410 and 390 nm for solution and film, respectively, and the absorption becomes negligible at wavelengths longer than 450 nm. The spectrum for the film was corrected for Fresnel losses at the interfaces of the film and substrate.

The refractive index dispersion used to calculate these losses is presented in Ref. [55]. Notice that before correction the spectrum shows significant losses due to the large refractive index of the hb–Polyyne film.

I. 4. 3 THG measurements

The NL optical behavior of the hb–Polyyne was studied in solid films using the guest (molecule) guest (polymer) approach. Ratios of 70:30 wt% of polystyrene (PS) and the hb–Polyyne were dissolved in chloroform. The solid films were deposited on fused silica substrates (1 mm thick) by using the spin coating technique. The prepared films had thickness $\sim 15 - 100$ nm with good optical quality showing negligible light scattering at visible and NIR wavelengths. The film thicknesses were measured with a surface profiler (Dektak 6M, Veeco).

To study the nonlinearities of hb–Polyyne via THG we followed the THG Maker–fringes approach.

The expressions for harmonic intensities are obtained by considering Maxwell’s equation in which the NL polarization of the medium acts as a source term. Assuming the propagation equation for both the fundamental and harmonic frequencies have plane wave equations, the wave equation in Gaussian units is:

$$\nabla^2 \vec{E}_{3\omega} + \frac{n^2(3\omega)}{c^2} \frac{\partial^2 E_{3\omega}}{\partial t^2} = -\frac{4\pi}{c^2} \frac{\partial^2 \vec{P}_{NL}(3\omega)}{\partial t^2} \quad 1.8$$

The general solution of Eq. (1.8) is a free wave, $\vec{E}_{3\omega}^f(\vec{r}, t)$:

$$\vec{E}_{3\omega}^f(\vec{r}, t) = \frac{1}{2} \left[\vec{E}_{3\omega}^f(\vec{r}) e^{i(\vec{k}_{3\omega} \cdot \vec{r} - 3\omega t)} + c. c. \right] \quad 1.9$$

and the particular solution of the homogenous equation is called the bound wave (because it follows the polarization) $\vec{E}_{3\omega}^b(\vec{r}, t)$:

$$\vec{E}_{3\omega}^b(\vec{r}, t) = \frac{1}{2} \left[\vec{E}_{3\omega}^b(\vec{r}) e^{i(3\vec{k}_\omega^b \cdot \vec{r} - 3\omega t)} + c. c. \right] \quad 1.10$$

where

$$k_\omega^b = \frac{\omega n(\omega)}{c} \quad 1.11$$

and

$$k_{3\omega}^f = \frac{3\omega n(3\omega)}{c} \quad 1.12$$

By substituting the bound wave (Eq. 1.10) into Maxwell's equation (Eq. 1.8), one gets the bound wave amplitude:

$$\left[|k_\omega^b|^2 - \frac{n^2(3\omega)}{c^2} (3\omega)^2 \right] E_{3\omega}^b = \frac{36\pi}{c^2} P_{NL} \quad 1.13$$

Which yields

$$E_{3\omega}^b = \frac{4\pi P_{NL}}{\Delta\varepsilon} \quad 1.14$$

where $\Delta\varepsilon = n^2(\omega) - n^2(3\omega)$ is the dielectric constant dispersion. Consequently, the third-harmonic wave propagating in the NL medium is the sum of both free and bound waves,

$$\vec{E}_{3\omega}(\vec{r}, t) = \frac{1}{2} \left[\vec{E}_{3\omega}^f(\vec{r}) e^{i(\vec{k}_{3\omega}^f \cdot \vec{r} - 3\omega t)} + \vec{E}_{3\omega}^b(\vec{r}) e^{i(3\vec{k}_{3\omega}^b \cdot \vec{r} - 3\omega t)} + c. c. \right] \quad 1.15$$

Due to the refractive index dispersion, both waves propagate with different velocities and interfere giving rise to Maker fringes, which give rise to an intensity modulation in the material. The output third-harmonic intensity is thus an oscillating function of the propagation distance.

The THG Maker-fringes setup consisted of a Nd-YAG laser-pumped optical parametric oscillator (OPO) that delivered pulses of 8 ns at a repetition rate of 10 Hz, see Figure 1.20. The idler beam of this OPO system, tuned at IR wavelengths in the range between 1100 and 1600 nm, was then focused into the films under test by using a 30 cm focal length lens to form a spot with a radius of approximately 150 μm . Typical energies in our measurements were set below 2 mJ per pulse at sample position (corresponding to peak intensities of 0.36 GW/cm^2).

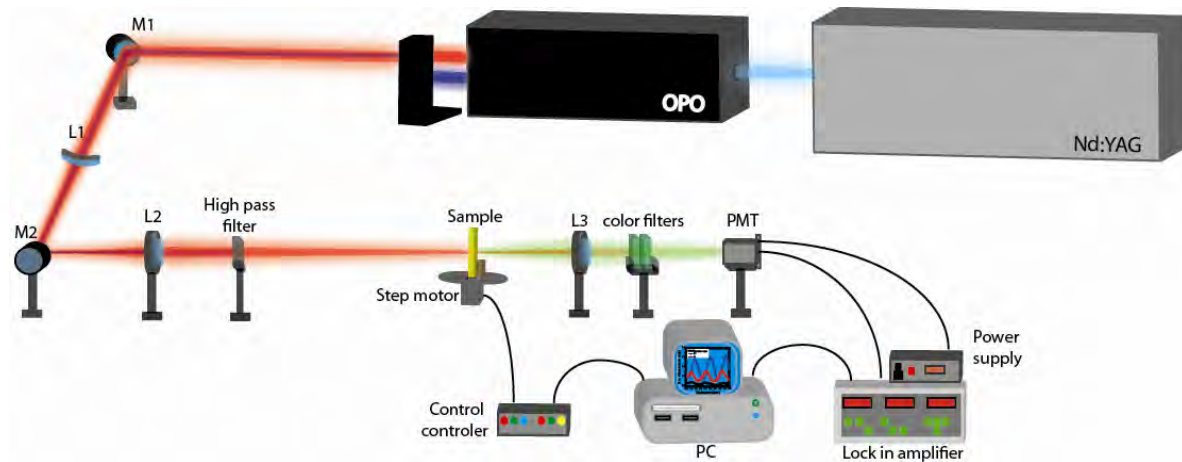


Figure 1.20 THG Maker-fringes experimental set up.

In the Maker-fringes technique, the third-harmonic peak intensity $I^{3\omega}$ from the substrate-film structure is compared to one produced from the substrate alone⁵⁶. Then, the NL susceptibility $\chi^{(3)}$ in a film of thickness L_f is determined from:

$$\chi^{(3)} = \chi_s^{(3)} \frac{2}{\pi} L_{c,s} \left(\frac{\alpha/2}{1 - \exp(-\alpha L_f/2)} \right) \left(\frac{I_f^{3\omega}}{I_s^{3\omega}} \right)^{1/2}, \quad 1.16$$

where $\chi_s^{(3)}$ and $L_{c,s}$ are the NL susceptibility and coherence length, respectively, for the substrate at the fundamental wavelength. Equation 1.2 is valid when the condition $L_f \ll L_{c,s}$ is satisfied. In any case, our samples satisfied the condition $L_f \ll L_{c,s}$ in which the Eq. (1.16) is valid.

Figure 1.21 shows typical plots of the THG signal from a 15-nm-thick hb-Polyyne film on glass substrate and from the substrate alone as a function of the incident angle for the excitation beam.

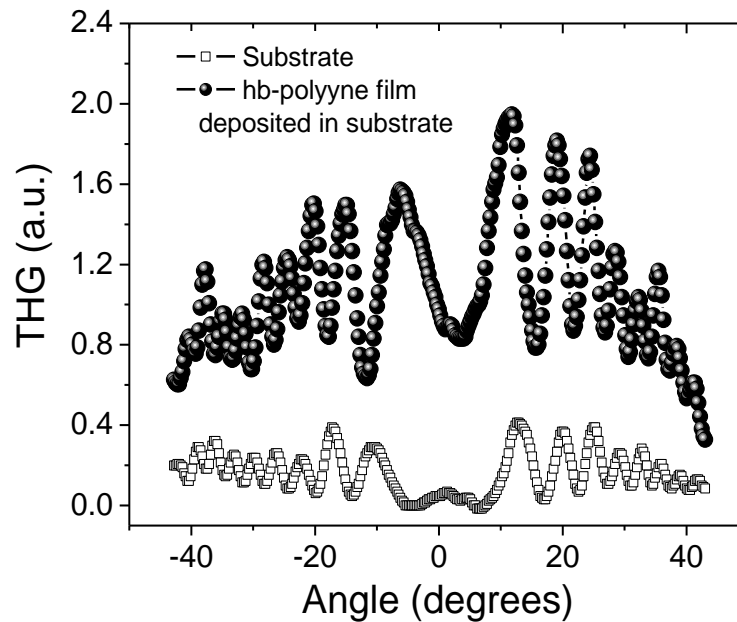


Figure 1.21 THG Maker-fringe patterns for (i) a 15-nm-thick hb-Polyyne film on glass substrate; (ii) a 1-mm-thick substrate without a film deposited on it. The fundamental wavelength is 1200 nm.

The excitation wavelength in this case is 1200 nm (THG signal at 400 nm). As we can see, the THG curves display an oscillatory behavior (Maker-fringe pattern) with an average

value in the substrate–film structure that is about 6 times more intense with respect to the substrate alone (thickness of 1 mm).

To perform $\chi^{(3)}$ calculation by using (1.16) we considered $\chi_s^{(3)} = 3.1 \times 10^{-14}$ esu which is practically constant within the 1100–1600 nm wavelength range⁵⁷. $L_{c,s}$ values at specific wavelengths were calculated from tabulated values of refractive index for fused silica. $L_{c,s}$ varied between 7 μm and 15.5 μm in the wavelength range 1100–1600 nm. The results for the NL susceptibility $\chi^{(3)}$ of hb–Polyyne measured at various laser wavelengths are shown in Figure 1.22 together with its linear absorption spectrum.

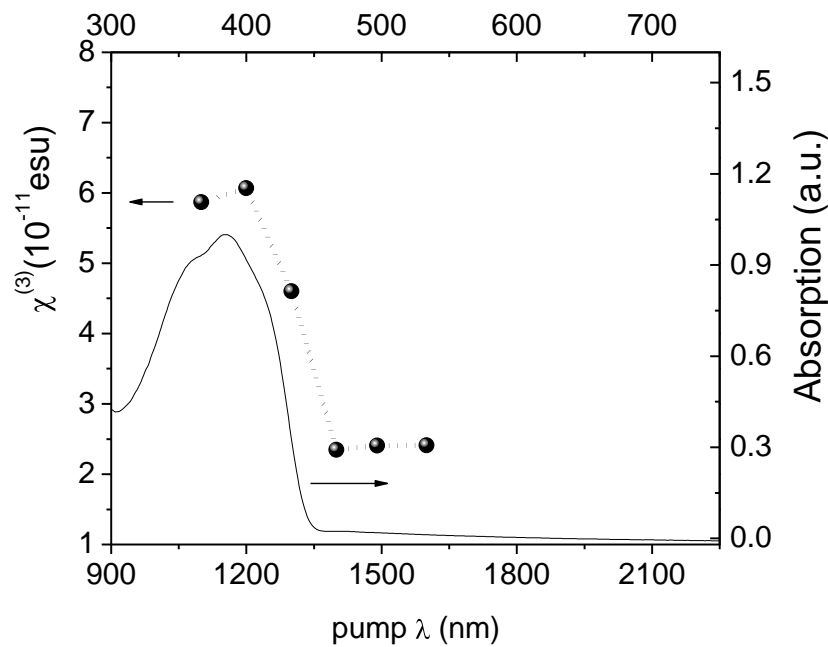


Figure 1.22 Wavelength dependence of the third order NL susceptibility for hb–Polyyne film. As a reference it is displayed the absorption spectra for hb–Polyyne (*top* and *right* axes).

One can divide the scale for the pump wavelength by 3 and observe that the dispersion curve of $\chi^{(3)}$ coincides with the linear absorption curve.

A maximum (resonant) value of NL susceptibility $\chi^{(3)} = 6.1 \times 10^{-11} \text{esu}$ is reached at the fundamental wavelength of 1200 nm. According to the absorption peak located at 390 nm, one observes an enhancement in $\chi^{(3)}$ due to three photon resonances. In regard to off-resonance wavelengths, the NL susceptibility decreases about a factor of three from the peak resonance value, i.e., between 1400 and 1600 nm of fundamental wavelength the susceptibility $\chi^{(3)} \sim 2.4 \times 10^{-11} \text{esu}$.

It is worth to compare the THG response of the hb-Polyyne with respect to CV and MEH:PPV, a well-known octupolar and conjugated polymer, respectively. Figures 1.23 a) and 1.23 b) show the $\chi^{(3)}$ spectrum for a 60 nm-thick MEH:PPV film and aprox. 150 nm-thick CV film, respectively. The $\chi^{(3)}$ spectrum of MEH:PPV reproduces its linear absorption spectrum, as happened for the hb-Polyyne.

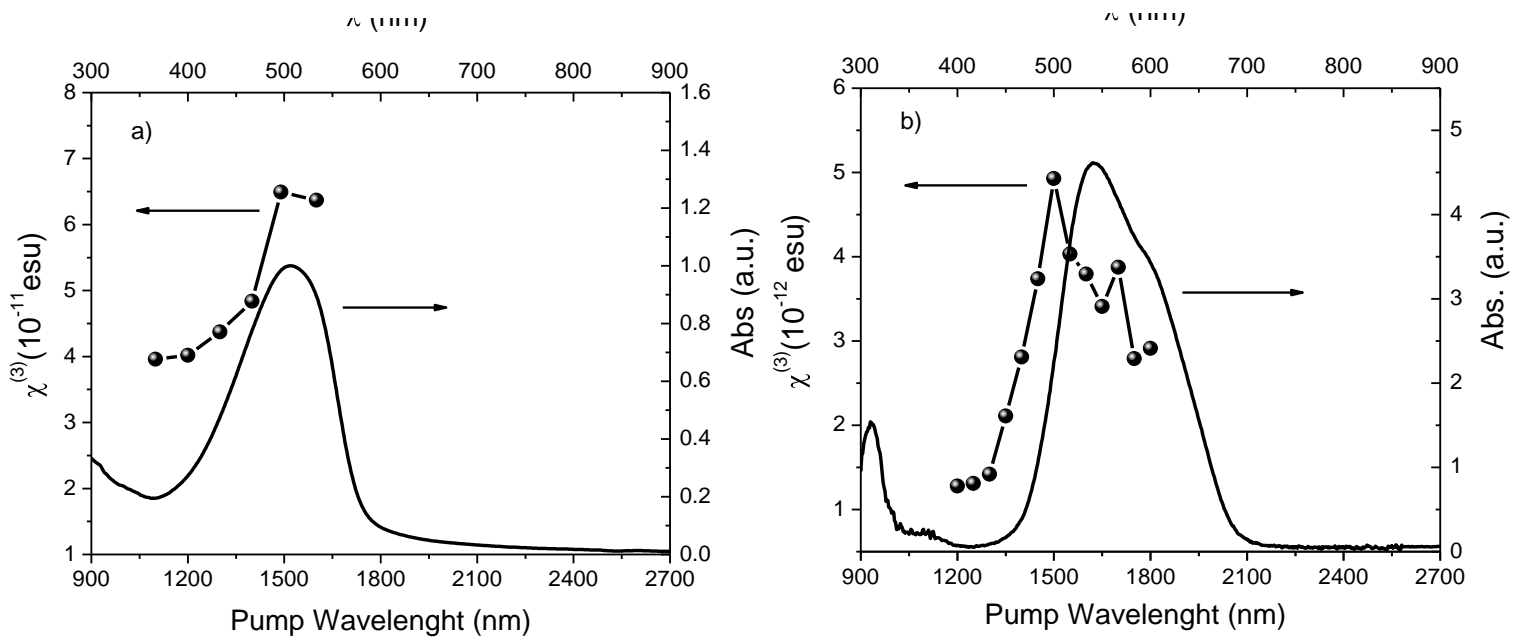


Figure 1.23 Wavelength dependence of the third order NL susceptibility for **a)** MEH:PPV polymer film and **b)** CV film. As references, the absorption spectra for MEH:PPV and CV are included.

Notice that the maximum (resonant) values of $\chi^{(3)}$ for hb-Polyyne and MEH:PPV are very similar, and even though the off-resonance values are smaller in hb-Polyyne, this

compound exhibits better transparency than MEH:PPV for most of the visible wavelength range.

On the other hand, Figure 1.23b) shows the maxima of $\chi^{(3)}$ for fundamental wavelength in the range 1200–1800 nm in CV film. Unlike hb–Polyene and MEH:PPV the $\chi^{(3)}$ spectrum not reproduce the absorption spectrum. This is mainly because $\chi^{(3)}$ could be enhanced by one, two and three–photon resonance, showing that $\chi^{(3)}$ would be complex near a resonance⁵⁸⁻⁵⁹.

The macroscopic NL susceptibility $\chi^{(3)}$ of hb–Polyene was used to calculate the second hyperpolarizability γ per monomer repeated unit, through $\langle\gamma\rangle = \chi^{(3)}/L^4 N_s$ where $N_s = \rho N_A/M_W$ is the number of the average monomer unit per cubic centimeter in the polymer film where N_A is Avogadro’s number, $\rho = 1g/cm^3$ is the mass density and M_W the molecular weight of the monomer. $L = (n^2 + 2)/3$ is the correction factor due to local field effects where n is the refractive index. Notably, the off-resonance γ value (per monomer repeated unit) in the wavelength range of 1400–1600 nm (telecommunication window) resulted to be 1.3×10^{-33} esu. Thus, the high transparency beyond 450 nm and the relatively large off-resonance nonlinearity of hb–Polyene make this a promising material for photonic applications.

I. 4. 4 NL absorption contributions

The intense monochromatic radiation from a laser can induce profound changes in the optical properties of a material. NL absorption refers to the change in transmittance of a material as a function of pump intensity. At sufficient high intensities, the probability of a material absorbing more than one photon before relaxing to the ground state can be greatly enhanced. As early as 1931, Göpper–Mayer derived the two–photon transition probability in a system using second order quantum perturbation theory. Since the invention of laser, not only this phenomenon of the simultaneous absorption of two photons has been observed in a wide variety of materials, multiphoton (>2) absorption has also been widely studied. In addition, population redistribution induced by intense

laser fields leads to interesting counterplays of stimulated emission and absorption, complicated energy transitions in complex molecular systems, and the generation of excited states. These phenomena are manifested optically in a reduced (saturable) or increased (reverse saturable) absorption. The many different effects produced by NL absorption in the frequency dependent transmittance of a material have led to several applications in science and technology. These include diverse areas as NL spectroscopy and optical power limiting. The NL phenomenon of TPA is shown in Figure 1.24.

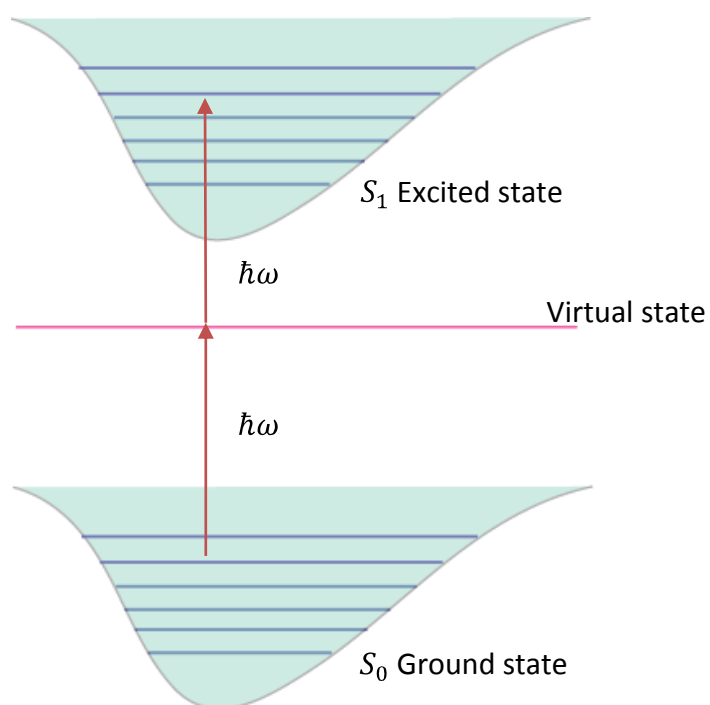


Figure 1.24 Schematic diagram of two-photon absorption (TPA).

TPA involves a transition from the ground state of a system to a higher-lying state by the simultaneous absorption of two photons from an incident radiation field or fields. This process involves different selection rules than those of singlet-photon absorption. Hence

TPA spectroscopy complements linear absorption spectroscopy in studying the excited states of systems.

Two possible situations of TPA can be observed in Figure 1.25: Self-TPA and Pump-probe TPA. For our immediate purposes, we focus on Self-TPA. Self-TPA is the case where two photons from the same optical field oscillating at frequency ω are absorbed to make the transition, which is approximately resonant at 2ω . The intermediate (or virtual) state is not real (i.e., does not involve a real stationary state of the system). Hence the system must absorb the two photons simultaneously. This makes the process sensitive to the instantaneous optical intensity.

The NLA in this case is proportional to the square of the instantaneous intensity. The differential equation describing the optical loss is given by

$$\frac{dI}{dz} = -\alpha I - \beta I^2 \quad 1.17$$

where α is the linear absorption coefficient and β is the TPA coefficient. The TPA coefficient β is a macroscopic parameter characterizing the material. Often, we are interested in the individual molecular TPA property that is described by the TPA cross-section σ_2 . The relation between β and σ_2 is given by

$$\sigma_2 = \frac{\hbar\omega\beta}{N}, \quad 1.18$$

where N is the density of molecules in the system, and $\hbar\omega$ is the energy of photons in the incident optical field.

The TPA coefficient is also related to the third-order susceptibility

$$\beta = \frac{3\pi}{\epsilon_0 n^2 c \lambda} \text{Im}[\chi_{xxx}^{(3)}(-\omega; \omega, \omega, \omega)] \quad 1.19$$

Notice that it is the imaginary part of $\chi^{(3)}$ that determines the strength of the NLA. Hence the susceptibility is complex, meaning that once of the resonant frequency denominators

is near zero and hence the imaginary part of the transition frequency is not negligible, as is assumed in purely reactive phenomena (i.e., NLR index). This frequency denominator corresponds to the energy transition of the system, which is resonant near $2\hbar\omega$.

Although Z-scan is a perfect technique to measure the NLA phenomenon, this technique requires concentrations of at least 10^{-3} M to carry out the measurements. We were limited by the disposal of material, so we decided to carry out our measurements through the two photon excited fluorescence (TPEF) technique⁶⁰.

For TPEF experiments chloroform solutions of hb-Polyyne were prepared. To calculate the cross section of the TPEF action in hb-Polyyne we used methanol solutions of laser dyes as references. The references were Rhodamine 6G, Rhodamine B and Coumarin 480, acquired from Exciton Inc.

The TPA action of hb-Polyyne was studied by the TPEF technique using a Ti:Sapphire laser (Spectra-Physics). This laser provided pulses of 100 fs of duration at a repetition rate of 80 MHz in the interval of 725–860 nm. The experimental setup is shown in the Figure 1.25.

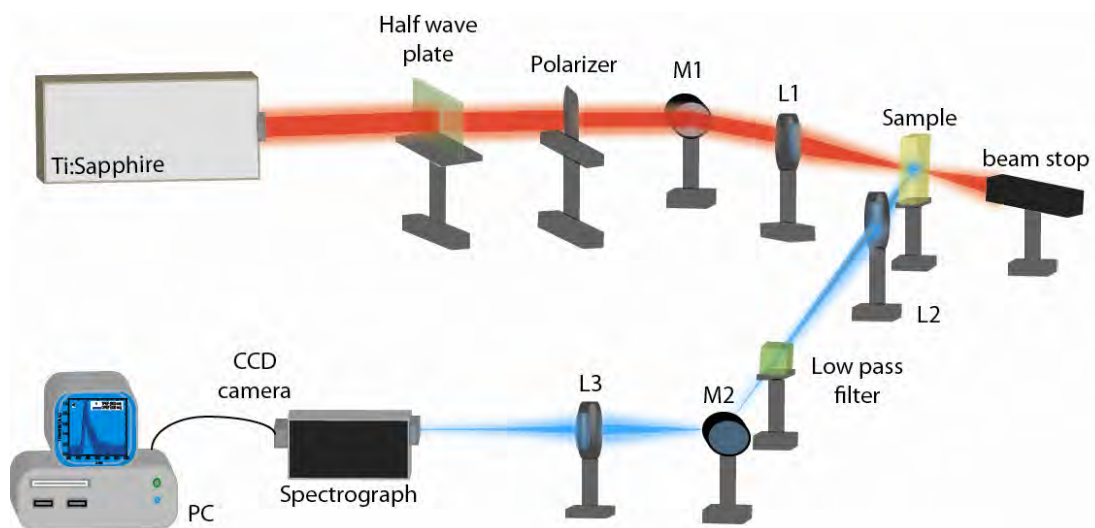


Figure 1.25 TPEF experimental set up. The pump is focusing inside the sample contained in a cell of 1 cm. Fluorescence is collected at 90° .

The induced two-photon fluorescence was collimated by a lens (L2) at a direction perpendicular to the pump beam. To minimize the attenuation of fluorescence due to

linear absorption effects, the excitation beam was focused as closely as possible to the lateral wall of the quartz cell. The TPEF was then focused (L3) into the input slit of an imaging spectrograph and recorded at the exit with a CCD camera. Under the same experimental conditions, the TPEF signals from laser dyes used as references were also obtained.

To calculate the TPEF cross section (σ^{TPEF}) and the TPA cross section (σ^{TPA}) for hb–Polyne we followed the TPEF method described by Albota, Xu and Webb⁶⁰. Following this method the cross sections (σ^{TPEF} and σ^{TPA}) for hb–Polyne are measured, according to

$$\begin{aligned}\sigma^{TPEF} &= \sigma^{TPA} \phi = \sigma_{ref}^{TPEF} \frac{c_{ref} n_{ref} F}{c n F_{ref}} \\ &= \sigma_{ref}^{TPA} \phi_{ref} \frac{c_{ref} n_{ref} F}{c n F_{ref}}\end{aligned}\tag{1.20}$$

Here c and n are the concentration and refractive index of the hb–Polyne solution respectively, and c_{ref} and n_{ref} are the corresponding parameters for the reference. With this formalism the cross sections σ^{TPA} and σ^{TPEF} can be calculated at different excitation wavelengths by using the fluorescence quantum yield ϕ_{ref} and the tabulated values of TPA cross sections σ_{ref}^{TPA} of the reference. In the use of (1.20) it is customary to assume that the fluorescence quantum yield for one-photon and TPEF is the same, and that these yields remain constant at different excitation wavelengths. We adopted Rhodamine 6G and Rhodamine B as reliable references since they were recently characterized in detail for fs excitation at several wavelengths⁶¹ and because they exhibit notorious TPEF which allowed high experimental sensitivity in the used range of wavelengths.

In order to know the quantum efficiency we carried out One–Photon Excited Fluorescence (OPEF) experiments, where we doubled the laser frequency with the help of a KDP NL crystal, see Figure 1.26. With OPEF the fluorescence quantum yield of hb–Polyne in chloroform was determined using an integrating sphere and a fluorescence standard with

known quantum yield (Coumarin 480, quantum yield 0.95⁶². This dye is also known in the literature as Coumarin 102).

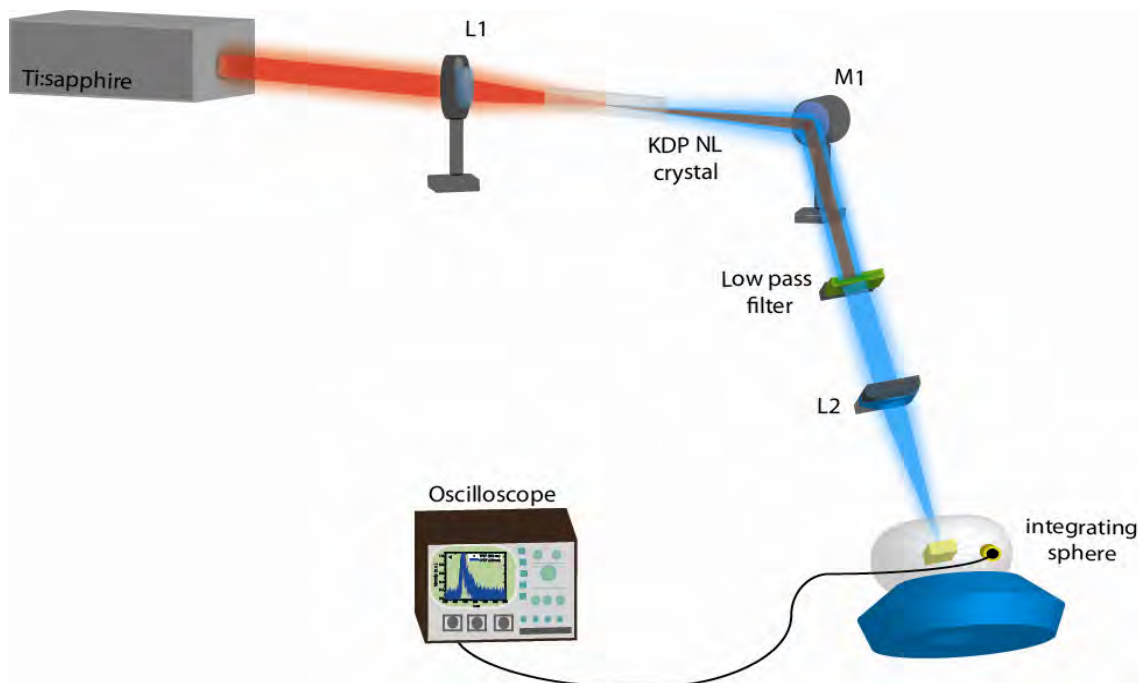


Figure 1.26 Experimental set up to measure the fluorescence quantum efficiency.

I. 4. 4. 1 OPEF and TPEF measurements

When pumped with fs pulses within the tunability of the Ti:Sapphire laser (725–860 nm), the hb–Polyne solutions emit very intense blue upconverted fluorescence, with a maximum of TPA \sim 445 nm. On the other hand, the upconverted fluorescence spectrum was identical to the spectrum corresponding to OPEF obtained under excitation of 400 nm, indicating that the intense blue light from TPEF and OPEF originates from the same lowest lying transition in the singlet manifold, Figure 1.27. The inset in the Figure 1.27 shows the picture of the intense fluorescence emission.

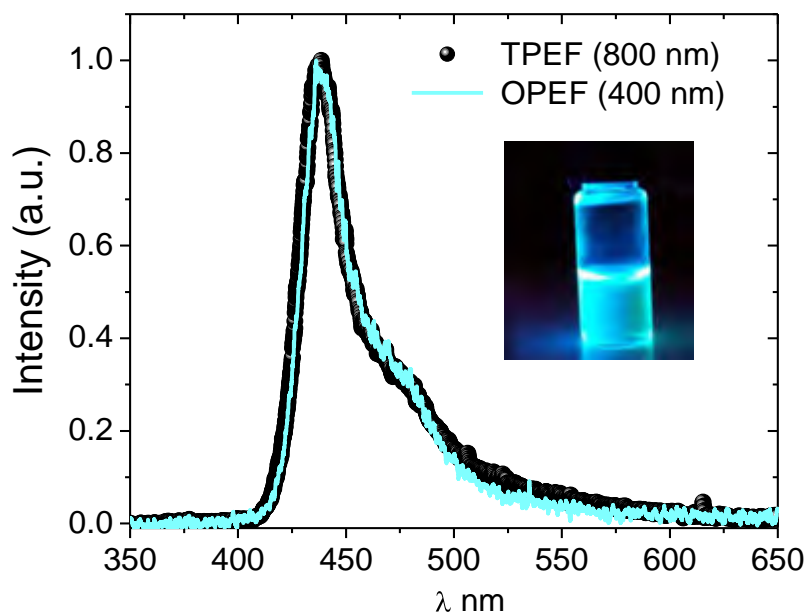


Figure 1.27 OPEF and TPEF emissions spectra excited at 400 and 800 nm respectively. For 1×10^{-7} mol/L chloroform solutions of hb-Polyne. Inset: picture of the hb-polyne sample excited at 400 nm.

By using an integrating sphere with one photon excitation at 400 nm and using Coumarin 480 as a fluorescence standard⁶², the fluorescence quantum yield (ϕ) in hb-Polyne was 0.57. Under excitation at 800 nm, the fluorescence intensity is basically proportional to the square of the input laser power, as demonstrated in Figure 1.28, confirming that the upconverted fluorescence is indeed induced by TPA. After 450 mW of intensity excitation, the TPA feature fades. This is perhaps by the saturation of the phenomenon of the hb-Polyne compound at those intensities.

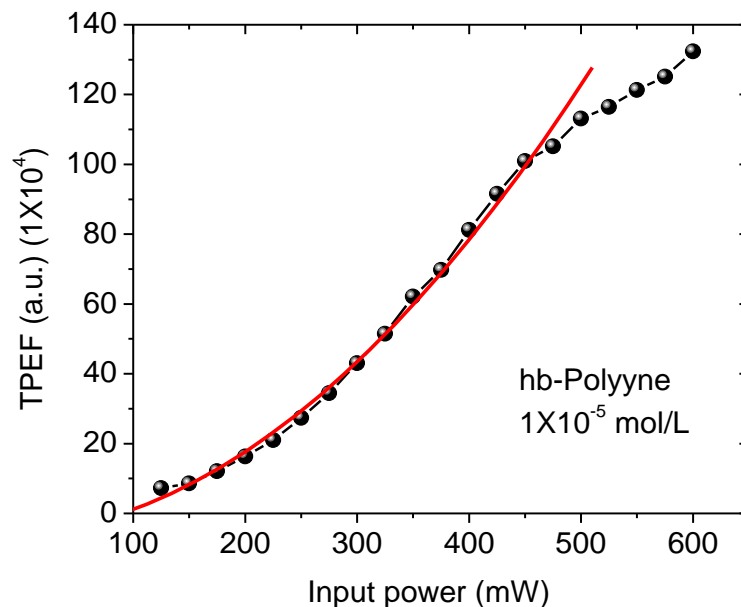


Figure 1.28 Spectrum of TPEF as intensity function.

Figure 1.29 shows the TPEF spectrum from a solution of hb-Polyyne along with the TPEF spectra corresponding to solutions of the dyes Rhodamine 6G, Rhodamine B and Coumarin 480 at the excitation wavelength of 725 nm. In order to avoid saturation effects all solutions were pumped at 180 mW and each solution was at the concentration of 10^{-5} mol/L. From this figure there is a much higher intensity of the TPEF signal from hb-Polyyne as compared with the dyes; in fact, the difference in peak intensities are two orders of magnitude.

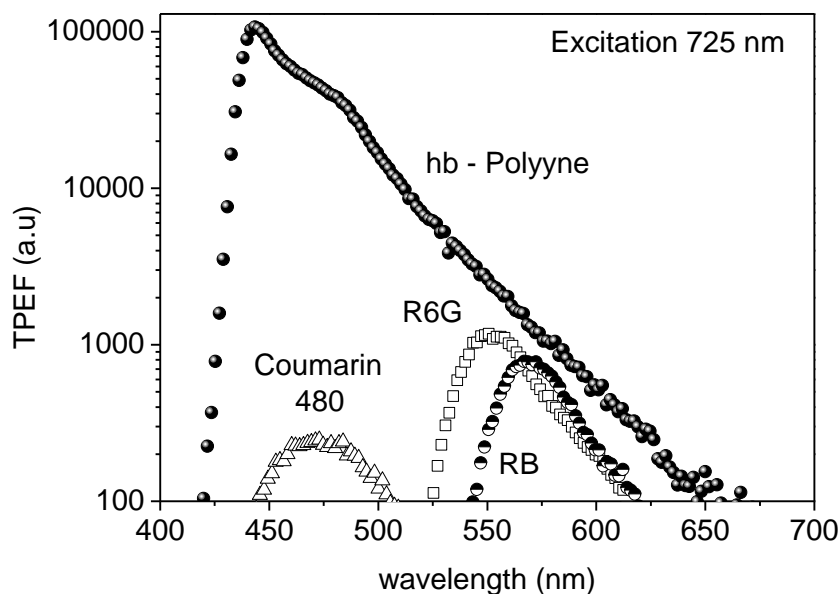


Figure 1.29 TPEF emission spectra from solutions of hb-polyyne, Coumarin 480, Rhodamine 6G (R6G) and Rhodamine b (RB). Each solution is at the concentration of 10^{-5} mol/L. In all cases the pump was set to 180 mW.

Figure 1.30 shows the σ^{TPA} values as a function of the excitation wavelength obtained from (1.20). We point out that the resulting values for σ^{TPA} were practically the same by using the references Rhodamines 6G and B, in spite of the fact that their quantum yields differ appreciably, being 0.95 and 0.45, respectively⁶¹. This means that our experimental setup was well calibrated. As reference the linear absorption spectrum for hb-Polyyne is included (dotted line).

We see in Figure 1.31 that the σ^{TPA} has a minimum value of 271 GM ($1 GM = 10^{-50} cm^4 s$) at 860 nm, but it increases constantly at shorter wavelengths, reaching a maximum value of 9068 GM around 740 nm. In regard to σ^{TPEF} , a maximum value of 5169 GM was obtained considering that $\phi = 0.57$.

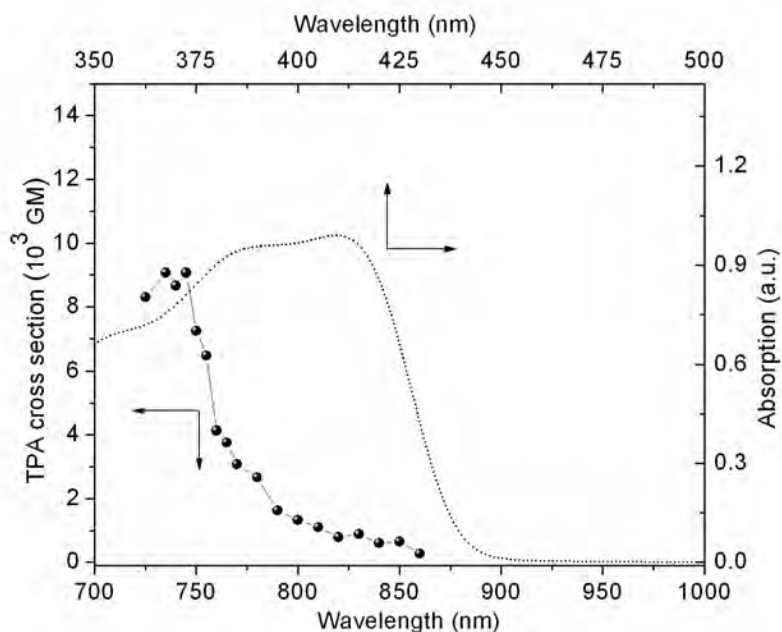


Figure 1.30 Wavelength dependence of the TPA cross section for hb-Polyyne.

These remarkably large values of σ^{TPA} and σ^{TPEF} are comparable with the largest TPA cross section values reported for organic compounds, which are in the range of $10^3 - 10^4$ GM. It is worth pointing out that this is the range where practical applications of TPA phenomena are feasible⁶³.

We can compare the performance of the hb-Polyyne with other octupolar systems. Figure 1.31 shows several of the NL optical structures with large TPA cross section to be compared with the hb-Polyyne TPA response. Table 1.6 reports the TPA cross sections σ^{TPA} for these molecules and valuable information regarding the characterization: molar concentration, the characterization technique, the laser type and the pump wavelength.

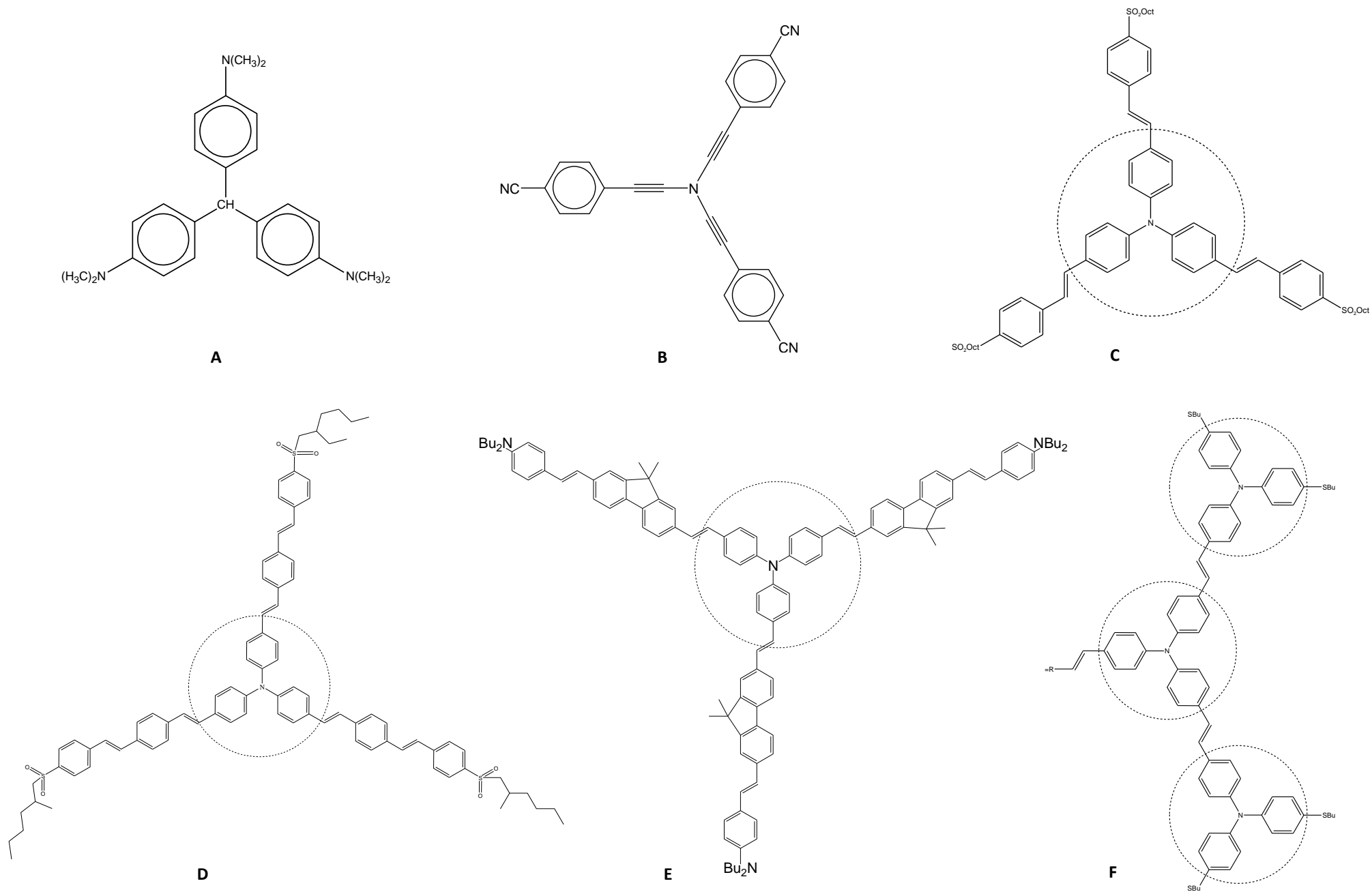


Figure 1.31 NL optical systems with large σ^{TPA} . **A** Crystal Violet, **B** Trialkynilamine, **C** Triphenylamine moiety with extended units of Octylsulfonylbenzene, **D** Triphenylamine moiety with extended units of ethylhexane – sulfonyl, **E** Triphenylamine moiety with extended units of fluorine; compound with butylamine and **F** second generation of a triphenylamine unit with four-arm; R= OC₁₀H₂₁

Table 1.6 Comparison of the general properties of the set of molecules presented in Figure 1.32 respect our hb-Polyyne.

Molecule	Concentration	Technique	Pump	σ^{TPA} [GM]	Ref.
A	10^{-5} M	TPEF	120fs, 1 kHz 800 nm	1980	64
B	10^{-5} M	TPEF	100 fs, 82 MHz 840 nm	581	64
C	Not mentioned	TPEF	80 fs, 80 MHz 705 nm	*35.92 $10^{-50} \text{cm}^4 \text{s photon}^{-1}$ molecule ⁻¹	65
D	10^{-3} M	TPEF	6ns, 10 Hz 856 nm	3700	66
E	10^{-6} M	TPEF	150 fs, 76 MHz 735 nm	9400	67
F	10^{-5} M	TPEF	150 fs, 1kHz 840 nm	11000	74
hb-Polyyne	10^{-5} M	TPEF	100 fs 80MHz 750 nm	9068	76 (this work)

Molecules A and B in Figure 1.31 could represent the main structural compositions of our hb-Polyyne. We can visualize the hb-Polyyne as repeated octupolar systems similar in structure to compound A. Especially compound A⁶⁴, which is based on a central acceptor atom interacting with surrounding donor moieties in a trigonal arrangement, reflects the high degree of conjugation between donor and acceptor groups. On the other hand, D. Beljonne et al⁶⁴. show the importance and strength of the coupling through compound B. Compound B as well as our hb-Polyyne is formed by repeated bonds of alkynes $-C \equiv C-$, as a matter of fact, the hb-Polyyne is represented by multiple-alkyne, bonding

repeated triphenylamine moiety. The amplitude of the TPA response can be modulated through cross-talk between the three arms of the octupolar molecule⁶⁴.

The design of octupolar compounds with enhanced TPA cross sections requires of cores that allow electronic delocalization through strong inter-arm-interaction (such a C⁺ or N centers) and arms leading to an optimal polarization. Molecules C⁶⁵, D⁶⁶ and E⁶⁷ perfectly fit these features. Furthermore, molecules C, D and E have in common that, they combine the advantages of octupolar systems with the advantages of multibranch systems. In multibranch systems, the interbranch coupling plays a central role. Depending on the extent and strength of this coupling, the ground state and the excited state will be either localized or delocalized⁶⁸, and optical properties such as TPA responses can show cooperative enhancement⁶⁹⁻⁷¹, additive behavior or weakening⁷²⁻⁷³. Thus, molecules C, D and E show that with the appropriate tuning of the number of branches, the coupling between them, the symmetry, and the modulation of the intramolecular CT from the core to the periphery, could constitute a substantial way for obtaining amplification in the TPA responses.

Finally, the strategy followed in the design of molecule F⁷⁴ as well as in our hb-Polyyne (through repeated triphenylamine moieties) shows that compounds gathered through a central core exhibit important TPA cooperative enhancement due to branching effects, i.e., molecular NL optical response of branched molecules may increase faster than the number of their constituent subunits, which is an indication of cooperative enhancement⁷⁵.

In conclusion, significant NL optical properties of hb-Polyyne solutions and films are reported. Two-photon excitation experiments demonstrate that the hb-Polyyne exhibits exceptionally high TPA cross sections under femtosecond excitation around 800 nm. The maximum TPA value (9068 GM) for hb-Polyyne is within the range of 10³–10⁴ GM. The high TPA cross sections and the relatively high fluorescence quantum yield of 0.57 exhibited by this compound can be of interest for multi-photon microscopy and optical

power limiting applications. In addition, hb-Polyyne films exhibited a third-order NL susceptibility $\chi^{(3)}$ of the order $(2.4-6.1) \times 10^{-11}$ esu. These values were in the order of magnitude of the third-order NL optical response of the well known conjugated polymer MEH:PPV.

Finally, taking into account the NL optical results of CV presented in the Fig. 1.23 and the table 1.6, we can confirm the cooperative effect from repeated octupolar moieties presented in the hb-Polyyne. Even, this type of configuration (hb-Polyyne) proved to be more efficient than the polymer MEH:PPV. Further, the polymer MEH:PPV is composed by 1700 monomer units and its molecular weight is of 996,000 gr/mol, unlike our hb-Polyyne that is composed by 60 octupolar units and its molecular weight is of 2400 gr/mol. All these confirm the following: polymers containing repeated octupolar units present more electronic delocalization which reflects higher NL optical behavior.

1.5 References

1. I. Ledoux and J. Zyss, *C. R. Phys.* **3**, (2002), 407.
2. J. Zyss, *J. Chem. Phys.* **98**, (1993) 6583.
3. D. M. Burland, *Chem. Rev.* (special issue) **94**, (1994) 1.
4. J. Zyss, C. Dhenaut, T. Chau Van, I. Ledoux, *Quadratic, Chem. Phys. Lett.* **206**, (1993), 409.
5. J.H. Park, M. Cha, M.-Y. Jeong, B.R. Cho, *J. Korean Phys. Soc.* **45**, (2004) 371.
6. X. Zhou, J.-K. Feng, A.-M. Ren, *Chem. Phys. Lett.* **403**, (2005) 7.
7. J.E. Ehrlich, X.L. Wu, I.-Y.S. Lee, Z.-H. Hu, H. Röckel, S.R. Marder, J.W. Perry, *Opt. Lett.* **22**, (1997) 1843.
8. W. Denk, J.H. Strickler, W.W. Webb, *Science* **248**, (1990) 73.
9. H. E. Pudavar, M. P. Joshi, P. N. Prasad, B. A. Reinhardt, *Appl. Phys. Lett.* **74**, (1999) 1338.
10. W. Denk, *Proc. Natl. Acad. Sci. USA* **91**, (1991) 6629.
11. R. M. Williams, D. W. Piston, W. W. Webb, *Fed. Am. Soc. Exp. Biol. J.* **8**, (1994) 804.
12. J. Zyss, I. Ledoux-Rak, H.-C. Weiss, D. Bläser, R. Boese, P. K. Thallapally, V. R. Thalladi, G. R. Desiraju, *Chem. Mater.* **10**, (2003) 3063.
13. V. Le Floch, S. Brasselet, J. Zyss, B. R. Cho, S. A. Lee, S. A., S.-J. Jeon, M. Cho, K. S. Min, M. P. Suh, *Adv. Mater.* **17**, (2005) 196.
14. P.N. Prasad, D.J. Williams, *Introduction to nonlinear optical effects in molecules and polymers* (Wiley, New York, 1990).
15. H.S. Nalwa, S. Miyata, *Nonlinear optics of organic molecules and polymers* (CRC Press, Boca Raton, 1997).
16. M.G. Kuzyk, C.W. Dirk, *Characterization techniques and tabulations for organic nonlinear optical materials* (Marcel Dekker, New York, 1998).
17. C.C. Chang, C.P. Chen, C.C. Chou, W.J. Kuo, R.J. Jeng, *J. Macromol. Sci. C, Polym. Rev.* **45**, (2005) 125.
18. S.K. Yesodha, C.K.S. Pillai, N. Tsutsumi, *Prog. Polym. Sci.* **29**, (2004) 45.
19. D. A. Tomalia, J.M.J. Fréchet, *J. Polym. Sci. A, Polym. Chem.* **40**, (2002) 2719.
20. H. Ma, S. Liu, J. Luo, S. Suresh, L. Liu, S. Ho Kang, M. Haller, T. Sassa, L.R. Dalton, A.K.-Y. Jen, *Adv. Funct. Mater.* **12**, (2002) 565.
21. J. Luo, M. Haller, H. Ma, S. Liu, T.-D. Kim, Y. Tian, B. Chen, S.-H. Jang, L.R. Dalton, A.K.-Y. Jen, *J. Phys. Chem. B* **108**, (2004) 8523.
22. P.A. Sullivan, A.J.P. Akelaitis, S.K. Lee, G. McGrew, D.H. Choi, L.R. Dalton, *Chem. Mater.* **18**, (2006) 344.
23. B. Voit, *J. Polym. Sci. A, Polym. Chem.* **38**, (2000) 2505.
24. J. Chen, H. Peng, C.C.W. Law, Y. Dong, J.W.Y. Lam, I.D. Williams, B.Z. Tang, *Macromolecules* **36**, (2003) 4319.
25. J. Xie, L. Hu, W. Shi, X. Deng, Z. Cao, Q. Shen, *J. Polym. Sci. B, Polym. Phys.* **46**, (2008) 1140.

26. D.Wang, S. Zhang, Y. Zhang, H.Wang, J. Mu, G.Wang, Z. Jiang, *Dyes Pigments* **79**, (2008) 217.
27. Z. Li, A. Qin, J.W.Y. Lam, Y. Dong, Y. Dong, C. Ye, I.D.Williams, B.Z. Tang, *Macromolecules* **39**, (2006) 1436.
28. J. Xie, X. Deng, Z. Cao, Q. Shen, W. Zhang, W. Shi, *Polymer* **48**, (2007) 5988.
29. J.M.J. Fréchet, *Proc. Natl. Acad. Sci. U.S.A.* **99**, (2002) 4782.
30. S. Hecht, J.M.J. Fréchet, *Angew. Chem., Int. Ed.* **40**, (2001) 74.
31. C. Li, C. Liu, Q. Li, Q. Gong, *Chem. Phys. Lett.* **400**, (2004) 569.
32. M. Häussler, J. Liu, R. Zheng, J.W.Y. Lam, A. Qin, B.Z. Tang, *Macromolecules* **40**, (2007) 1914.
33. H. Peng, J.W.Y. Lam, B.Z. Tang, *Macromol. Rapid Commun.* **26**, (2005) 673.
34. R. W. Boyd, *Nonlinear Optics* (Academic Press, 2008), 3th Edition.
35. M.G. Kuzyk and C. W. Dirk (Marcel Dekker, 1998).
36. M. Sheik-Bahae, A. A. Said, T. H. Wei, D. J. Hagan and E. W. Van Stryland, *J. Quantum Electron. QE-26*, (1990) 760.
37. Q. M. Ali and P.K. Palanisamy, *Optik* **116**, (2005) 515.
38. Jean-Michel Ménard, M. Betz, I. Sigal and H. M. van Driel, *Appl. Optics* **46**, (2007) 2119.
39. Shao-Chen Yang, Qiu-Ming Qian, Li-Peng Zhang, Pei-Hua Qiu, and Zhi-Jiang Wang, *Optics Lett.* **16**, (1991) 548.
40. A. Gnoli, L. Razzari and M. Righini, *OPTICS EXPRESS*, **13**, (2005) 7976.
41. S. J. Sheldon, L. V. Knight and J. M. Thorne, *Appl. Opt.* **21**, (1982) 1663.

42. D. Rativa, R. E. de Araujo, Cid B. de Araújo, A. S. L. Gomes and L. R. P. Kassab, *Appl. Phys. Lett.* **90**, (2007) 231906.
43. A. S. L. Gomes, E. L. Falcão Filho and Cid B. de Araújo, *Opt. Express* **15**, (2007) 1712.
44. S. Couris, M. Renard, O. Faucher, B. Lavorel, R. Chaux, E. Koudoumas and X. Michaut, *Chem. Phys. Lett.* **369**, (2003) 318.
45. N. L. Boling, A. J. Glass, A. Owyong, *IEEE J. Quantum Electron* **14**, (1978) 601.
46. W. Adam and G. Cilento, *Chemical and Biological generation of excited states*, Academic Press, Inc. New York 1982.
47. M. Falconieri, G. Salvetti, *Appl. Phys. B* **69**, (1999) 133.
48. A. Nakahara, Y. Shirasaki, K. Kawai, O. Ohara, J. Mizuno and, S. Shoji, *Microelectronic Engineering* **88**, (2011) 1817.
49. T. Zako, H. Hyodo, K. Tsuji, K. Tokuzen, H. Kishimoto, M. Ito, K. Kaneko, M. Maedaand, K. Soga, *J. of Nanomaterials Article ID 491471* (2010).
50. I. Goykhman, B. Desiatov, and U. Levy, *Appl. Phys. Lett.* **97**, (2010) 081108.
51. J. Zyss, T.C. Van, C. Dhenaut, I. Ledoux, *Chem. Phys.* **177**, (1993) 281.
52. Y.-K. Lee, S.-J. Jeon, M. Cho, *J. Am. Chem. Soc.* **120**, (1998) 10921.

53. W.-H. Lee, H. Lee, J.-A. Kim, J.-Ho. Choi, M. Cho, S.-J. Jeon, B.R. Cho, *J. Am. Chem. Soc.* **123**, (2001) 10658.
54. G. Ramos-Ortiz, J.L. Maldonado, M.A. Meneses-Nava, O. Barbosa-García, M. Olmos and, M. Cha, *Opt. Mat.* **29**, (2007) 636.
55. M. Häußler, R. Zheng, J. W. Y. Lam, H. Tong, H. Dong, and B. Z. Tang, *J. Phys. Chem. B* **108**, (2004) 10645.
56. Blanca M. Muñoz, Rosa Santillan, Mario Rodríguez, José Manuel Méndez, Margarita Romero, Norberto Farfán, Pascal G. Lacroix, Keitaro Nakatani, Gabriel Ramos-Ortíz, José Luis Maldonado, *J. of Org. Chem.* **693**, (2008) 1321.
57. F. Kajzar, J. Messier, *Phys. Rev. A* **32**, (1985) 2352.
58. W.-H. Lee, M. Cho, S.-J. Jeon, B. R. Cho, *J. Phys. Chem.* **104**, (2000) 11033.
59. P.N. Prasad, D.J. Williams, *Introduction to Nonlinear Optical Effects in Molecules and Polymers*, John & Wiley, New York, 1991.
60. M.A. Albota, C. Xu, W.W. Webb, *Appl. Opt.* **37**, (1998) 7352.
61. N.S. Makarov, M. Drobizhev, A. Rebane, *Opt. Express* **16**, (2008) 4029.
62. G. Jones II, W.R. Jackson, C.Y. Choi, W.R. Bergmark, *J. Phys. Chem.* **89**, (1985) 294.
63. N.S. Makarov, A. Rebane, M. Drobizhev, H. Wolleb, H. Spahni, *J. Opt. Soc. Am. B* **24**, (2007) 1874.
64. D. Beljonne, W. Wenseleers, E. Zojer, Z. Shuai, H. Vogel, S. J. K. Pond, J. W. Perry, S. R. Marder and Jean-Luc Brédas, *Adv.Funct Mater.*, **12**, (2002) 631.
65. C. Katan, F. Terenziani, O. Mongin, M. H. V. Werts, L. Porrès, T. Pons, J. Mertz, S. Tretiak, and Mireille Blanchard-Desce, *J. Phys. Chem. A* **109**, (2005) 3024.
66. H.J. Lee, J. Sohn, J. Hwang, and S.Y.Park, *Chem. Mater* **16**, (2004) 456.
67. C. Katan, S. Tretiak, M. H. V. Werts, A. J. Bain, R. J. Marsh, N. Leonczek, N. Nicolaou, E. Badaeva, O. Mongin, and M. Blanchard-Desce, *J. Phys. Chem. B* **111**, (2007) 9468.
68. T. G. Goodson III, *Acc. Chem. Res.* **38**, (2005) 99.
69. A. Abbotto, L. Beverina, R. Bozio, A. Facchetti, C. Ferrante, G. A. Pagani, D. Pedron, R. Signorini, *Chem. Commun.* (2003) 2144.
70. M. Drobizhev, A. Karotki, Y. Dzenis, A. Rebane, Z. Suo, C. W. Spangler, *J. Phys. Chem. B* **107**, (2003) 7540.
71. J. Yoo, S. K. Yang, M-Y Jeong, H. C. Ahn, S.-J Jeon, B. R. Cho, *Org. Lett.* **5**, (2003) 645.
72. A. Adronov, J. M. J. Fréchet, G. S. He, K. -S. Kim, S.-J. Chung, J. Swiatkiewicz, P. N. Prasad, *Chem. Mater.* **12**, (2000) 2838.
73. S.-J. Chung, T.-C. Lin, K.-S. Kim, G. S. He, J. Swiatkiewicz, P. N. Prasad, G. A. Baker, F. V. Bright, *Chem. Mater.* **13**, (2001) 4071.
74. M. Drobizhev, A. Rebane, Z. Suo and, C. W. Spangler, *J. of Luminescence* **111**, (2005) 291.
75. F. Terenziani, C. Katan, E. Badaeva, S. Tretiak, M. Blanchard-Desce, *Adv. Mater.* **20**, (2008) 1.
76. R. Castro-Beltran, G. Ramos-Ortiz, C.K.W. Jim, J.L. Maldonado, M. Häußler, D. Peralta-Dominguez, M.A. Meneses-Nava, O. Barbosa-Garcia, B.Z. Tang *Appl. Phys. B*, **97**, (2009) 489.

CHAPTER II

SECOND AND THIRD-ORDER NL OPTICAL EFFECTS IN NOVEL FOUR-COORDINATED ORGANOBORON DERIVATIVE AND THEIR BIDENTATE LIGANDS: THE EFFECT OF THE N→B BOND

Organometallic systems provide many interesting and unique structure and bonding schemes for molecular engineering of new materials. Furthermore, insertion of a metal unit in a conjugated structure significantly influences the π -electron behavior that can have important manifestations in optical nonlinearity. Besides, they offer the prospect of the tailorability of metal-organic ligand interactions.

II. 1 Background

New materials with desirable NL optical properties have been the subject of intense interest because these materials may provide an efficient means of controlling and processing signal-carrying light beams used in photonic technologies. Materials with significant quadratic and/or cubic NL optical properties are therefore of importance. Our group has been very interested in the use of organometallic compounds as NL optical chromophores in view of efficient OLEDs and OPVs applications, and in view of materials with strong $\chi^{(2)}$ and $\chi^{(3)}$ responses. The presence of metal atoms in the structures of organometallic molecules adds an additional flexibility to the design of NL chromophores and might lead to effects that are not readily available in classical organic chromophores because of, for example, problems with chemical stability. Furthermore, contribute by providing their electrons to the overall conjugation. In this context, coordination complexes have recently emerged as efficient compounds for second and third-order NL optical materials¹⁻³. Stronger intramolecular charge transfers (ICT) can be expected in metal complexes including conjugated ligands, because of the effective overlapping of the π -electron orbitals of ligands with the metal atom orbitals, i.e., in such compounds the

accessibility of multiple oxidation states may afford compounds with reversible (“switch”) nonlinearity⁴. In the search for new NL optical systems, considerable attention has centered on organic molecules having the inclusion of boron atom⁵⁻⁷. The vacancy in the p_z orbital makes it attractive to applications and studies in NLO. Besides, it allows the conjugation of organic π -system with and through boron, improving the electronic delocalization. There are several studies on the properties and possible applications of three-coordinate boron compounds⁸⁻¹⁰, especially for their inherently electron deficient characteristic. On the other hand, there are also studies about the NL optical properties in four-coordinate boron compounds^{7, 10-12}. Figure 2.1 shows the general structures of three-coordinate and four-coordinate boron compounds.

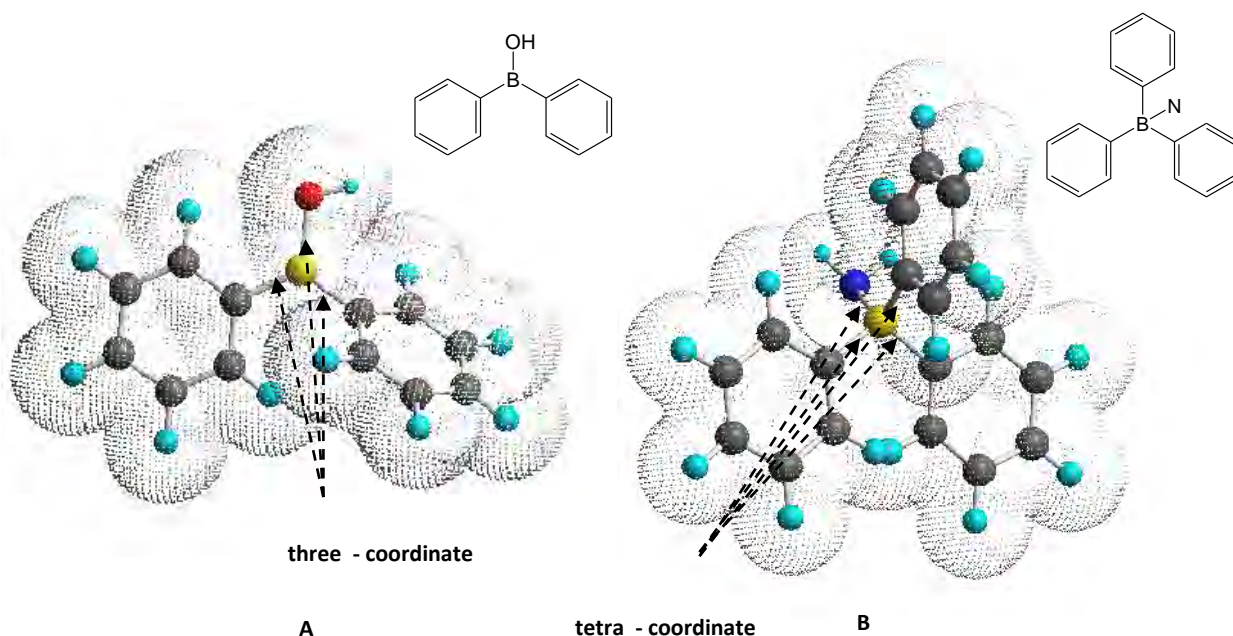


Figure 2.1 A Three-coordinate organoboron compound and B Four-coordinate organoboron compound.

Yellow circle: Boron, Red circle: Oxygen and Blue circle: Nitrogen.

The importance of studying tetra-coordinate compounds is because of their intrinsic high electron affinity, large capacity to perturb the electronic structure by decreasing the LUMO level, the possibility to obtain very stable compounds, besides presenting higher transparency and have much higher $\mu \cdot \beta_0$ values due to their increased dipole moments.

A great number of fascinating π -electron systems have been synthesized¹³, see for example Figure 2.2.

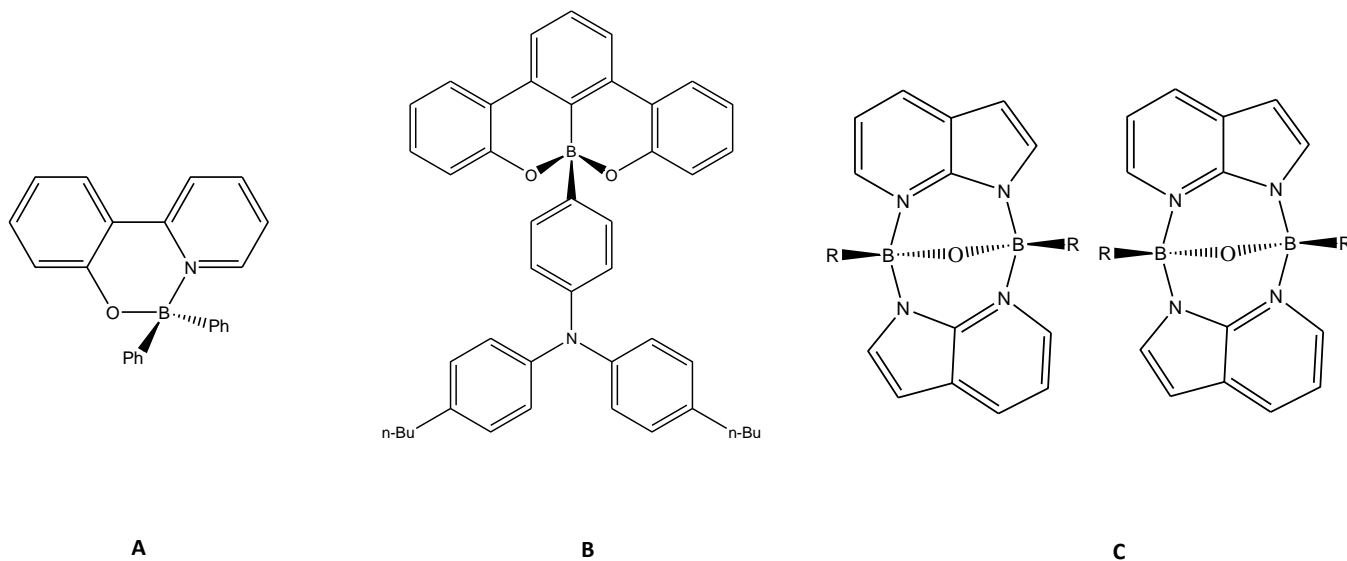


Figure 2.2 **A** bidentate chelate compound, **B** donor-functionalized molecule and **C** N,N-chelate compounds.

For all these characteristics, four-coordinate boron compounds have emerged as very attractive materials for various optoelectronic applications including, electron-transport materials, host/hole-blocking materials for organic light-emitting diodes (OLEDs), sensors and biological imaging materials, and photoresponsive materials¹².

Recently, the GPOM has been very interested in the NL optical characterization of organoboron compounds in view of possible optoelectronic application. For instance, there are some studies, previous to this thesis in which the GPOM investigated the boron complexes performance in NL devices¹⁴. They decided to explore the application of electro-optic chromophores (see Figure 2.3) to make thick, solid photorefractive (PR) films, to be used in dynamic holography.

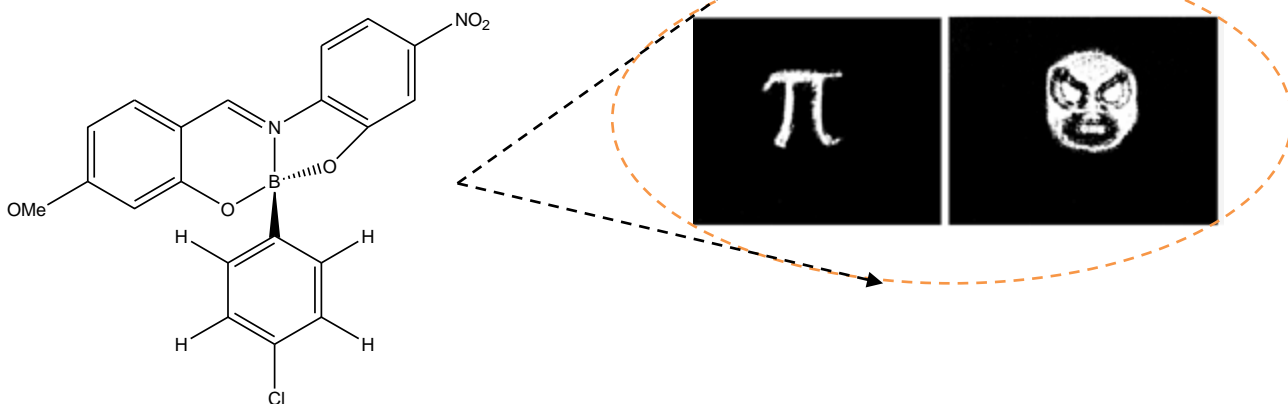


Figure 2.3 Electro-optic chromophore (2-(p-chlorophenyl)-(3' -nitrobenzo[d])- (4''-methoxybenzo[h])-1,3-dioxo-6-aza-2-boracyclonon-6-ene, a push-pull molecule. In inset, holographic image of an object transmitted through the PR sample.

In Fig. 2.3, the holographic images obtained with polymer PR films doped with the chromophore shown a good quality, and were formed and erased in ~ 0.5 s a reasonably fast response time. On the other hand, Mario Rodríguez et al. carried out NL optical and photoluminescence characterizations of a novel series of boronates (see Figure 2.4) as well as studies on crystal growth from these boron complexes¹⁵.

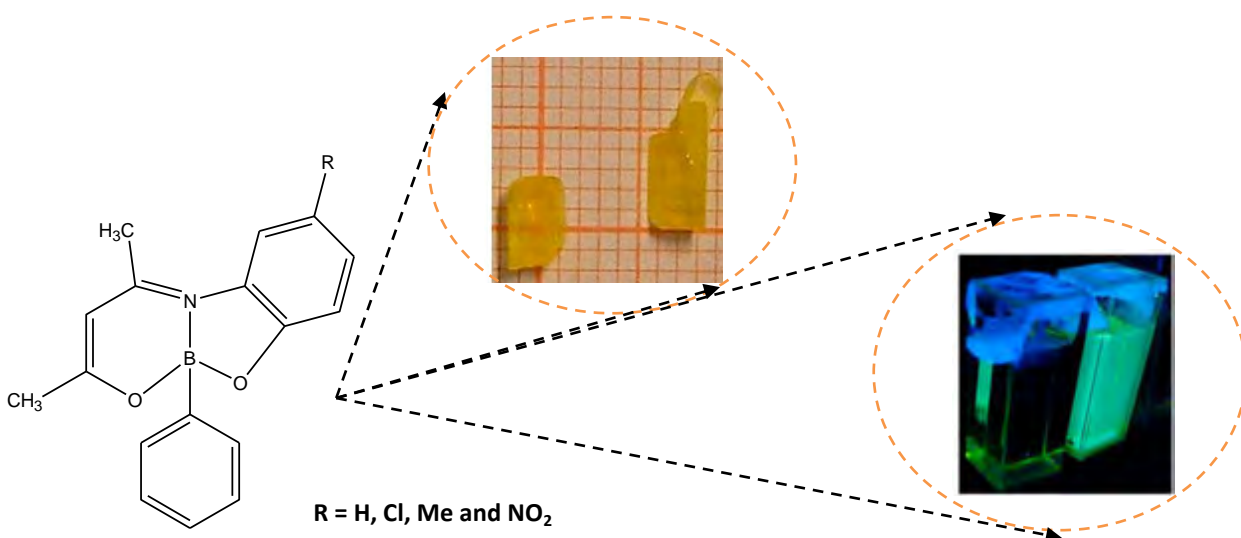


Figure 2.4 Novel boronates synthesized by the single step reaction of 2,4-pentanedione, aminophenol and phenylboronic acid.

The inset in the Fig. 2.4 shows the photograph of single crystals of compounds used and the photoluminescence from the boronate in a chloroform solution. These new series of boronates were interesting since the crystal packing of some of them resulted in noncentrosymmetric solids. NL optical studies confirmed that the SHG efficiency of these crystals is in average 4 times larger than in urea and 26 times larger than in KDP.

Further, these crystals exhibit notorious fluorescence induced by one and two-photon absorption at the resonant wavelengths about 400 and 800 nm, respectively. In summary, both analyses showed that organoboron compound possess stronger NL properties, related to the parameters μ , $\Delta\alpha$ and β . In addition, the second analysis was the first report about the preparation of organic crystals in the scale of millimeters with boron derivatives and offers the opportunity to investigate other organoboron compounds in NL organic crystals.

We are interested in investigate the NL optical properties conferred on aza electronic π -system present in bi- or three-dentate ligand and how they are modified by the presence of the coordination bond. In this way, extensive research about NLO properties has been performed on boronates and borinates compounds¹⁶⁻¹⁸. Elongation of the main π -backbone on boron complexes structures showed high second NL responses and theoretical analysis indicate that N→B coordinative bond favors the polarization of the electronic π -system¹⁷.

The following study is a continuation of the research work done by the GPOM, about the structural-property responses in boron-containing systems. In order to get more information about the N→B coordinative bond and how this favors the electronic polarization through the molecule, we will conduct second and third-order NL optical characterization. In this work we present studies of NL absorption and harmonic generation in hetero-aromatic π -conjugated systems containing four-coordinated boron and their corresponding ligands. Structural analysis of π -backbone was carried out using X-ray diffraction and experimental data of the bond distance was used for calculate the Bond Length Alternate (BLA) parameter. Electronic transitions were evaluated by

absorption spectroscopy and the NL properties were evaluated using EFISH (which is explained as the study unfolds) and THG techniques.

II.2 Four-coordinated organoboron compounds and their ligands: general aspects.

The synthesis and X-ray diffraction analysis of the following compounds were carried out by a group of collaborators in CINVESTAV and UNAM. Reagents for the preparation of the ligands and boronates were obtained from Sigma-Aldrich (USA) and were used without any further treatment. Solvents as ethyl acetate, ether ethylic and methanol for synthesis and purification process were purchased from QUIMICURT, México.

The bidentate ligands were prepared from the reaction between the appropriated aromatic alcohol and the corresponding cinnamaldehyde derivative in methanol at reflux temperature with yield from 80–95%. All compounds (ligands and boronates) were soluble in common organic solvents, enabling their optical characterization by Z-scan, EFISH and THG Maker-fringe techniques. Crystals suitable for X-ray diffraction analysis were prepared by slow evaporation technique from saturate solution of methanol and dichloromethane. Figure 2.5 shows the structures of ligands (L1, L2 and L3) and borinates (B1, B2 and B3) while general information related with them is presented in Table 2.1.

The BLA parameter is used in order to quantify the NL optical capabilities of the push-pull molecules having a polyenic linker. Marder et al.^{19,20} has suggested that the degree BLA, expressed as the difference between the length of carbon-carbon double and single bonds in a polyenic chain, found in dipolar molecules has a critical bearing on their NL optical properties. There is an optimum BLA value equal to 0.04 Å, which leads to the largest NL optical response. In the present case, the BLA values obtained by X-ray diffraction analysis are provided for the $-C=C-C-$ linkage shown in Table 2.1.

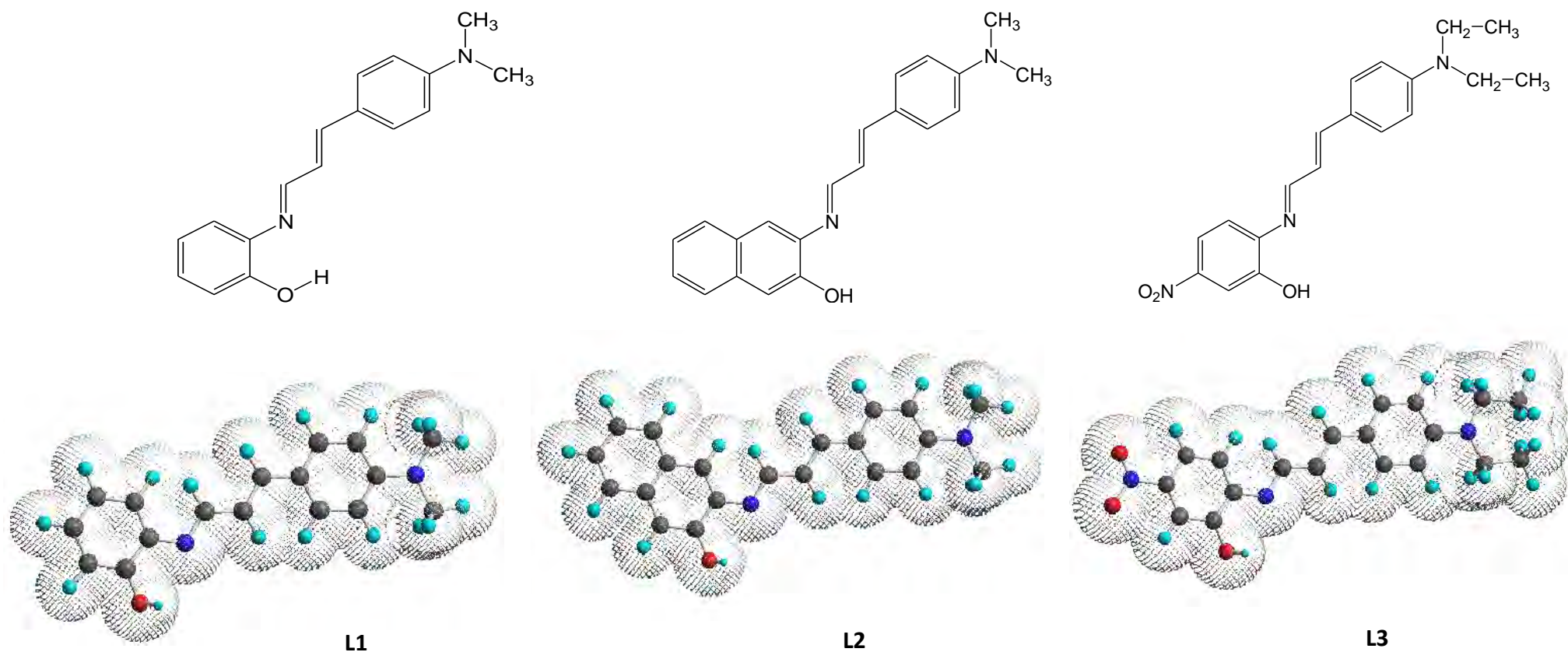


Figure 2.5 Molecular structures of ligands L1, L2 and L3 and borinates B1, B2 and B3.

Table 2.1 Structural effects induced by boron complexation, with related BLA parameter (see text), in the polyenic fragment for molecules L1 – L3 and B1 – B2.

Compound	Donor group	Acceptor group	–C = C –	= C – C =	–C = N –	BLA/Å
L1	(CH ₃) ₂	C ₆ H ₅	1.337	1.424	1.2827	0.087
L2	(CH ₃) ₂	C ₁₀ H ₇	1.339	1.425	1.281	0.086
L3	(CH ₂ – CH ₃) ₂	NO ₂	1.338	1.423	1.282	0.085

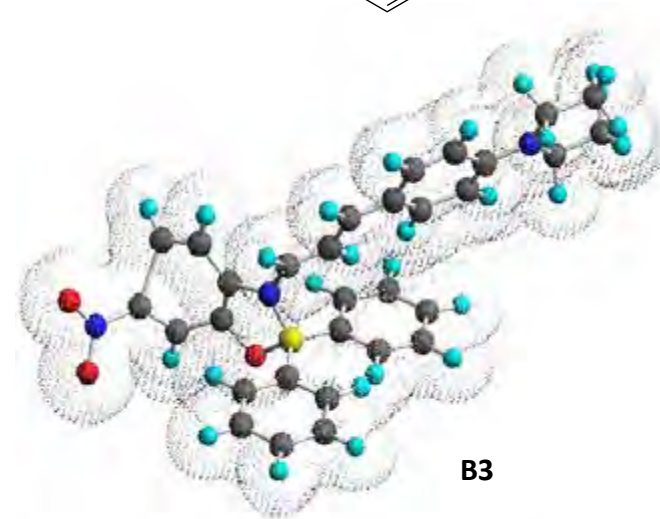
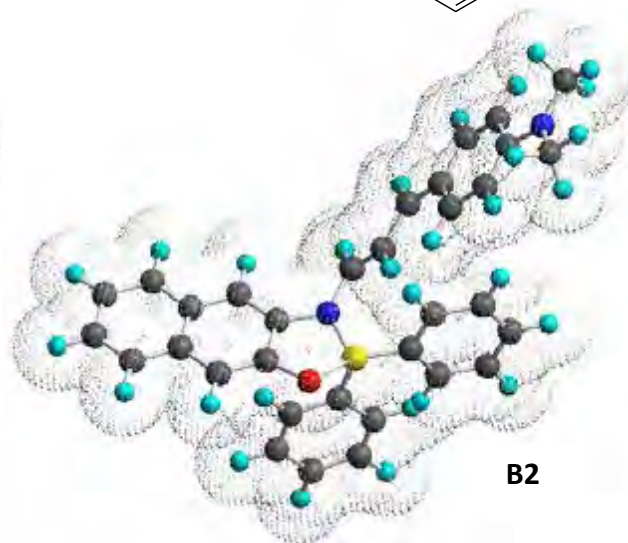
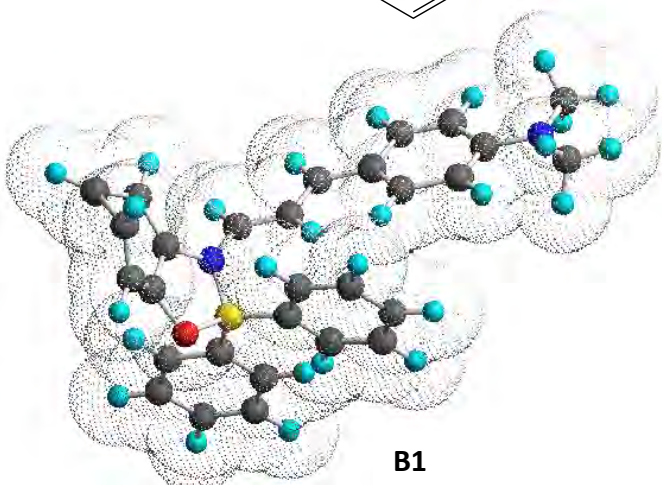
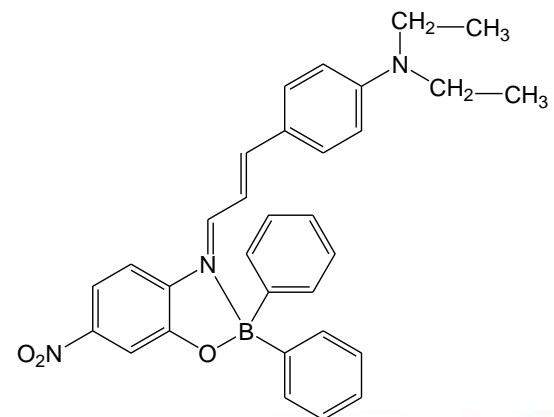
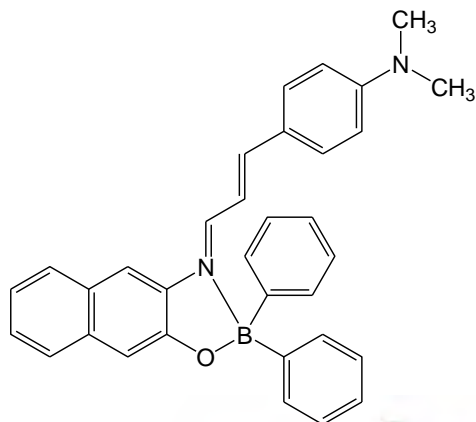
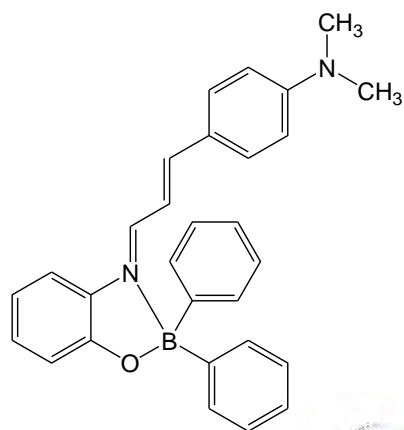


Figure 2.5 Continued

Table 2.1 continued.

Compound	Donor group	Acceptor group	-C = C -	= C - C =	-C = N -	BLA/Å
B1	(CH ₃) ₂	C ₆ H ₅	1.347	1.409	1.316	0.062
B2	(CH ₃) ₂	C ₁₀ H ₇	1.357	1.41	1.314	0.053
B3	(CH ₂ - CH ₃) ₂	NO ₂	1.360	1.389	1.315	0.029

The six compounds show the same backbone ($ph - N = C - C = C - ph$). L1 and B1 consist of dimethylamine [$N(CH_3)_2$ –donor] and phenyl [(C_6H_5) –acceptor] groups. L2 and B2 consist of dimethylamine and naphthyl [$(C_{10}H_7)$ –acceptor] groups. Finally L3 and B3 are composed by diethylamine [$N(CH_2-CH_3)_2$ –donor] and nitro [NO_2 –acceptor] groups. Here, it is important to be aware of the strength of the donor and acceptor groups; Table 2.2 shows the relative strengths of electron donation and electron withdrawing of these groups compared with other groups.

Table 2.2 Ranking of most common donors and acceptors strengths. R corresponds to any radical.

	Strong	Moderate	Weak
Donor	NH_2 , NHR , $N(CH_2-CH_3)_2$, OH	$N(CH_3)_2$, OCH_3 , (OC_2H_5, \dots) , $NHCOCH_3$	CH_3 , (C_2H_5, \dots)
Acceptor	NO_2 , $(CH_3)_3^+$, CN , $COOH$, $COOR$,	SO_3H , CHO , COR	F , Cl , Br , I , C_6H_5 , $C_{10}H_7$

Referring to Table 2.2, $N(CH_2-CH_3)_2$, $N(CH_3)_2$, NO_2 , C_6H_5 and $C_{10}H_7$ are the substituents that conform our ligands and organoboron compounds. In relation to these groups, $N(CH_2-CH_3)_2$ and NO_2 are the strongest electron-donor and electron-acceptor groups, respectively. On the other hand, C_6H_5 and $C_{10}H_7$ are the weakest acceptors. Under this assumption, and knowing that strong donor/acceptor substituents can enhance the optical nonlinearity²¹, it is possible to predict the NL behavior of our compounds. For instance, we expect that the strength of the NL response of our compounds could be in the following order: $L3 > L2 > L1$ and $B3 > B2 > B1$. Possibly the group L3-B3 may be the group with stronger NL behavior, this is precisely because they are the compounds with the strongest donor and acceptor groups. What really matters here is the understanding for role of boron atoms as part of the conjugated system. Boron atoms have the ability to work as strong acceptor group and with this to complete the push–pull system, and in most cases, improve the electronic mobility and the planarity of the π –system. Boron–functionalized chromophores have been typically designed following two structural principles: 1) Boron may be inserted into the main chain as an integral part of the π –conjugated system (Figure 2.6 A), this approach requires use of two boron valencies for

the formation of the backbone. 2) Boryl substituents are placed either at one terminal position of the molecular axis in push–pull systems or at both terminals (Figure 2.6 B).

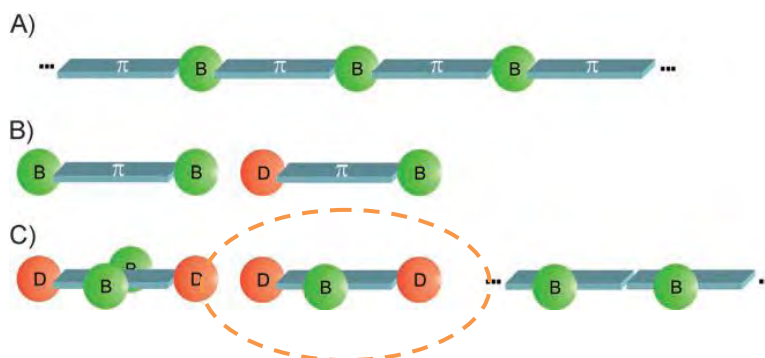


Figure 2.6 Schematic presentation of π -conjugated systems having the boryl group in **A)** in the chromophore chain, **B)** at the terminal position(s), and **C)** at the lateral positions. D=substituents groups, B=boryl group.

Within these molecular architectures, the boryl group is essentially an acceptor unit that may extend the π -system. The new design concept highlighted herein departs from these previous approaches in that it introduces boryl substituents at the lateral positions of the π -conjugated framework (Figure 2.6 C). Our systems fall in the latter case where the boryl substituents are at the lateral positions of the π -conjugated framework.

In order to get further insight about the effect of the π -electronic polarization, the second and third-order nonlinearities due to the formation of the N \rightarrow B coordinative bond, in this chapter we present studies of NL absorption and harmonic generations in hetero-aromatic- π -conjugate systems containing four-coordinated boron; the NL responses of this systems are compared with their precursor bidentate ligands.

The studies of the nonlinearities of the compounds were carried out through the Z-scan open aperture, THG and EFISH techniques. Due to laboratory conditions and the available material, we did not characterize all the compounds under the same experimental conditions.

II.3 Experimental results and discussions

II.3.1 Linear Absorption

The absorption maxima (λ_{max}) for the L1, L2, L3, B1, B2 and B3 compounds in DCM solutions are 400, 421, 471, 510, 529 and 566 nm, respectively, see Figure 2.7. These spectra are characterized by absorption bands attributed to $\pi[\text{N}(\text{CH}_3)_2] \rightarrow \pi^*$ (aryliminic) for L1, L2, B1 and B2 compounds. However, for compounds L3 and B3, their spectra are characterized by absorption bands attributed to $\pi[\text{N}(\text{CH}_2\text{-CH}_3)_2] \rightarrow \pi^*$ (aryliminic) electronic transitions. The difference in the absorption maxima in L1, L2 and L3 are mainly to the combination of the substituents. For instance, the ligand L3 presents the maximum red-shifted property because it is the ligand with the strongest electron acceptor and electron donor, NO_2 and $\text{N}(\text{CH}_2\text{-CH}_3)_2$, respectively.

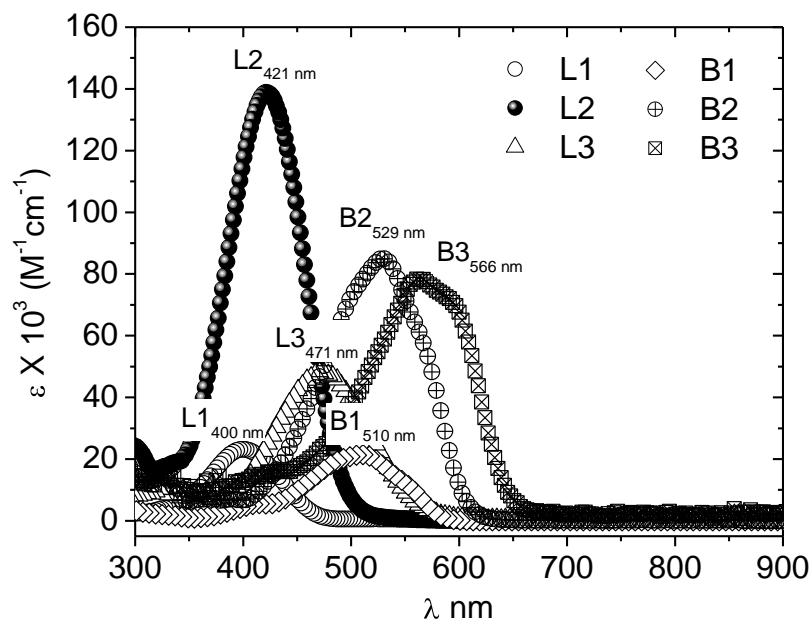


Figure 2.7 Linear absorption spectra of compounds L1, L2, L3, B1, B2 and B3 in DCM.

These combinations of substituents favors the ICT over the π -backbone in L3 compound compared with the low efficiency promoted in the L1 and L2 compounds by their Phenyl and naphthyl groups, respectively. An important effect (red shift) of complexation is shown in the Figure 2.7 when the boron compounds (B1, B2 and B3) are present. In the case of boron complexation from L1 to B1 a wavelength shift of $\Delta\lambda_{B1-L1} = 110$ nm is observed, from L2 to B2 a $\Delta\lambda_{B2-L2} = 108$ nm and finally, from L3 to B3 a $\Delta\lambda_{B3-L3} = 95$ nm. Precisely, the set 1 (B1-L1) and set 2 (B2-L2), present the maximum values of shift. In both sets, the boron complexion causes that the push pull system is complete. Therefore, the strength of ligand ICT seems to play the major role in the modification of the absorption spectrum upon complexation, regardless of its dimensionality.

II.3.2 NL absorption

To study the NLA properties in solutions, Z-scan measurements were performed with fs and ns laser pulses. The sensitivity to NL refraction is entirely due to the aperture, and removal of the aperture completely eliminates the effect. However, in this case, the Z-scan will still be sensitive to NL absorption.

In the first case a fs Ti:sapphire regenerate amplifier delivering pulses of 280 fs (1 kHz repetition rate) at 800 nm was used. In the second case, 7 ns pulses at 532nm (10 Hz) were obtained from a frequency doubled Qswitched Nd:YAG laser. The Z-scan curves were taken in a 1mm quartz cell, which is less than the Rayleigh range for the focused beams. To avoid sample degradation, the peak intensity was kept below $60 \text{ GW}/\text{cm}^2$ and $90 \text{ MW}/\text{cm}^2$ for fs and ns excitation, respectively. The NL absorption coefficient β was obtained from open-aperture Z-scan data using the relations²²:

$$T(z, s = 1) = \sum_{m=0}^{\infty} \frac{[-q_0(z)]^m}{(m+1)^{3/2}}$$

$$\text{where } q_0(z) = \left[\frac{\beta I_0 L_{eff}}{(1+z^2/z_0^2)} \right] < 1. \quad 2.1$$

Here I_0 is the peak irradiance, $L_{eff} = (1 - \exp(-\alpha_0 L))/\alpha_0$ the effective thickness with L the sample thickness, while z is the sample position and z_0 the Rayleigh range. To verify the validity of the measurements, the Z-scan set-up was previously calibrated with the standard CS_2 .

Figures 2.8 a) and 2.8 b) shows the open and close-aperture Z-scan curves for L1 and B1 at the concentration of 10 mM, in this case using fs excitation with peak irradiance of 53 GW/cm^2 at the focal region. Figure 2.8 a) shows that at the focal region it is clearly observed that the B1 compound exhibits NL absorption while for the L1 compound such kind of absorption is practically zero or below the level of sensitivity of the experiment.

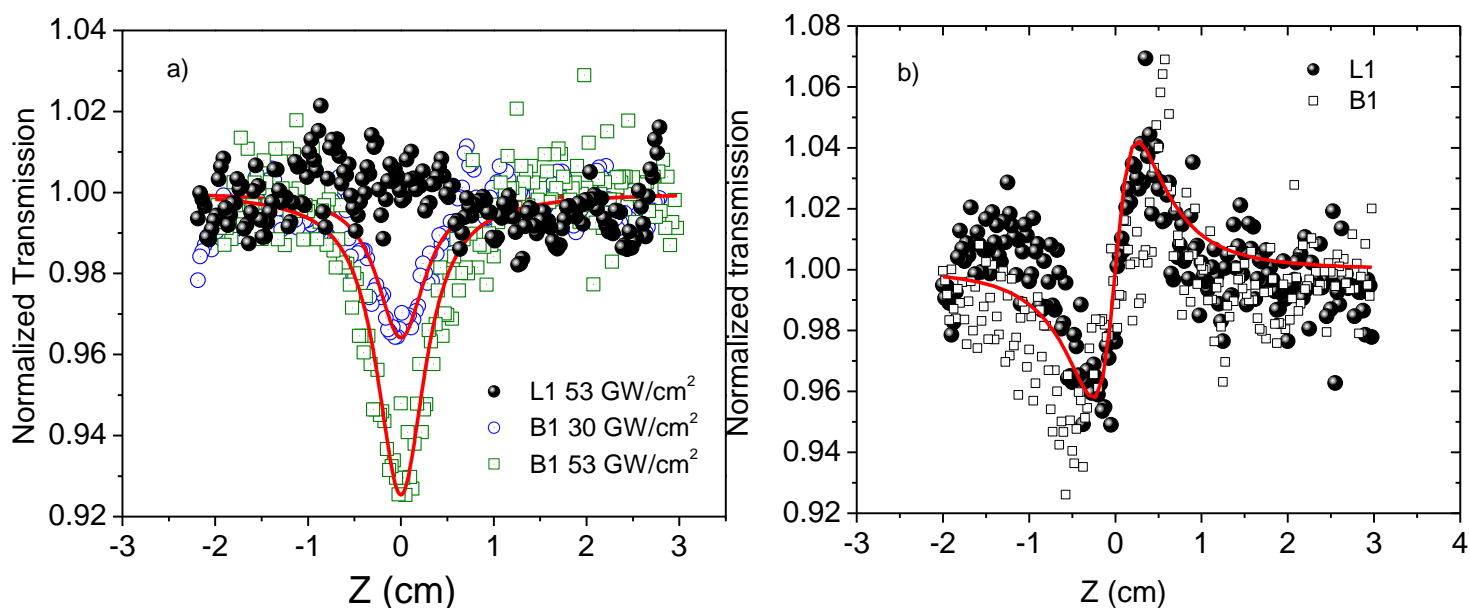


Figure 2.8 a) Normalized transmittance in open-aperture Z-scan experiments (fs excitation) for ligand L1 (filled circles) and borinate B1 (open squares) at irradiance of 53 GW/cm^2 and B1 at irradiance of 30 GW/cm^2 (open circles). **b)** closed-aperture ($S = 0.4$) Z-scan curves for L1 (filled circles) and B1 (open squares) at irradiance of 53 GW/cm^2 . Solutions of 10mM were employed. Continuous lines are theoretical fit to experimental data.

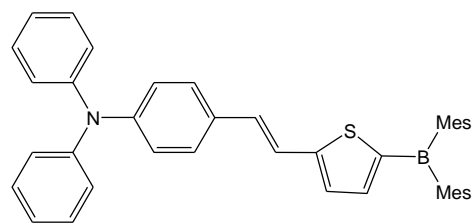
The figure also presents the Z-scan (open-aperture) for B1 at lower excitation, $\sim 30 \text{ GW/cm}^2$. Owing to the type of excitation (fs pulses far from the linear absorption band) it is then recognized that the origin of the NL absorption exhibited by the compound B1 is due to the TPA process.

We remark that the excitation wavelength (800 nm) should produce resonant TPA process in the case of compound L1 as its linear absorption spectrum has a main absorption band at 400 nm. This fact however did not lead to an observable TPA effect. In contrast, compound B1 is out of resonance and exhibited appreciable TPA, see Figure 2.7. We ascribe these results to the formation of the N \rightarrow B coordinative bond that increases the nonlinearities in the boronate with respect to its ligand.

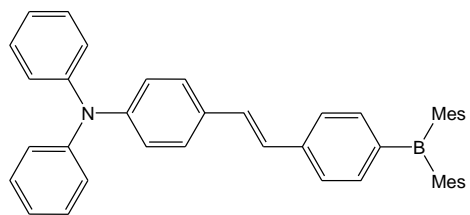
Figure 2.9 b) presents the ratio of closed-aperture Z-scan curves for both L1 and B1 compounds where the effect of NLA was eliminated by dividing these curves by their respective open-aperture curves. Here the NLR responses for solutions of both molecules were positive and did not differ appreciably from that exhibited by the solvent.

The σ_{TPA} can be evaluated from $\sigma_2 = \frac{\hbar\omega\beta}{N}$ (see eq. 1.4 in chapter I), giving a value of 152 GM ($1\text{GM} = 10^{-50} \text{ cm}^4 \text{ s photon}^{-1}$) for B1. Although this value is moderate, it demonstrates the effectiveness of the N \rightarrow B coordinative bond to enhance the NL absorption.

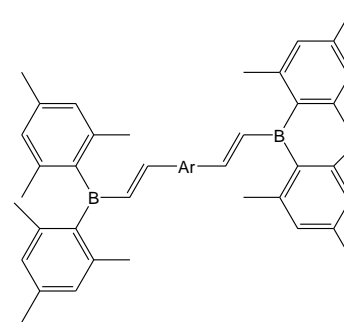
We compared the TPA cross section σ_{TPA} for compound B1 with other values reported in the literature with boron-containing molecules, see Figure 2.9. In regard to other boron-containing compounds, the TPA cross section value measured for B1 is in the range of those exhibited by a series of push-pull type compounds comprising the trivalent boron B(Mes)₂ group as electron acceptor²³, Figure 2.9 a) and 2.9 b). In those compounds the measured σ_{TPA} values ranged from 74 to 300 GM when pumped with 200 fs pulses in the 700–900 nm wavelength range.



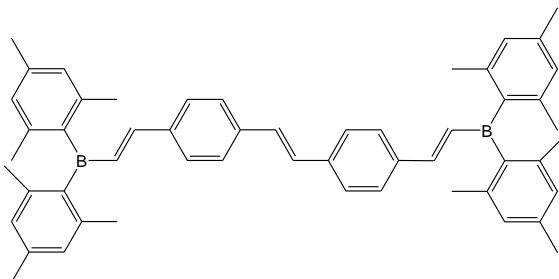
a)



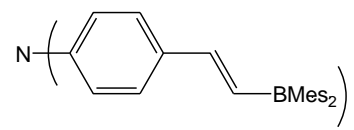
b)



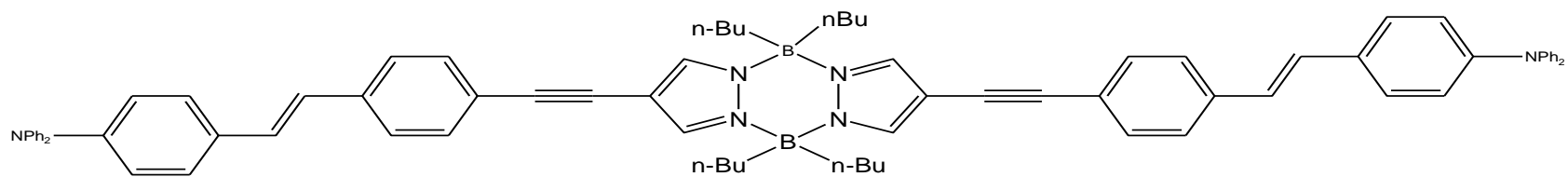
c)



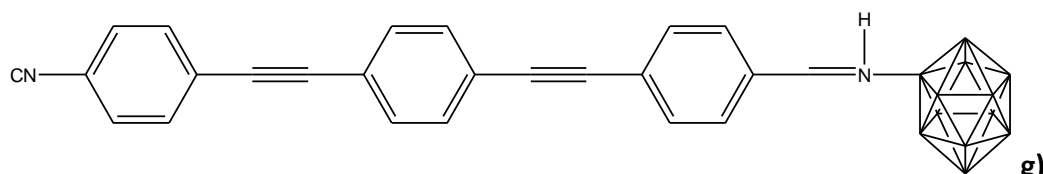
d)



e)



f)



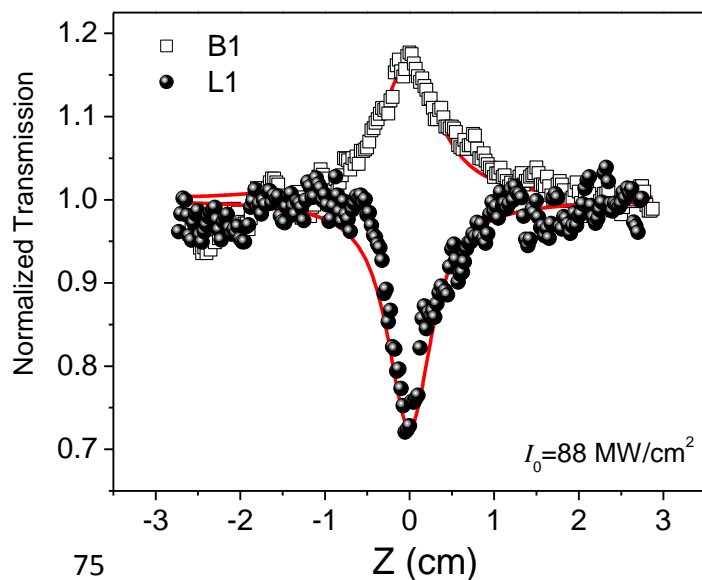
g)

Figure 2.9 Structures reported in literature of boron-containing compounds.

The values of σ_{TPA} in compounds C and D were further enhanced up to 377^{24} and $1340 GM^{25}$ by using dimesitylboryl as end-group in acceptor- π -acceptor quadrupoles, and up to approximately $1000 GM$ by using dimesitylboryl as acceptor group in octupolar compound²⁶, Fig. 2.9 e). Similar values ($1350 GM$) were observed in a $\pi - \sigma - \pi$ systems comprising a cyclodiborazane core²⁷, compound f). The TPA process has also been reported in closo-dodecaborate clusters with σ_{TPA} of $35 GM^{28}$, compound g). On the other hand, very recent theoretical studies suggest that values near to $10^4 GM$ are possible in three-branched compounds with a boron center²⁹⁻³⁰. Note that in all these cited works the σ_{TPA} values were measured through TPEF experiments about 800 nm with fs excitation; in our case, however, the two-photon transition was directly measured through NL transmission experiments since L1 and B1 are not fluorescent molecules. The use of the Z-scan technique with fs pulses allowed us to observe instantaneous two-photon transitions, i.e., other types of effects such as NLA due to excited state absorption are precluded with this very ultrashort optical excitation. To evaluate NLA effects originated by non - instantaneous two-photon transitions, the following present NLA experiments with ns excitation.

We measured the NLA of molecules L1 and B1 with ns laser excitation at the visible wavelength of 532 nm. We note that at this wavelength, the compounds show linear absorption. Figure 2.10 shows the obtained open aperture Z-scan curves using irradiance of $88 MW/cm^2$.

Figure 2.10 Normalized transmittance in open-aperture Z-scan experiments (ns excitation) for L1 (filled circles) and boronate B (open squares) at irradiance of $88 MW/cm^2$. Solutions of 100 and 25 μM were employed for L1 and B2, respectively. Continuous lines are theoretical fit to experimental data.



Following similar data fitting as in the fs excitation case, the ligand L1 exhibits a β value of $9.2 \times 10^{-8} \text{ cm/W}$ while the boronate B1 now exhibits a negative β value of $-7.8 \times 10^{-8} \text{ cm/W}$. In contrast to the simultaneous TPA that occurred in B1 under fs excitation, in the ns regime it is reasonable to assume sequential single-photon absorption to explain the NL effect²².

The observed NL transmission in Figure 2.10 for compound B1, is then explained by a five-level model involving singlet S_n ($n = 0,1,2$) and triplet T_n ($n = 1,2$) manifolds, see Figure 2.11.

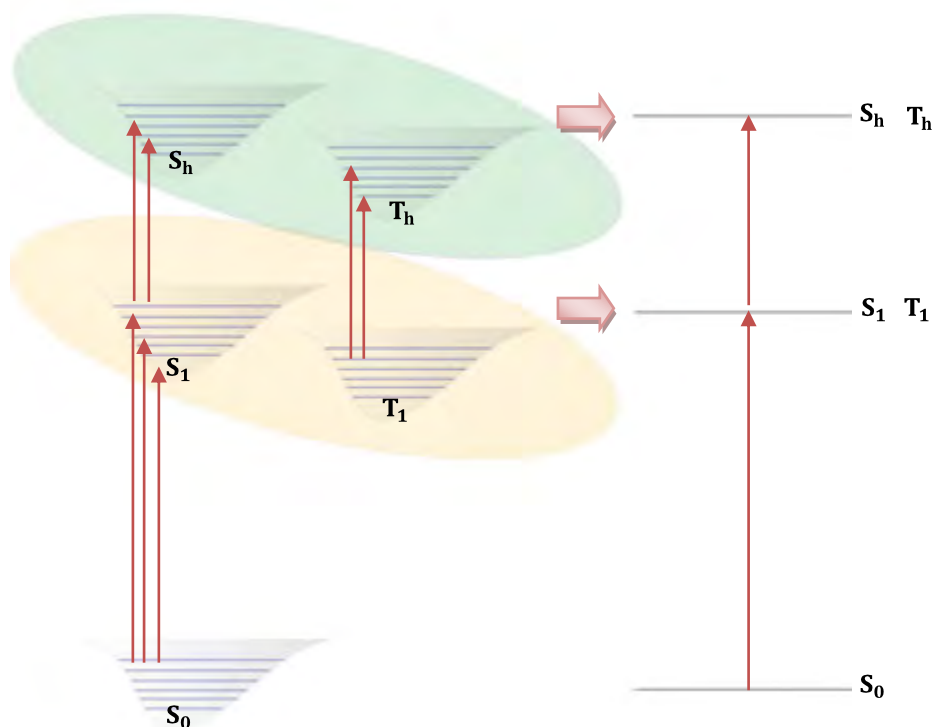


Figure 2.11 Schematic diagram of a five-level system. Absorption of an incident photon promotes an electron to the first excited singlet state. From this state, one to three things may happen: **i)** The electron can relax to the ground state by a radiative or by nonradiative transition. **ii)** The electron to undergo a spin-flip transition to a triplet state (intersystem crossing). **iii)** The molecule may absorb another photon, which promotes the electron to a higher-lying singlet state, from which it then relaxes back to the first excited singlet state.

From S_1 the electron will experience one of three possible processes as follows: **i)** relaxes to S_0 , **ii)** undergoes a spin-flip transition to T_1 and **iii)** promoted to S_h by absorbing another single photon. For an excited electron in T_1 , there are only two possibilities that it may relax to S_0 by another spin-flip transition or be promoted to T_h by absorbing another single photon. The five-level system can be simplified by a one step three photon absorption model (3PA), in which S_1 and T_1 (S_h and T_h) are combined to S_1T_1 (S_hT_h). In this model, the system simultaneously absorbs one photon, promoting an electron from S_0 to S_1T_1 . Subsequently, the electron can be excited to S_hT_h by absorbing another single photon, resulting in one-PA-induced excited states absorption (ESA). Note that this kind of multi-photon transitions were not present for the fs excitation because at 800 nm the linear absorption was too weak and because such ultra-fast excitation is much shorter than the typical lifetime of excited states in organic compounds.

It follows that L1 exhibits reverse saturable absorption (RSA) since the excited state absorption dominates over the initial absorption, as proved by computing the ratio between the excited (σ_{exc}) and ground (σ_0) state absorption cross sections, which is ($\sigma_{exc}/\sigma_0 \sim 1.9$). To perform this calculations, and owing to the fact that the population of excited states depends on the fluence F_0 rather than the intensity, it was necessary to replace βI_0 by $\alpha_0 \sigma_{exc} F_0 / 2h\nu$ in Equation 2.1. Note that for B1 the ratio becomes $\sigma_{exc}/\sigma_0 \sim 0.0013$ such that now the absorption saturates, which means that during the interval of time when excitation is present (ns interval), the ground state population is significantly depleted.

Table 2.3 summarizes the NLA results for the L1 and B1 compound, furthermore this shows the contribution of the boron atom when the N→B is presented.

Table 2.3 Linear and NL absorption of L and B compounds.

Compound	$\lambda(max)$	$\beta(cm/GW)$ fs at 800nm	σ_{TPA} [GM]	$\beta(cm/GW)$ ns at 532nm	σ_{exc}/σ_0
L1	400	To weak to be detected	-	92	1.9
B1	510	0.037	152	-78	0.0013

According to experimental observations, the boron complexes show a higher π -electronic mobility with respect to the corresponding conjugate ligands, which has been related to electronic properties conferred by the N \rightarrow B coordinative bond to aza π -backbone. Figure 2.12 shows the main resonance structures for ligands and boronates. The ligands and boronates have the neutral aromatic rings, but upon photoexcitation there is a redistribution of the π -electrons over the backbone to produce the resonance forms shown.

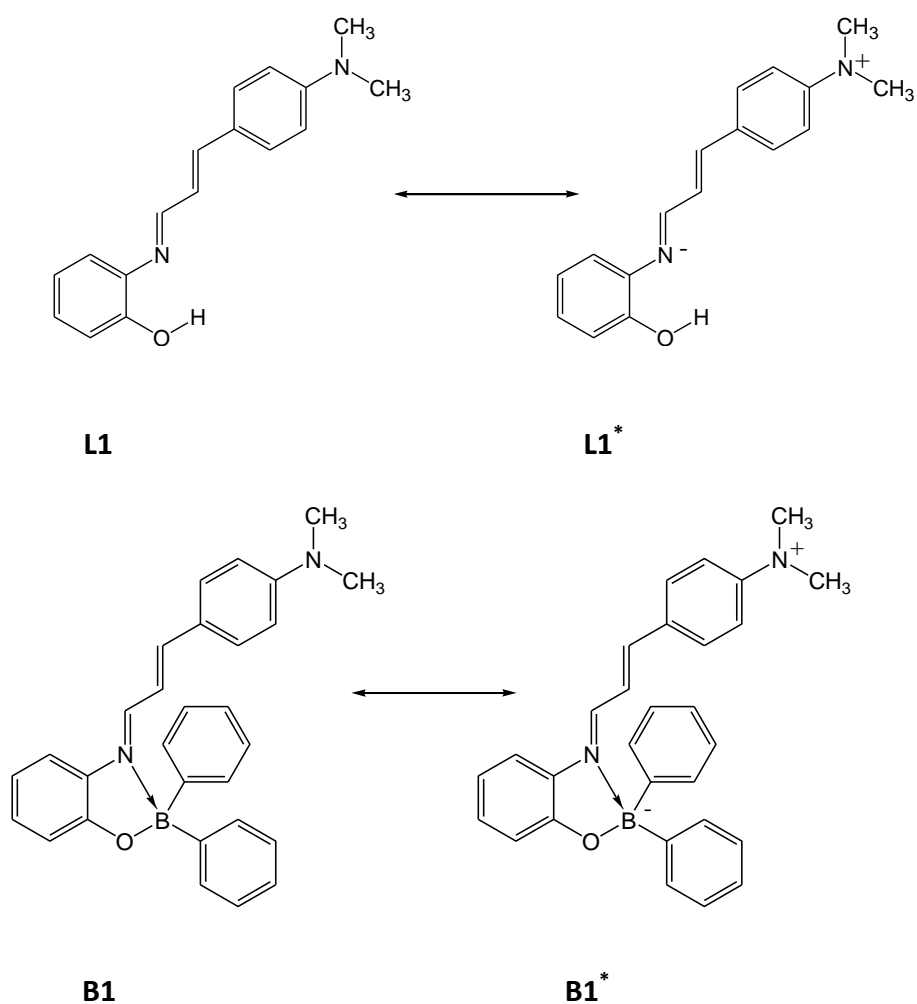
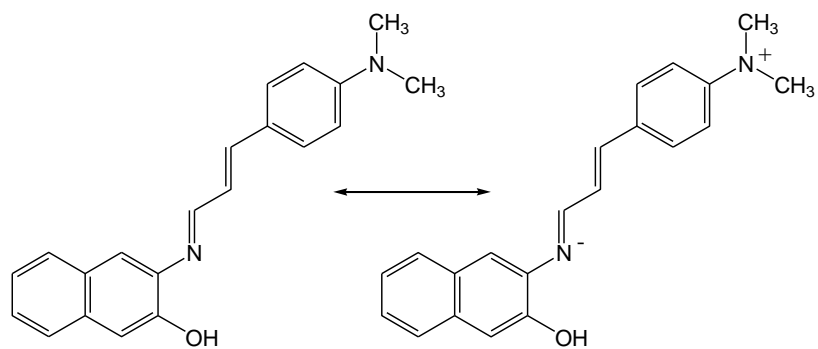
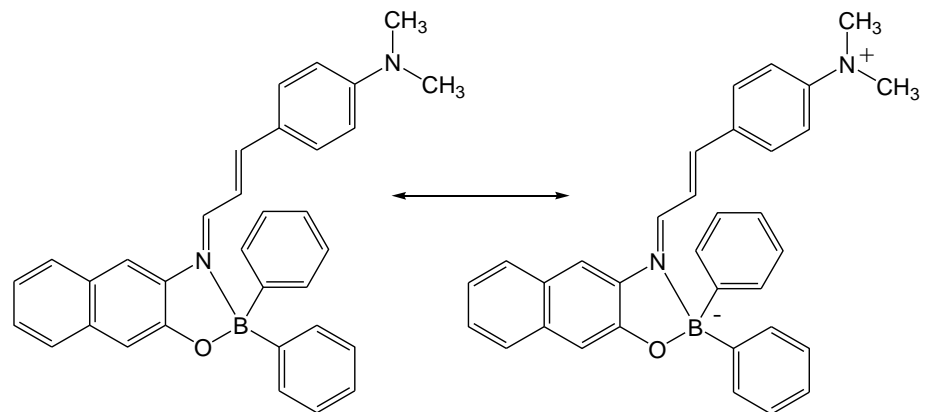


Figure 2.12 Main resonance forms for ligands and boronates.



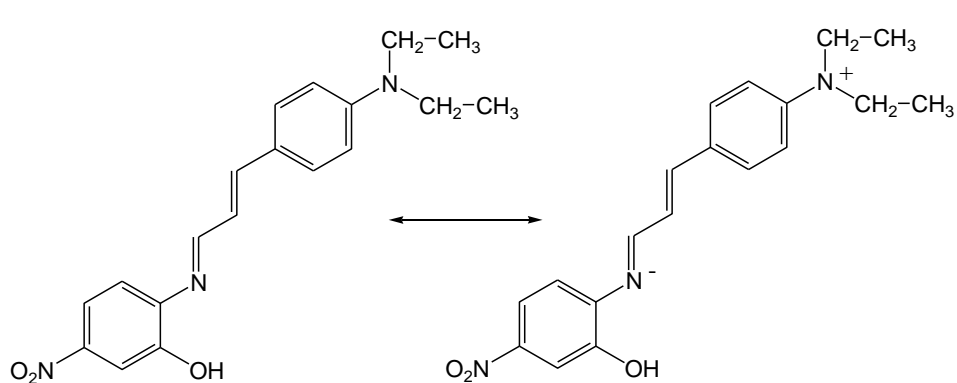
L2

L2*



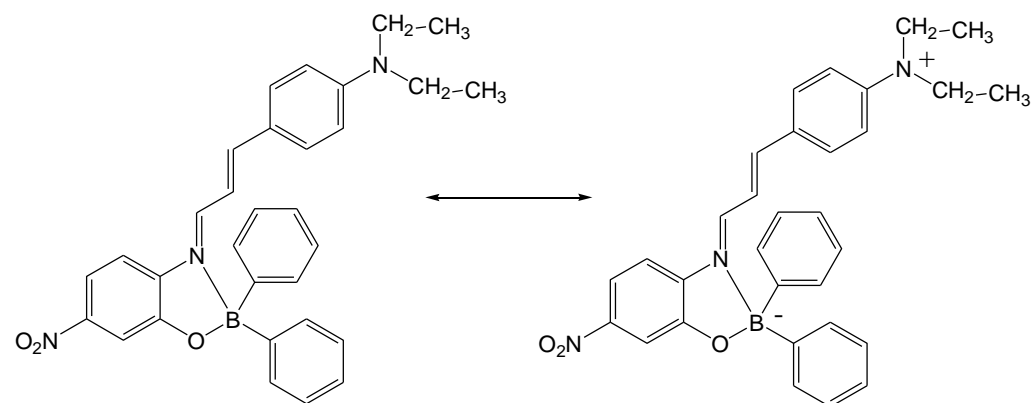
B2

B2*



L3

L3*



B3

B3*

Figure 2.12 Continued

Thus, the presence of the N→B bond favors the increase of the NL responses due to a larger contribution to the CT process in the resonance structure (borinates) and probably due to the fact that the boron atom stabilizes the negative charge more efficiently than the nitrogen in ligands, at the time that the nitrogen–boron bond changes from coordinative to a sigma bond. This behavior is consistent with previous investigations where the transition energies were calculated by ZINDO method, showing that compounds containing coordinative N→B bond has a clear reduction of the transitions energy values¹⁶⁻¹⁸.

II.3.3 EFISH measurements

The first hyperpolarizabilities as a $\mu\beta$ product for compounds L2, L3, B1, B2 and B3 compounds were evaluated experimentally by Electric Field–induced Second Harmonic (EFISH) generation technique³¹. EFISH is the standard method for the determination of molecular second–order susceptibilities. The basic idea of the method is to measure the frequency doubling efficiency of the NL optical molecule in dilute solutions; diluted solutions are used in order to reduce intermolecular effects. Because of the isotropic symmetry of a liquid, however, the macroscopic second–order susceptibility vanishes and no coherent frequency doubled light can be observed. This problem is solved by applying a static electric field which partially orients the dipolar molecules and thus breaks the symmetry of the liquid.

A static electric field E^0 partially orients the molecules due to the coupling to the dipole moment. The solution becomes noncentrosymmetric and a laser beam E^ω incident to the solution produces a second–harmonic (SH) signal. The macroscopic polarization at the SH frequency is defined by

$$P_i^{2\omega} = \epsilon_0 d_{ijk}^{(-2\omega, \omega, \omega)}(E^0) E_j^\omega E_k^\omega. \quad 2.2$$

We choose the polarization of the incoming wave and the applied electric field in the x_3 –direction. The only susceptibility component producing a SH signal is then the diagonal component along this direction, $d_{333}(E^0)$.

For weak fields $d_{333}(E^0)$ becomes proportional to the external field. If the molecular z –axis is chosen to lie parallel to the ground state dipole moment μ_g , the $P_3^{2\omega}$ is written as

$$P_3^{2\omega} = \varepsilon_0 \Gamma_L (E_3^\omega)^2 E_3^0 \quad 2.3$$

$$\text{with } \Gamma_L = \frac{d_{333} E_3^0}{E_3^0} = N f^0 (f^\omega)^2 f^{2\omega} \left(\gamma + \frac{\mu_g \beta_z}{5kT} \right), \quad 2.4$$

where N is the number of the molecules and f^0 , f^ω and $f^{2\omega}$ are local field factors evaluated at the indicated frequency. The microscopic quantities γ and β_i are given by

$$\gamma = \frac{1}{5} \gamma_{iijj} \quad 2.5$$

$$\text{and } \beta_i = \sum_j \beta_{ijj} \quad 2.6$$

The equation 2.4 means that besides β , the permanent dipole moment μ_g also has to be determined. EFISH does not allow the determination of single tensor elements but only of a combination of several components. μ_g can be obtained by measuring the dielectric constant of the substance of interest. The microscopic quantity that can actually derived from the measurements in the EFISH experiment is given by

$$\gamma' = \langle \gamma \rangle + \frac{\mu_g \beta_z}{5kT} \quad 2.7$$

where $\mu_g \beta_z$ is the scalar product of the dipole moment vector with the vector part of the hyperpolarizability tensor and $\langle \gamma \rangle$ is the scalar orientationally averaged part of the third-order hyperpolarizability tensor with components γ_{ijkl} and is given by

$$\langle \gamma \rangle = \frac{1}{5} (\gamma_{xxxx} + \gamma_{yyyy} + \gamma_{zzzz} + 2\gamma_{yyzz} + 2\gamma_{zzxx} + 2\gamma_{xxyy}) \quad 2.8$$

Because all materials have nonzero value of $\langle \gamma \rangle$, an electric field-induced contribution to γ' will be provided by the solvents and solutes in the EFISH cell as well as from the glass in the region of the dc field. Where contributions from $\mu_g \beta_z$ to the signal at 2ω are weak these contributions must be carefully accounted for.

Using THG experiments the third-order hyperpolarizability $\gamma(-2\omega, \omega, \omega, 0)$ has been shown to contribute less than 10% to γ' for strongly conjugated molecules. For instance, the orientation contribution is usually assumed to be predominant over the electronic term $\langle \gamma \rangle$ for small molecules; this could be different for large molecular systems, such as polyenes with a large conjugation length; in that case the contribution of the cubic hyperpolarizability could be significant.

The EFISH experiment is conducted by directing the beam at fundamental frequency ω through the cell in the presence of the dc field and translating the cell with respect to the beam, Figure 2.13. Filters and/or monochromators are used to reject light at the fundamental frequency from the detector. The cell is then translated with respect to the beam and the harmonic intensity is recorded as a function of position. Translation of the cell in the x direction produces a path length variation Δl . The relationship between the translation distance Δx and Δl is given by

$$\Delta l = \Delta x \tan \alpha. \quad 2.9$$

The need for the wedge geometry and measurement of signal intensity at 2ω as a function of path length is associated with phase mismatch between the fundamental and harmonic waves propagating through the medium.

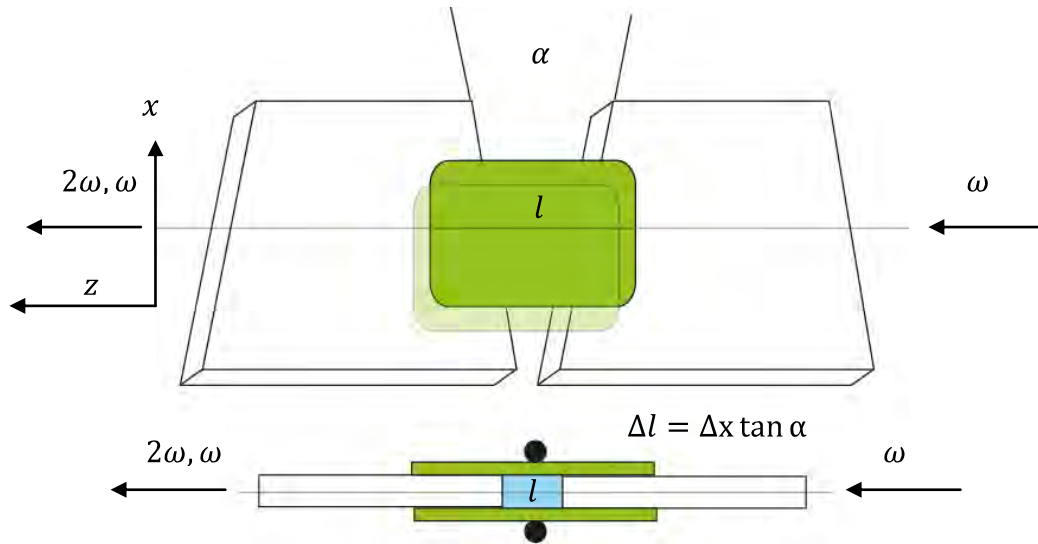


Figure 2.13 Top view (above) and edge view (below) of a cell used for EFISH measurements. The glass is about 3mm thick and about 1 cm long. The gap in which the liquid is confined is 1-2 mm, and the electrodes extend about five times the gap spacing to avoid nonuniform electric field at the glass-liquid interface. The cell is translate in the x direction with respect to the beam to produce the fringes.

Second harmonic (SH) generation is a phase-sensitive process so that the flow of energy between the fundamental and harmonic waves depends on the phase relationships between the waves. As the harmonic field propagates through the sample, overlapping the fundamental wave, energy will flow back and forth between these waves, depending on their phase relationships, until the NL interaction is terminated. On either side of the interface a free and reflected harmonic wave is created whose amplitude depends on the optical constants and other boundary conditions at the interface.

This process can be seen more clearly by considering the representation of the electric part of an electromagnetic wave

$$E(z, t) = \frac{1}{2} (E^0 e^{(i\omega t - \phi(z))} + c.c.) \quad 2.10$$

E^0 is the amplitude of the field and the time and positional oscillatory behavior are described by the first and second terms in the exponent, respectively. The propagation of

the NL polarization $P^{2\omega}$, which is proportional to E_{ω}^2 , is governed by the refractive index at ω , while that for the SH wave $E_{2\omega}$ is governed by that at 2ω . This generates a phase angle difference between the two waves given by

$$\Delta\phi = \frac{2\pi l}{\lambda} \Delta n \quad 2.11$$

where λ is the wavelength corresponding to frequency ω . The characteristic distance or coherence length l_c over which the waves will dephase is given by $l\Delta n$. The intensity distribution between the fundamental, free, and reflected waves is determined solely by the phase relationships between the waves during the last coherence length where the interaction is terminated by an interface as determined by the boundary conditions at the interface. The term free wave is used to describe the electric field component propagating at the harmonic frequency with wave vector $k_{2\omega}$. In the absence of optical absorption the harmonic intensity $I(2\omega)$ is given by

$$I(2\omega) = 2I_m \sin^2 \frac{\Delta\phi}{2} \quad 2.12$$

The quantity I_m is related to the optical properties of the interface and NL polarization in the media on either side of the interface. If the contribution from glass is small compared to the liquid of interest and $\gamma \ll \mu_g \beta_z / 5kT$ then $I_m \propto (\mu_g \beta_z)^2$. The $\mu\beta$ value of the investigated chromophore can then be inferred from the amplitude and period of the resulting so-called "Maker Fringes".

The EFISH measurements were performed at $\lambda = 1.907 \mu m$ as fundamental wavelength. The laser excitation at $1.907 \mu m$ was provided by a 1 m-long hydrogen Raman cell of high-pressure (50 bars) pump by a Q switched $Nd^{3+}:YAG$ laser. NL optical experiments were performed with dichloromethane (DCM) solutions at concentrations of 5 and 10×10^{-3} M. For EFISH measurements the $\mu\beta$ value could be inferred from the amplitude and period of

the Maker fringes which were obtained through harmonic intensity variation as a function of cell translation.

As an example of typical curves for EFISH measurements, Figure 2.14 presents the traces for L3 and B3 compounds and as reference the signal produced by used solvent (DCM) is also presented. There is an increase in the SH intensity after boron complexation. Furthermore, the presence of boron atom in the conjugated structure significantly influences the π -electron behavior that has an important manifestations in the NL optical response, see Table 2.4.

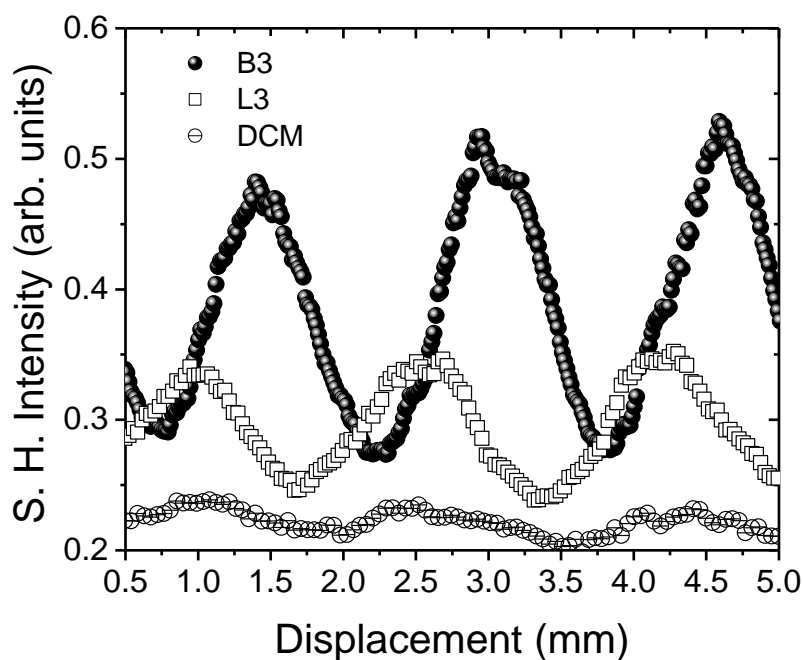


Figure 2.14 Example of an EFISH measurement for B3, L3 and DCM at 1.907 μm .

We can infer of this behavior that organoboron compounds offer the prospect of the tailorability of metal–organic ligand interactions.

Table 2.4 shows the results of EFISH measurements for the set of compounds. In general, all the compounds have conjugate electronic π -systems with different push-pull character such that their NL optical response are expected from moderate to high.

Table 2.4 First Hyperpolarizabilities deduced from EFISH measurements at 1.907 μm .

Compound	$\lambda(\text{max})$	$\mu\beta \times 10^{-46} \text{ esu}$ (SHG _{signal} 953nm)
L1	400	-
L2	421	2.6
L3	471	8.9
B1	510	7.3
B2	529	5.2
B3	566	26.1

On imine L3, efficient “push-pull” architecture is present and for borinate B3 a N→B coordinative bond is added to π -system. However, in L2 compound a less efficient architecture is observed and for its boron complex → B2 an improvement of the donor–acceptor electronic features is expected with the formation of N→B bond.

L3 have NL optical properties larger than that L2 compound due to more efficient “push-pull” architecture. The important second NL optical responses shown by the ligands are generated mainly by the conjugate electronic π -system. As clearly is noticed in Table 2.4, Four-coordinate Organoboron compounds (B1–B3) give relatively large $\mu\beta$ values respect to their corresponding ligands. An increase factor of 3 times on the first hyperpolarizability is observed from ligand L3 to boronate B3. This enhance is clearly promoted for the formation of N→B coordinate bond which produces a high delocalization of π -electrons, confirmed by redshifted in absorption spectra from ligand to borinates, see Figure 2.7.

The NL response of the B2 compound was not as efficient as L3, B1 and B3 compounds. On the other hand, this is slightly higher than the L2 compound. Although the boron atom can act as an acceptor (especially where the conjugated systems present weak push–pull characteristics) the strength of this does not compare with the strength of the NO₂ group; see the L3 and B2 NL optical results. On the other hand, we can compare the B1 and B2 NL

optical responses. The B1 response was higher than the B2 compound, which leads us to think that the phenyl group works more efficiently than the naphthyl group.

The $\mu\beta$ value obtained for the more efficient π -system in this work, B3 with N(Et)₂ donor group, is equal to $26.1 \times 10^{-46} \text{ esu}$, which is higher than previous reported for borinate that have a NMe₂ group as a donor group ($15.6 \times 10^{-46} \text{ esu}$)¹⁸. Compound B3 have the highest optical respond of the boron complexes reported for our group in recent studies (Table 2.5). Comparing the SH value of B3 with other Four-coordinate boron complexes and zwitterionic species reported, this new borinate have an excellent value³¹.

Table 2.5 Comparison of SH response in B3 respect to other boron complexes reported in our group.

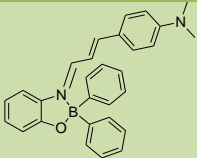
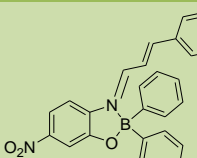
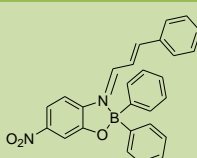
	Boron compounds		
			
$\mu\beta$ (10^{-46} esu)	7.3 Ref. 18	15.62 Ref. 17	26.1 (this work)

Table 2.5 shows the evolution of structural design that has been followed in our group respect to the Four-coordinate Organoboron compounds. B3 compound shows the higher NL response compare with other, the diethylamine group (donor group) works more efficiently than the diethylamine group. Furthermore, the NO₂ improves the π -electron delocalization in these structures. In general, the N→B coordinative bond present in an efficient π -system, i.e., in which a NO₂ and diethylamine group are presented too, result in a great redistribution of the π -electron over the backbone, thus increasing the NL response.

II.3.4 THG measurements

By available material, we conducted cubic NL optical measurements only in L1 and B2 compounds. The cubic NL responses $\chi^{(3)}(-3\omega; \omega, \omega, \omega)$ for L1 and B1 compounds were estimated through the use of THG technique. Details of the experiments and procedure were explained in the Chapter I in the section 1. G. 2 of this dissertation. We carried out THG measurements at the IR wavelength of 1550 nm. The THG measurements were performed on thin polymer (polystyrene: PS) films deposited on glass substrate doped with the ligands and boronates at a loading level of 30 wt.% (weight percent). Film thickness was controlled with the rotation speed of our spin-coater and with the viscosity of solutions, so that thicknesses were 120 and 125 nm for L1 and B1 compounds, respectively. In any case, the films had excellent optical quality showing negligible light scattering at visible and NIR wavelengths. Typical pump irradiances at sample position was 0.5 GW/cm^2 . With these conditions, the third-order NL susceptibility $\chi^{(3)}(-3\omega; \omega, \omega, \omega)$ resulted to be 4.4×10^{-12} esu and 7.5×10^{-12} esu for L1 and B1, respectively.

The macroscopic NL susceptibility $\chi^{(3)}$ was used to calculate the second hyperpolarizability γ , which is the molecular parameter of interest, through $\gamma = \chi^{(3)}/L^4 N_s$ where N_s is the density of molecules in the polymer films, $L = (n^2 + 2)/3$ is the correction factor due to local field effects and n is the refractive index. Assuming for the films the refractive index and density of polystyrene, and using a molecular doping level of 30%, the γ values for the boronate and its ligand resulted to be 4060×10^{-36} and 1440×10^{-36} esu, respectively. Then we have that the boronate exhibits an enhanced NL response of about a factor of three with respect to its ligand

Note that the study of third-order nonlinearities in boron compounds through THG spectroscopy at infrared wavelengths has not been extensively reported. For example, in a study on the structure-property in π -conjugated asymmetric and symmetric dimesitylboranes, performed by using THG at 1907 nm, maximum second

hyperpolarizability resulted about 229×10^{-36} esu [6,32-34]. The order of magnitude here reported for γ in the boron compound B1 is certainly much larger than those reported for dimesitylboranes, but it must be considered that in the former case resonant NL response plays an important role as the measurements were performed at 1550 nm, i.e., the γ value is enhanced by a three-photon resonance since the THG wavelength (517 nm) almost coincides with the peak of linear absorption band of the molecule. In the case of dimesitylboranes, however, the γ values at 1907nm are out of resonance.

In summary, the formation of the N→B coordinative bond increases the nonlinearities in hetero-aromatic π -conjugate systems. In particular, under ultra-fast (fs) excitation at 800 nm the NL process of TPA was increased in the boronate 2 with respect to its ligand 1, i.e., the boronate exhibited two-photon absorption characterized by a cross section of 152GM, while such effect was practically absent for the ligand. These results suggest that the N→B bond allows more effective delocalization of the π -system and that the boron atom stabilizes the negative charge more efficiently than the nitrogen in the ligand. At the second-order level, the observation of an enhancement in the range of 2–3 times of the NL optical response between the series suggests that the N→B bond allows more effective delocalization of the π -system; the $\mu\beta$ values were in the order of 10^{-46} esu . On the other hand, through THG spectroscopy the resonant second hyperpolarizability γ for the boronate resulted in the order of 10^{-33} esu, this under ns excitation at the telecommunications wavelength of 1550 nm.

Further work is in progress in order to incorporate the N→B coordinative bond to more efficient organic systems in order to improve their nonlinear response.

II.4 References

1. N. J. Long, *Angew. Chem. Int. Ed. Engl.* **34**, (1995) 21
2. S. K. Hurst, M. G. Humphrey, T. Isoshima, K. Wostyn, I. Asselberghs, K. Clays, A. Persoons, M. Samoc, and B. Luther-Davies, *Organometallics* **21**, (2002) 2024.
3. C. E. Powell, J. P. Morrall, S.A. Ward, M. P. Cifuentes, E. G. A. Notaras, M. Samoc, and M. G. Humphrey, *J. Am. Chem. Soc.*, **126**, (2004) 12234.
4. T. Weyland, I. Ledoux, S. Brasselet, J. Zyss, C. Lapinte, *Organometallics* **19**, (2000) 5235.
5. C. D. Entwistle and T. B. Marder, *Angew. Chem. Int. Ed.*, **41**, (2002) 2927.
6. Z. Yuan, N. J. Taylor, R. Ramachandran and T. B. Marder, *Appl. Organometallic Chem.* **10**, (1996) 305.
7. M. J. G. Lesley, A. Woodward, N. J. Taylor, T. B. Marder, I. Cazenobe, I. Ledoux, J. Zyss, A. Thornton, D. W. Bruce, and A. K. Kakkar, *Chem. Mater.* **10**, (1998) 1355.
8. M. Lequan, R. M. Lequan, K. C. Ching, *J. Mater. Chem.* **1**, (1991) 997.
9. W. Kaim, A. Schulz, *Angew. Chem.* **96**, (1984) 611.
10. C. D. Entwistle and T. B. Marder, *Angew. Chem. Int. Ed.* **41**, (2002) 2927.
11. C. Lambert, s. Stadler, G. Bourhill, C. Bräuchle, *Angew. Chem.* **108** (1996) 710.
12. Ying-Li Rao and Suning Wang, *Inorganic Chemistry*, in press.
13. A. P. Kulkarni, C. J. Tonzola, A. Babel, S. A. Jenekhe, *Chem. Mater.* **16** (2004) 4556.
14. J. L. Maldonado, G. Ramos-Ortíz, O. Barbosa-García, M. A. Meneses-Nava, L. Márquez and M. Olmos-López, *Int. J. of Mod. Phy. B* **21**, (2007) 2625.
15. Mario Rodríguez, Gabriel Ramos-Ortíz, Martha I. Alcalá-Salas, José Luis Maldonado, Karla A. López-Varela, Yliana López, Oscar Domínguez, Marco A. Meneses-Nava, Oracio Barbosa-García, Rosa Santillan, Norberto Farfán, *Dyes and Pigments* **87** (2010) 76.
16. B. M. Muñoz, R. Santillan, M. Rodríguez, J. M. Méndez, M. Romero, N. farfán, P. G. Lacroix, K. Nakatani, G. Ramos-Ortiz, J. L. Maldonado, *J. Organomet. Chem.*, **693**, (2008) 1321.
17. M. Rodríguez, J. L. Maldonado, G. Ramos-Ortiz, J. F. Lamère, P. G. Lacroix, N. Farfán, M. E. Ochoa, R. Santillan, M. A. Meneses-Nava, O. Barbosa-García and K. Nakatani, *New J. Chem.*, **33** (2009) 1693.
18. M. Rodríguez, R. Castro-Beltrán, G. Ramos-Ortiz, J. L. Maldonado, N. Farfán, O. Domínguez, J. Rodríguez, R. Santillan, M. A. Meneses-Nava, O. Barbosa-García, J. Peón, *Synthetic Metals*, **159** (2009) 1281.
19. S. R. Marder, C. B. Gorman, F. Meyers, J. W. Perry, G. Bourhill, J. L. Brédas and B. M. Pierce, *Science* **265**, (1994) 632.
20. F. Meyers, S. R. Marder, B. M. Pierce and J. L. Brédas, *J. Am. Chem. Soc.*, **116** (1994) 10703.
21. Ch. Bosshard, K. Sutter, Ph. Pretre, J. Hulliger, M. Flörsheimer, P. Kaatz and P. Günter, *Organic Nonlinear Optical Materials*, Gordon and Breach Science Publishers SA.
22. M.G. Kuzyk, C.W. Dirk (Eds.), *Characterization Techniques and Tabulations for Organic Nonlinear Materials*, Marcel Dekker, Inc., 1998.
23. Z.-Q. Liu, Q. Fang, D. Wang, D.-X. Cao, G. Xue, W. -To Yu, H. Lei, *Chem. Eur. J.* **9** (2003) 5074.
24. M. Charlot, L. Porrès, C.D. Entwistle, A. Beeby, T.B. Marder, M. Blanchard-Desce, *Phys. Chem. Chem. Phys.* **7** (2005) 600.
25. Z.-Q. Liu, Q. Fang, D.-X. Cao, D. Wang, G.-B. Xu, *Org. Lett.* **6** (2004) 2933.

26. J.C. Collings, S.-Y. Poon, C.L. Droumaguet, M. Charlot, C. Katan, L.-O. Pålsson, A. Beeby, J.A. Mosely, H.M. Kaiser, D. Kaufmann, W.-Y. Wong, M. Blanchard-Desce, T.B. Marder, *Chem. Eur. J.* **15** (2009) 198.
27. A. Hayek, J. Francois Nicoud, F. Bolze, C. Bourgogne, P.L. Baldeck, *Angew. Chem. Int. Ed.* **45** (2006) 6466.
28. R. Bernard, D. Cornu, P.L. Baldeck, J. Čáslavský, J.-M. Létoffé, J.-P. Scharff, P. Miele, *Dalton Trans.* (2005) 3065.
29. L. Zhao, G. Yang, Z. Su, L. Yan, *J. Mol. Struct. Theochem.* **855** (2008) 69.
30. X.-B. Zhang, J.-K. Feng, A.-M. Ren, X.-J. Zhao, C.-C. Sun, *J. Mol. Struct. Theochem.* **764** (2006) 69.
31. J.-L. Oudar, *J. Chem. Phys.* **67** (1977) 446.
32. Z. Yuan, C.D. Entwistle, J.C. Collings, D. Albesa-Jové, A.S. Batsanov, J.A.K. Howard, N.J. Taylor, H.M. Kaiser, D.E. Kaufmann, S.-Y. Poon, W.-Y. Wong, C. Jardin, S. Fathallah, A. Boucekkine, J.-F. Halet, T.B. Marder, *Chem. Eur. J.* **12** (2006) 2758.
33. C.D. Entwistle, T.B. Marder, *Chem. Mater.* **16** (2004) 4574.
34. Z. Yuan, J.C. Collings, N.J. Taylor, T.B. Marder, C. Jardin, J.-F. Halet, *J. Solid State Chem.* **154** (2000) 5.

CHAPTER III

TELLURITE GLASSES AS NL OPTICAL MATERIALS

Other of the interests of the group is the study of the NL optical properties of inorganic materials in view of possible photonic applications, i. e., as power stabilizers, all-optical switches, and so forth. For instance, we have carried out studies on sol–gel materials. The sol–gel process is a method for preparing glasses at room temperature, which an organic dye can be doped within an inorganic glass. Recently our interest has focused on trying to apply the individual characteristics of organic and inorganic compounds in a unique device that involves both, i.e., hybrid materials. Hybrid materials (organic–inorganic) have extraordinary opportunities to be applied as luminescent solar concentrators, sensors for environmental and biological impurities, lasers tunable in the visible spectrum, active waveguides and materials for NL optics based on nanosized particles in glass bulks and glass films, etc.

A very important step in the characterization of these hybrid materials, and their great possibilities to be applied as optoelectronic and photonic devices, is through the individual study of their components, i.e., the separate study of the NL optical properties of organic compounds and glasses.

The follow study aims to provide that glasses have extraordinary possibilities as NL optical materials. We carried out studies of third–order NL optical responses and photoluminescence behavior in a particular chalcogenide glass. Although this Chapter is focuses only in the NL optical study of a set of photonic glasses, there is an enormous interest in applying them as part of an optoelectronic device, and in addition, as an integral part of something where the benefits are involved the benefits of a hybrid material.

III.1 Background

With the increasing interest in photonic devices, the appeal for employing optical glasses has grown, because such materials may be chemically and mechanically stable, being ideal for advantageous substituting crystalline systems in many situations^{1,2}. The suitability of a given material for photonic applications is mainly determined by its linear and NL optical properties and therefore it is very important to characterize its optical parameters. A good starting point is the choice of glasses with constituents that present high polarizabilities, implying that the resulting linear refractive index, n_0 , is high. Based on Miller's rule³, which relates the linear and the third-order susceptibilities, we may conclude that the NL refractive index, n_2 , is also high, allowing these materials to be used in light-controlled-by-light devices^{1,2}.

Heavy-metal oxide glasses (HMO) were considered as candidate materials for optical devices by many authors^{1,2,5-7}. Also chalcogenide (ChGs) glasses have shown to be very promising for NL optical applications, because they incorporate elements such as S, Se, and Te that have high polarizabilities. Here, ChGs glasses are an important class of amorphous semiconductors used in phase-change memories, solar cells, sensors and photonics. ChGs contain as a major constituent one or more of the chalcogen elements from group 6a of the periodic table (sulphur, selenium and tellurium), covalently bonded to network formers such as As, Ge, Sb, Ga, Si, P, Zn and Mg. The existence of a broad range of possible glass-forming system with large composition space and good resistance to crystallization yields glasses with optical properties such as nonlinearity, photosensitivity and IR transparency, which can all be optimized for photonic applications. ChGs are comprised of covalently bonded heavy elements, and this gives them some unique properties for IR, NL and waveguide optics. Due to their inter-atomic bonds are weak relative to those in oxides, the bandgap of ChGs is redshifted to the visible or near-IR region of the spectrum. The vibrational energies of the bonds are low because the constituent atoms are particularly heavy. This means that ChGs are transparent into the

mid-IR and, as a consequence, their low phonon energies make them interesting hosts for rare-earth dopants⁸. Typically, ChGs transmit to $\sim 11 \mu\text{m}$ - $\sim 20 \mu\text{m}$. However, physical attributes such as the glass transitions temperature (T_g), glass hardness, strength and durability generally deteriorate with weaker bonding and therefore decrease with long-wave transparency. A low value of T_g means that precision glass moulding becomes a viable approach for fabrication low-cost optical components for applications such as thermal imaging⁹. Glass densities are also high relative to oxide glasses and, when combined with strong polarizability, this leads to high refractive index of $n \sim 2 - 3$. This is reflected in a high NLR index and it has been confirmed by measurements¹⁰⁻¹¹ that reveals ultrafast third-order (Kerr) nonlinearities up to a thousand times of silica, making ChGs attractive for all-optical signal processing¹².

Among the ChGs glass families, tellurite glass is considered as a kind of NL optical glasses in many potential applications. The good characteristics such as third-order NL optical performance, optical bi-stability and up-conversion property of tellurite glasses were reported¹³⁻¹⁶ more often in these years, i.e., such as laser devices, broadband amplifiers, up-conversion emission and photonic crystal fibers¹⁷⁻²². For these photonic applications, tellurite glasses offer advantages over both semiconductors and organic materials because of their good transmission in the visible and IR regions, fast response times, good mechanical properties as well as affordability and processability. Moreover, when compared with other glass families, tellurites offer relatively low phonon energies and are mostly less toxic and more chemically and thermally stable²⁰⁻²⁸. In the development of tellurite glasses for optical signal processing and all-optical switching applications it is necessary to combine large NLR indices with desirable thermo-mechanical properties. Since the optical and thermo-mechanical characteristics depend on the glass composition, it is of great interest to know the correlation of the different glass formers as well as various possible network modifiers on these characteristics. Recently, a lot of work on composition and material properties has been reported for different glass families. For instance, the incorporation of alkali metals as network modifiers has been studied in order to improve the thermo-mechanical properties as well as the optical properties²⁶⁻³³. In

regard to tellurite glasses, we recently reported the effect of alkali metal oxides R_2O ($R = \text{Li, Na, K, Rb and Cs}$) and network intermediate MO ($M = \text{Zn, Mg, Ba and Pb}$) on the thermo–mechanical and chemical properties³⁴. In this study, the experimental results showed that alkali metals with small ionic radii decrease the thermal expansion coefficient, the glass transition temperature (T_g) and the chemical durability. As for the optical properties, the results showed that small ionic radii also favor the increase of the linear refractive index n while THG experiments demonstrated also an increase in the NL third–order susceptibilities of the type $\chi^{(3)}(-3\omega; \omega, \omega, \omega)$ for fundamental wavelength at 1550 nm. THG experiment not provide the value of n_2 , being the latter parameter of paramount interest for all–optical switching applications. Motivated by this fact, in this work we present direct measurements of n_2 for a series of TeO_2 glasses composed using various network modifiers and intermediates, in order to associate their NL optical responses with their glass composition.

To explore the effect of alkali metals and network intermediates on the NL refractive index of tellurite glasses, compositions such as $\text{TeO}_2\text{-MO-R}_2\text{O}$ were studied. For this purpose, four TeO_2 -based glasses were prepared in a way that they had the same molar concentration of TeO_2 . The magnitude of the NLR index was determined using the standard Z-scan technique. Additionally, the TM Z-scan technique was also employed in order to identify possible contributions to n_2 from thermo–optical effects. Note that the use of different network modifiers and intermediates in tellurite glasses introduces changes in the coefficient of thermal expansion which can influence the overall NL response. Therefore, we applied TM Z-scan technique that enables to discriminate between nonlinearities of pure electronic origin and nonlinearities due to accumulative thermal effects. This information is important since only NL electronic processes can provide fast material response, which is of interest for photonic application including optical processing of information.

Finally, to obtain more information about the electronic structure in tellurite glasses, the effect of modifiers and intermediates on the formation of localized states was also studied through photoluminescence and pump–probe experiments.

III.2 Experimental results and discussions

III.2.1 NL optical materials

The glasses studied here with composition (mol%) $70\text{TeO}_2\text{-}20\text{MO-}10\text{R}_2\text{O}$ were prepared by the Advanced Materials and Nanophotonics group at the Centro de Investigaciones en Óptica (CIO). Details of the NL materials and their preparation are reported recently, see Ref. [35].

The network intermediates are $M = \text{Zinc (Zn)}$ or Magnesium (Mg) and the network modifiers are $R = \text{Lithium (Li)}$, Sodium (Na) and Potassium (K) . For characterization the samples were cut and polished to obtain $\sim 1\text{mm}$ thick slabs. Special care was taken to polish the samples in order to reduce errors in the NL optical characterization due to glass imperfections. The glass compositions and code used in this work for each sample are summarized in Table 3.1. This table also shows the linear refractive index at 800 nm obtained from calculated dispersion curves that resulted from direct measurements of the refractive index at 633, 830 and 1550 nm through the use of the prism coupler technique¹⁸.

Table 3.1 Code, glass composition (mol%) and refractive index for the tellurite glasses used in this study.

Glass	TeO ₂	ZnO	MgO	K ₂ O	Na ₂ O	Li ₂ O	n (800 nm)
TeZnK	70	20	–	10	–	–	1.887
TeZnNa	70	20	–	–	10	–	1.918
TeZnLi	70	20	–	–	–	10	1.956
TeMgLi	70	–	20	–	–	10	1.919

III.2.2 Absorption and optical bandgap

To estimate the optical band gap of the samples, linear absorption measurements have been performed. The absorption spectra were measured from 300 to 3000 nm using a spectrophotometer (Lambda 900, Perkin-Elmer) and are shown in Figure 3.1.

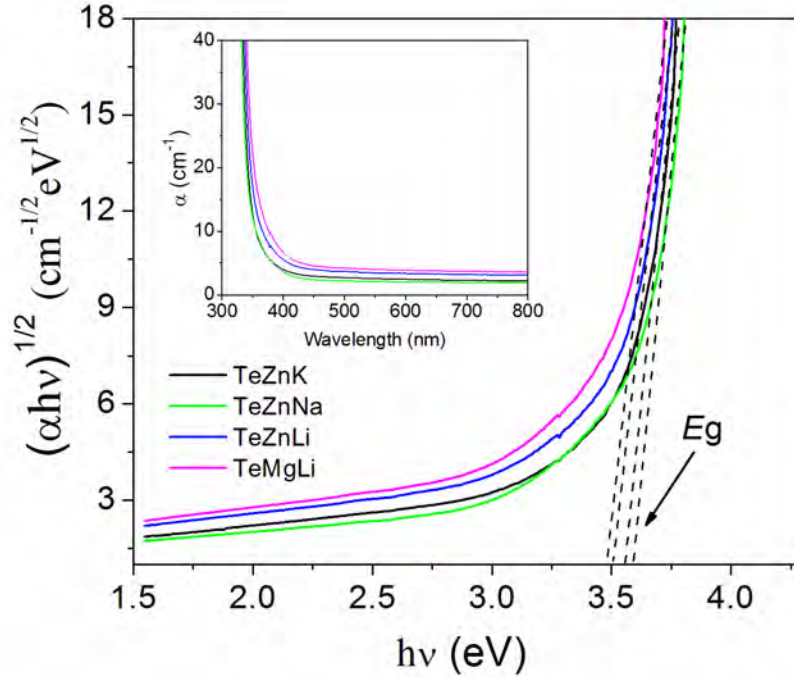


Figure 3.1 Dependence of $(\alpha \cdot hv)^{1/2}$ on the photon energy for tellurite glasses. Inset: absorption spectra of the tellurite glasses.

The tellurite glasses were optically transparent in the range of wavelengths from 450 nm (2.75 eV) to 2500 nm (0.49 eV) while a weak tail of linear absorption was present at 400 nm (3.10 eV). The optical band gap energy E_g for each sample was obtained from its absorption spectrum following the Tauc approach³⁶. By plotting $(\alpha \cdot hv)^{1/2}$ as a function of photon energy hv (α is the absorption coefficient in cm^{-1}) and extrapolating the linear regions of this function to zero absorption, optical bandgap values of 3.55eV, 3.59eV, 3.50eV and 3.48eV were obtained for TeZnK, TeZnNa, TeZnLi and TeMgLi, respectively. These values are larger than those reported in the literature for pure TeO_2 glasses which

are in the range 3.15–3.37 eV³⁷⁻³⁸, this means that the inclusion of modifiers and network intermediates shifts the band gap to higher energies. Our samples also show larger E_g than in tellurite glasses that use Bi as network intermediate, i.e., TeO₂ - Bi₂O₃-ZnO³⁹ but are smaller than those reported for rare earth doped tellurite glasses³⁷.

III.2.3 Nonlinear optical properties

The NL optical characterization of the set of glasses was conducted through Z–scan and TM Z–scan experiments. Details of the both techniques were reported in Chapter I in the section 1.2.1.

In Figure 3.2a examples of Z–scan traces for TeZnNa and TeZnK glasses are shown. The samples exhibited a self-focusing effect. Here a peak preceded by a valley in the normalized transmittance clearly indicates that glasses have a positive NL refractive index. These traces were obtained with a train of fs pulses at high repetition rate from the Ti:sapphire oscillator with a peak intensity of 9.0 GW/cm² at the sample position. Figure 3.2b shows the temporal evolution of the TM Z–scan signals at the positions of minimum (valley) and maximum (peak) transmittance for these two glasses. The signals exhibit negligible time evolution. The changes in normalized transmittance between peak and valley directly after excitation have been obtained by extrapolating the evolution curves to the time $t = 0$ and the corresponding electronic values of n_2 have been found to be 1.31 and 2.33 ($\times 10^{-15}$ cm²/W) for TeZnK and TeZnNa, respectively. The signals exhibit negligible time evolution. The changes in normalized transmittance between peak and valley directly after excitation have been obtained by extrapolating the evolution curves to the time $t = 0$ and the corresponding electronic values of n_2 have been found to be 1.31 and 2.33 ($\times 10^{-15}$ cm²/W) for TeZnK and TeZnNa, respectively.

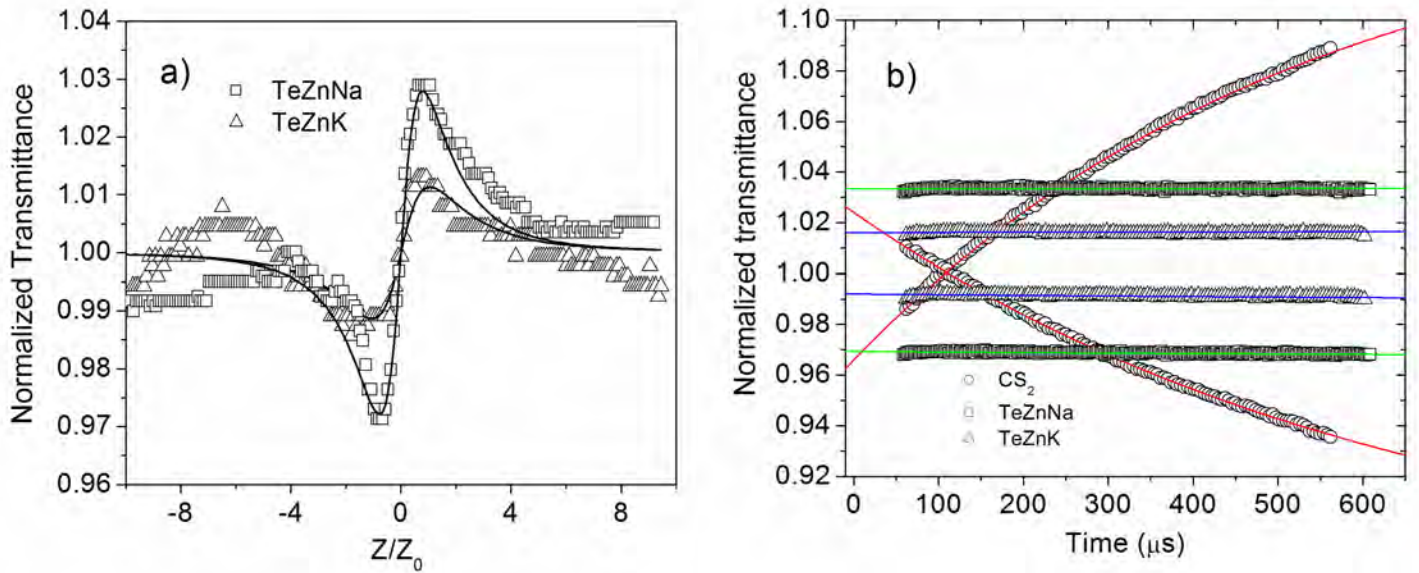


Figure 3.2 a) Normalized transmittance of standard Z-scan measurements for TeZnNa and TeZnK. The continuous lines are fittings to the experimental data. b) thermally managed Z-scan signals at valleys and peaks of traces shown in a). The traces of CS_2 are included as reference.

Figure 3.2b also shows the signal obtained from the standard reference CS_2 . In this case, the crossing of the two TM Z-scan curves reveals the presence of both self-focusing (electronic) and self-defocusing (thermal) effects that compete during the time that the sample is exposed to the train of fs pulses. It is evident that in CS_2 the electronic NL response dominates at early times, but the thermal nonlinearity dominates over the electronic response of the material after $\sim 100 \mu\text{s}$ as shown by the crossing of the TM Z-scan curves at such time. By extrapolating the evolution curves of CS_2 the electronic value of n_2 resulted to be $2.11 \times 10^{-15} \text{ cm}^2/\text{W}$, this is in good agreement with values previously reported for this material⁴⁰ and, thus, validates the calibration of our experimental apparatus. Following this procedure, the n_2 values for glasses TeZnLi and TeMgLi were found to be 2.37 and 2.81 ($\times 10^{-15} \text{ cm}^2/\text{W}$), respectively. For these glasses also no temporal evolution of the TM Z-scan signal was observed. The absence of a temporal evolution in the TM Z-scan signals from the tellurite glasses studied in this work clearly

shows that their third-order optical nonlinearity originated from pure electronic polarization.

Table 3.2 summarizes the NL refractive indices determined for our tellurite glasses as well as the real part of the third-order nonlinear susceptibility $\chi^{(3)}(-\omega; \omega, \omega, \omega)$. Both quantities are related through $n_2 = 3\chi^{(3)}/4\epsilon_0 n^2 c$ where n is the linear refractive index.

Table 3.2 Values of n_2 and third-order nonlinear susceptibility $\chi^{(3)}(-\omega; \omega, -\omega, \omega)$ measured through thermally-managed Z-scan technique.

Sample	n_2 [$10^{-15} \text{ cm}^2/\text{W}$]	$\chi^{(3)}$ (10^{-13} esu)
TeZnK	1.31±0.20	1.15
TeZnNa	2.33±0.42	2.06
TeZnLi	2.37±0.40	2.10
TeMgLi	2.81±0.5	2.5
CS ₂	2.11±0.45	1.87

By examining Table 3.2 for the glasses with the network intermediate Zn, it is observed that n_2 increases in the following order TeZnK < TeZnNa < TeZnLi, although the sample with Li as modifiers is barely larger than in the case of Na. It is also observed a further increase of nonlinearity when Zn is replaced by Mg as intermediate. The NL response is related with the degree of hyperpolarizability of the sample as a result of the structural changes inside the arrangement with the presence of modifiers and intermediates. Therefore, the trend exhibited by samples with Zn as intermediate can be attributed to the decrease in ionic radius from K to Li through Na that leads to a modification of the polarizability per unit volume⁴¹. Similarly, the NL response increases when Zn is substituted by Mg which has a smaller ionic radius. From this concept it follows that the number of ions per unit volume might increase as the ionic radii of the network modifiers and/or intermediates decrease. The corresponding ion radii for K, Na, Li, Zn and Mg are 1.33, 0.95, 0.68, 0.74 and 0.65 Å, respectively. Thus, more ions per unit volume can be polarized using Li and Mg as modifier and intermediate, respectively, and consequently,

the NL response is larger. In the opposite case, fewer ions per unit volume can be polarized with the use of K and Zn and consequently the nonlinear response is weaker. This trend was also observed in the NL susceptibilities of the type $\chi^{(3)}(-3\omega; \omega, \omega, \omega)$ measured by means of THG at 1.9 μm for binary glasses of the type $\text{TeO}_2\text{-R}_2\text{O}$ with $\text{R} = \text{K}, \text{Na}, \text{Li}$ ⁴¹. As for ternary glasses, a recent study on the optical properties of codoped tellurite glasses based in the matrix $\text{TeO}_2\text{-ZnO- Na}_2\text{O}$ showed a NL refractive index of $1.90 \times 10^{-15} \text{ cm}^2/\text{W}$ at 800 nm²⁷. The matrix reported in that work was similar to our TeZnNa sample although with a concentration of 5 mol % for the modifier Na_2O (and 20 mol% for ZnO). Thus, the values of n_2 measured in the present work for TeZnNa and in Ref. 27 for a similar glass composition show good agreement.

The NLR index for the series of glasses with Zn as network intermediate followed the order suggested by the semi-empirical Millers rule (stating that materials with larger linear refractive index possess larger NLR index), although they do not vary in proportion to the variation of their linear refractive index. However, the rule fails with the introduction of Mg as network intermediate (see Table 3.2). According to Millers Rule, TeMgLi shows an unexpected larger nonlinearity in comparison to TeZnLi, being their linear refractive index 1.919 and 1.956 at 800 nm, respectively. In this case, the nonlinearity increased when Zn was replaced by Mg in the glass composition to obtain a maximum value of $2.81 \times 10^{-15} \text{ cm}^2/\text{W}$. This is not surprising as other authors have also observed the failure of Millers rule⁴²⁻⁴³. Further, in our previous work³⁴, it was also observed that the introduction of Mg to replace Zn in the glass composition increased the third-order susceptibility tensor associated with the optical nonlinear effect of THG for IR wavelengths.

The Z-scan experiments demonstrate that the glass composition of our samples not only exhibit large values of n_2 but also have a good capacity to disperse the absorbed heat, precluding the appearance of accumulative thermal effects (thermal lensing) that could affect the nonlinear optical behavior. In our case, heat is produced from the residual linear

absorption at 800 nm (at this wavelength, NL absorption was not experimentally detected for the maximum peak powers available in our TM Z-scan experiment). The absorption coefficient was estimated to be in the range of $0.1 - 1 \text{ cm}^{-1}$ depending on the sample, and was calculated from the linear absorption spectra once the reflection losses were taken into account (typical transmittance in these glasses is about 80%). The capacity of the samples to disperse the absorbed heat was tested in various experimental conditions. For instance, it is worth to mention that for these TM Z-scan experiments, we change the duty cycle of our setup, the illumination time was $\sim 1 \text{ ms}$ followed by $\sim 36 \text{ ms}$ without illumination. This duty cycle was varied by simply changing the frequency of the chopper wheel and no appreciable thermal effect was detected even for longer times of illumination. Furthermore, standard Z-scan experiments were performed using a continuous wave Ti:Sapphire laser with 400 mW output power. In this case, a constant transmittance was observed and no evidence of thermal lensing was detected. These results are interesting in view of the thermo-optical response measured in other glasses with different techniques. For instance, in binary and ternary tellurite glasses with composition (in mol%) $80\text{TeO}_2\text{-}20\text{Li}_2\text{O}$ and $80\text{TeO}_2\text{-}15\text{Li}_2\text{O}\text{-}5\text{TiO}_2$ and with similar residual absorption than the corresponding to our samples ($\sim 1\text{cm}^{-1}$) small thermal lens effect was detected under cw Ar^+ laser excitation with 81 mW at 514 nm^{44} .

The values of n_2 for the tellurite glasses were independent of the peak intensities available for the laser oscillator used in the TM Z-scan experiments. In order to study the NL response at much higher intensities, we analyzed the samples using the standard Z-scan under fs pulses delivered by a Ti:Sapphire regenerative amplifier. Figure 3.3 shows an example of the nonlinear response of TeZnLi sample at three different peak intensities, 10.6, 34.6 and 57.8 GW/cm^2 .

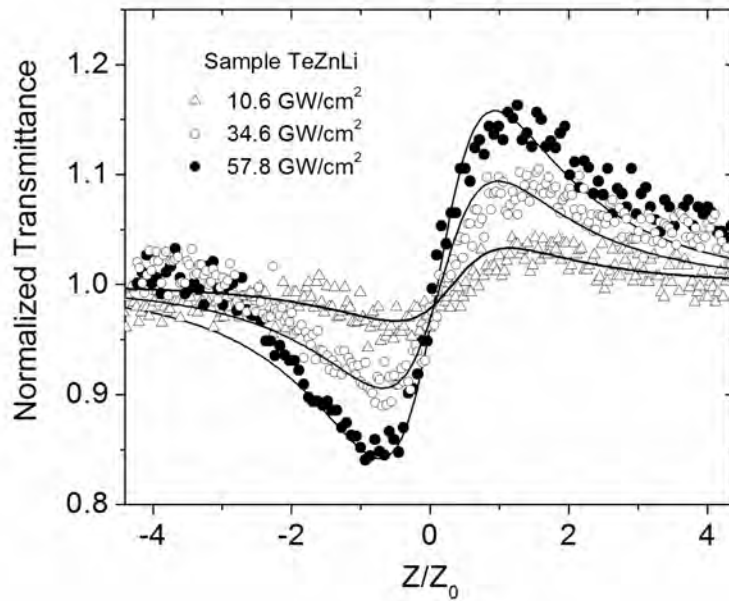


Figure 3.3 Normalized transmittance in standard Z-scan measurements for TeZnLi under excitation at 1 KHz pulse repetition rate and different intensities. The continuous lines are fittings to the experimental data.

From these Z-scan traces the values of n_2 resulted in 2.51, 2.24 and 2.07 ($\times 10^{-15} \text{ cm}^2/\text{W}$) respectively, showing that at high peak intensities the NL response saturates. Figure 3.4 presents the values of NLR index measured for all samples under study at 10.6 and 57.9 GW/cm^2 and for comparison the figure includes those values obtained with TM Z-scan at 9.0 GW/cm^2 .

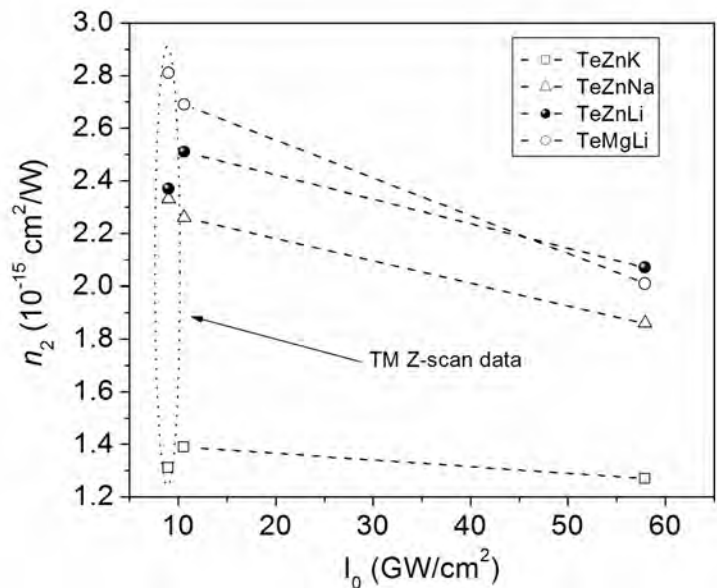


Figure 3.4 Variation of n_2 as a function of intensities obtained under excitation at 1 KHz pulse repetition rate. For comparison, the values of n_2 obtained through TM Z-scan experiments are included.

Notice the good agreement between the values of n_2 obtained at 10.6 GW/cm² with train of pulses at 1 KHz and those obtained through TM Z-scan at 9.0 GW/cm² with train of pulses at 80 MHz. This confirms that the NL response is free of accumulative thermal lensing effects even upon excitation at high frequencies of repetition rate with intensities of the order of 10 GW/cm². Moreover, at this level of intensities the experiment with pulses at 1 KHz also demonstrates that the order in which the nonlinearities increase as a function of the modifiers is the same than that observed in TM Z-scan experiments. However, when the peak intensities are further increased the values of n_2 decrease to some extent, as it is observed in Figure 3.4 for the intensity of 57.8 GW/cm². The decrease of the measured NLR indices at very high intensities might be associated with the appearance of nonlinearities of higher order or other physical process that modify the material response. Nevertheless, it is worth to point out that during these experiments the glasses did not reveal apparent optical damage. This suggests that our samples are able to withstand high optical peak intensities without showing optical damage.

III.2.4 Photoluminescence and transient absorption

Photoluminescence (PL) and pump-probe measurements were obtained from tellurite glass samples.

Figure 3.5 shows a representative experimental setup of pump-probe experiments. Pump-probe measurements come in many flavors related to modes of detection and choice of pump and probe beams. In terms of detection, most pump-probe measurements utilize a detector with slow response time compared to that of the dynamics of interest. In such time-integrated detection, time resolution comes about due to the ability to scan the pump-probe delay precisely. Furthermore, pump and probe pulses may be either degenerate (pulses are essentially identical, are derived directly from the same laser, and occupy the same spectral band) or nondegenerate.

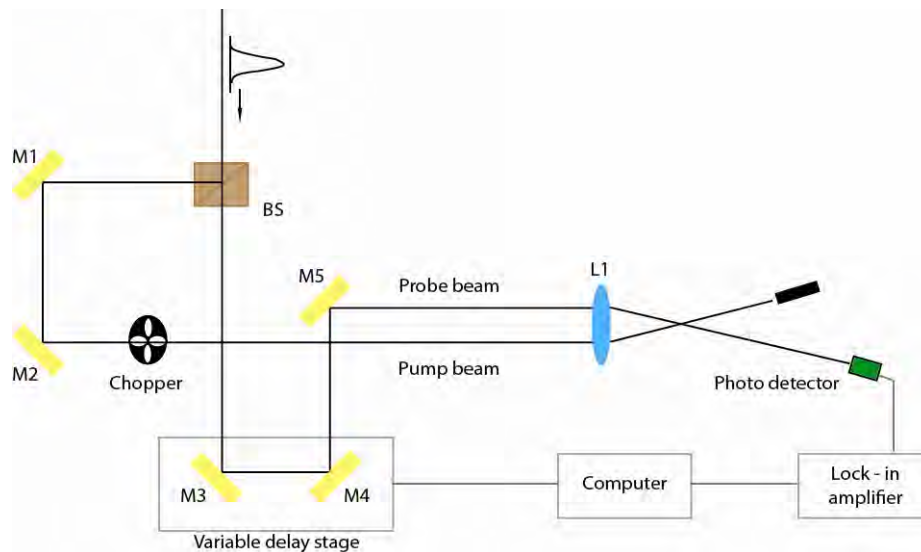


Figure 3.5 Representative experimental setup for pump-probe measurements in transmission geometry. The chopper and lock-in amplifier pull out the change in the power of the transmitted probe induced by the presence of the pump.

The pump and probe pulses are focused into an absorbing sample noncollinearly with controllable relative delay τ . The average power in the probe beam is measured using a time integrating detector as a function of τ .

In nondegenerate experiments pump and probe beams are spectrally nonoverlapping. Here the probe beam is often derived from the same laser as the pump, but frequency-conversion processes are used to shift the frequency of the pump, the probe, or both. For example, the pump may lie in the visible spectrum, while the probe beam may be elsewhere in the visible, in the ultraviolet or infrared, or even in more exotic frequency regions such as terahertz or X-ray. Furthermore, the process of continuum generation provides access to probe pulses with extremely broad frequency content.

Typically, spectra are recorded both with the pump on and with the pump blocked; subtracting these yields the differential transmission spectrum. Such differential spectra are then recorded as a function of probe delay. The resulting time- and frequency-resolved pump-probe data often provide much richer information than is possible in degenerate measurements.

Photoluminescence (PL) spectra from tellurite glass samples were obtained after excitation with the third-harmonic (355 nm) of a pulsed Nd:YAG laser (7 ns pulses at 10 Hz repetition rate) and with the second-harmonic (244 nm) of a CW Argon laser. In addition, the dynamics of electronic excitations in the glasses were studied through time-resolved pump-probe experiments. In this case, the transient change of transmission of the samples was measured in a non-degenerate setup employing femtosecond pump pulses at 440 nm (2.8 eV) with typical intensities in the range of 0.38 – 1.2 mJ/cm² and probe pulses at 516 nm (2.4 eV) with intensities a hundred times weaker with respect to pump pulses. The instrument response was evaluated through the cross correlation between the pump and probe pulses and gave a temporal resolution of 120 fs.

In Figure 3.6 the PL of TeZnLi after UV excitation is shown. Clearly, position and structure of the emission bands change depending on the excitation wavelength. All tellurite glass samples exhibited very similar emission spectra independently of the modifier or network intermediate in their composition, although TeZnLi showed the most intense PL signal. Low pump intensities were used to obtain these spectra.

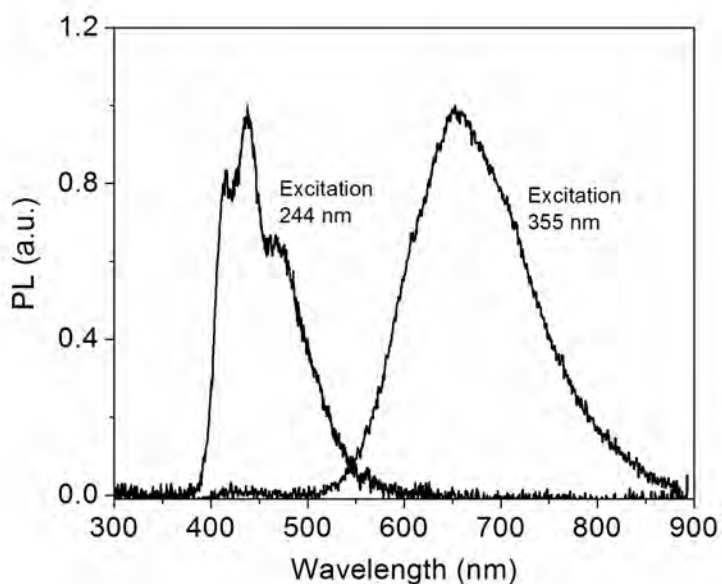


Figure 3.6 Normalized photoluminescence spectra for sample TeZnLi after excitation with 244 nm and 355 nm laser light.

Figure 3.6 shows a red emission band centered at 650 nm (1.90 eV) with a bandwidth of 140 nm after excitation at 355 nm (3.49 eV) and a blue emission band centered at 437 nm (2.83 eV) and with a bandwidth of 83 nm after excitation at 244 nm (5.08 eV). Both emission bands are the result of electron relaxation from electronic states with energies lying within the band gap as illustrated in the energy scheme in Figure 3.7, where ETb and ETr stand for the states responsible for blue and red emission bands, respectively.

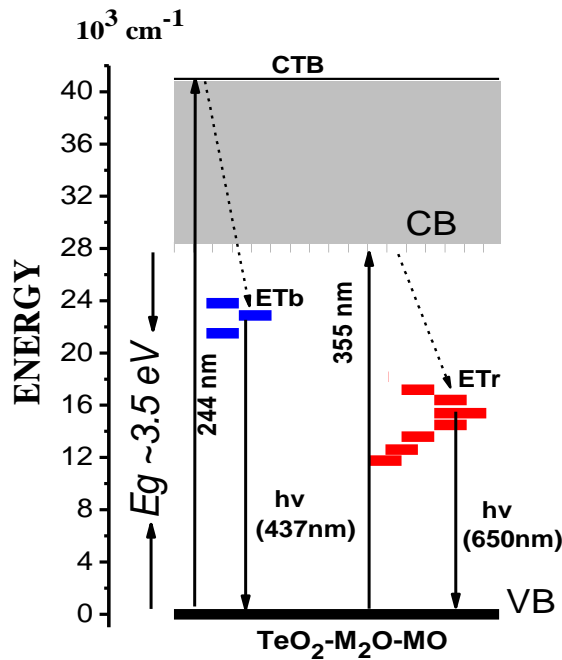


Figure 3.7 Schematic energy level diagrams for tellurite glasses. Dotted lines indicate nonradiative relaxations.

Those localized electronic states were produced by defects induced during the glass fabrication and can be probably related to the presence of both modifiers and network intermediates. Blue emission is likely associated with the presence of oxygen vacancies ($\Delta E_g \sim 2.8$ eV) as has been described for ZnO^{45} , while the red emission is probably associated with sites where the modifiers (Li, Na, K) constitute impurities⁴⁶⁻⁴⁷.

The observed PL dependence on the wavelength of excitation suggests two mechanisms for electronic transitions. Excitation at 355 nm promotes electrons from the valence band to the conductive band edge and after nonradiative relaxations ETr is populated; subsequently, radiative decays generate the red PL band. For 244 nm excitation, the

charge transfer band (CTB) is populated and successive nonradiative relaxations result in the population of the ETb state which generates the blue PL band. This is in agreement with the analysis of the CTB in TeO₂ glasses reported previously⁴⁸⁻⁴⁹.

To study the dynamics of the excited states, we performed nondegenerate pump–probe experiments with wavelengths corresponding to photon energies smaller than the optical bandgap. The samples were excited by strong pump pulses at 440 nm (2.8 eV) while delayed and weak probe pulses at 516 nm (2.4 eV) allowed us to measure transient changes of transmission ΔT induced by the pump pulses. The change in transmission is defined as $\Delta T = T_p - T$, where T_p and T are the transmission with and without pump, respectively. Figure 3.8 displays ΔT as a function of time delays between pump and probe pulses for the samples TeZnK, TeZnNa, TeZnLi and TeMgLi.

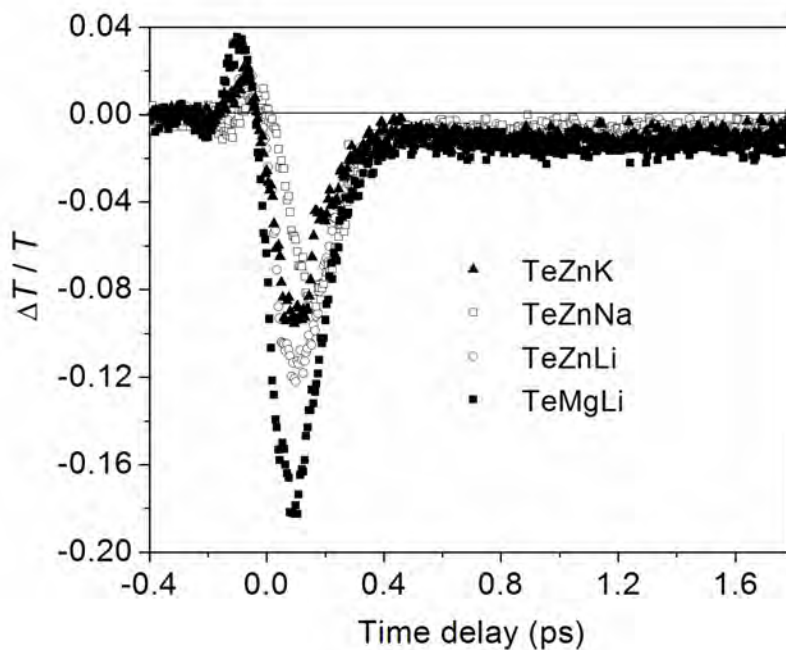


Figure 3.8 Transient changes of transmission of TeZnLi, TeZnNa and TeZnK samples for pump at 440 nm (2.8 eV) and probe at 516 nm (2.4 eV).

In this figure the major component is a fast transient induced absorption (i.e., decrease of transmission or negative values of $\Delta T/T$) of few hundreds of fs and a long and weak tail. This suggests that the $\Delta T/T$ decrease observed in all the samples might be associated with induced absorption from the localized states to the conduction band. Notice that the wavelength of the pump corresponds to an energy (2.8 eV) that is below the optical band gap (3.5 eV) of samples so that excitation can only occur into the localized states and from them subsequent absorption of the probe pulse promotes electron to the conduction band. Figure 3.8 also shows the presence of a fast $\Delta T/T$ increase ($\Delta T/T > 0$) just for early delays although that component might not represent population dynamics of electronic states but a coherent artifact produced by third-order nonlinear effects, i.e. cross phase modulation effects. In any case, these experiments confirm the existence of localized states and also demonstrate the fast response of the material.

In summary, the high material nonlinearity of tellurite glasses, combined with the ideal network modifiers and intermediate, makes them attractive as fast NL optical devices. This makes them a good platform for ultrafast NLO and a key technology for future ultrahigh-bandwidth optical communications systems. Tellurite glasses offer a unique set of properties among optical that make them an excellent choice for mid-IR science and NLO. The main challenge for all applications is to identify glasses that have the required stability and processability—from among the myriad of tellurite glass compositions currently available. If achieved, this intriguing range of optical glasses should have an extremely bright future.

III.3 References

1. R.L. Sutherland, Handbook of Nonlinear Optics (Marcel Dekker, New York, 1996).
2. M. Yamane, Y. Asahara, Glasses for Photonics (Cambridge University Press, Cambridge, UK, 2000).
3. P.N. Butcher, D. Cotter, The Elements of Nonlinear Optics (Cambridge University Press, Cambridge, UK, 1998).
4. M. Sheik-Bahae, D.C. Hutchings, D.J. Hagan, E.W. Van Stryland, IEEE J. Quantum Electron. QE-27, 1296 (1991)
5. K. Tanaka, J. Mater. Sci. 16, 633 (2005)
6. T.R. Oliveira, L. de S. Menezes, E.L. Falcão-Filho, A.S.L. Gomes, C.B. de Araújo, K. Sakaguchi, F.P. Mezzapesa, I.C.S. Carvalho, P.G. Kazansky, Appl. Phys. Lett. 89, 211 912 (2006)
7. See for instance: G. Poirier, C.B. de Araújo, Y. Messaddeq, S.J.L. Ribeiro, M. Poulain, J. Appl. Phys. 91, 10 221 (2002).
8. Sanghera, J. S., Shaw L. B. and Aggarwal, I. D. IEEE J. Sel. Top. Quant. **15**, (2009) 114.
9. Zhang, X. H., Guimond, Y. and Bellec, Y., J. Non-Cryst. Sol. **326**, (2003) 519.
10. Kosa, T. I. et al. J. Non-Cryst. Sol. **166**, (1993) 1219.
11. Harbold, J. M. et al. Opt. Lett. **27**, (2002) 119.
12. Pelusi, M. D. et al. IEEE J. Sel. Top. Quant. **14**, (2008) 529.
13. L.Jiang, Z.R.Sun, X.R.Zhu, H.P.Zeng, Z.Z.Xu,Z.G.Wang, J.Lin, W.H.Huang, R.S.Armstrong and P.A.Lay: Opt. Mater., **25** (2004) 401.
14. H.Lin, G.Meredith, S.Jiang, X.Peng, T.Luo, N.Peyghambarian and E.Y.B.Pun: J. Appl. Phys., **93** (2003) 186.
15. J.Lin, W.H.Huang, Z.R.Sun, C.S.Ray and D.E.Day: J. Non-Cryst. Solids, **336** (2004) 189.
16. A.P.Mirgorodsky, M.Soulis, P.Thomas, T.Merle-Mjean and M.Smirnov: Phys. Rev. B **73**, (2006) 134206.
17. R. Rolli, M. Montagna, S. Chaussedent, A. Monteil, V. K. Tikhomirov, and M. Ferrari, Opt. Mater. **21**, (2003) 743.
18. J. Jackson, C. Smith, J. Massera, C. Rivero-Baleine, C. Bungay, L. Petit, and K. Richardson, Opt. Express **17**, (2009) 9071.
19. S. Shen, A. Jha, X. Liu, M. Naftaly, K. Bindra, H. J. Bookey, and A. K. Kar, J. Am. Ceram. Soc. **85**, (2002) 1391.
20. X. Feng, W. H. Loh, J. C. Flanagan, A. Camerlingo, S. Dasgupta, P. Petropoulos, P. Horak, K. E. Frampton, N.M. White, J. H. Price, H.N. Rutt, and D. J. Richardson, Opt. Express **16**, (2008) 13651.
21. P. V. dos Santos, M. V. D. Vermelho, E. A. Gouveia, M. T. de Araújo, F. C. Cassanjes, S. J. L. Ribeiro, and Y. Messaddep, J. Chem. Phys. **116**, (2002) 6772.
22. S. Xu, H. Ma, D. Fang, Z. Zhang, and Z. Jiang, Mater. Lett. **59**, (2005) 3066.
23. M. Dutreilh-Colas, P. Thomas, and J. C. Champarnaud-Mesjard, Phys. Chem. Glasses **44**, (2003) 349.
24. F. Chen, T. Xu, S. Dai, Q. Nie, X. Shen, J. Zhang, and X. Wang, Opt. Mat. **32**, (2010) 868.
25. A. P. Mirgorodsky, M. Soulis, P. Thomas, and T. Merle-Méjean, Phys. Rev. B **73**, (2006) 134206.
26. R. F. Souza, M.A.R.C. Alencar, J.M. Hickmann, R. Kobayashi, and L.R.P. Kassab, Appl. Phys. Lett. **89**, (2006) 171917.
27. F. Eroni. P. dos Santos, F. C. Fávero, A. S. L. Gomes, J. Xing, Q. Chen, M. Fokine, and I. C. S. Carvalho, J. Appl. Phys. **105**, (2009) 024512.
28. J. C. McLaughlin, S. L. Tagg, and J. W. Zwanziger, J. Phys. Chem. B **105**, (2001) 67.
29. J. S. Wang, E. M. Vogel and E. Snitzer, Opt. Mater. **3**, (1994) 187.
30. H. Lin, S. Jiang, J. Wu, F. Song, N. Peyghambarian and E. Y. B. Pun, J. Phys. D: Appl. Phys. **36**, (2003) 812.
31. Y. Gao and C. Cramer, Solid State Ionics **176**, (2005) 2279.

32. S.P. Singh, Aman and A. Tarafder, *Bull. Mater. Sci.* **27**, (2004) 281.
33. H. Takebe, Y. Nageno, and K. Morinaga, *J. Am. Ceram. Soc.* **77**, (1994) 2132.
34. H. Desirena, A. Schülzgen, S. Sabet, G. Ramos-Ortiz, E. de la Rosa, and N. Peyghambarian, *Opt. Mater.* **31**, (2009) 784.
35. R. Castro-Beltrán, H. Desirena, G. Ramos-Ortiz, E. De la Rosa, G. Lanty, J. S. Lauret, S. Romero-Servin, Axel Schülzgen, in press.
36. J. Tauc, R. Grigorovici, and A. Vancu, *Phys. Status Solidi* **15**, (1966) 627.
37. L.M. Sharaf El-Deen, M.S. Al Salhi, and M. M. Elkholy, *J. Alloys Comp.* **465**, (2008) 333.
38. S.-H. Kim, T. Yoko, and S. Sakka, *J. Am. Ceram. Soc.* **76**, (1993) 2486.
39. E. Yousef, M. Hotzel, and C. Rüssel, *J. Non-Cryst. Solids* **353**, (2007) 333.
40. R. A. Ganeev, A. I. Rysanyansky, M. Baba, M. Suzuki, N. Ishizawa, M. Turu, S. Sakakibara, and H. Kuroda, *Appl. Phys. B* **78**, (2004) 433.
41. S.-H. Kim, *J. Mater. Res.* **14**, (1999) 1074.
42. Q. Liu, C. Gao, H. Zhou, B. Lu, X. He, Qian Shixiong, and X. Zhao, *Opt. Mater.* **32**, (2009) 26.
43. H. Guo, H. Tao, S. Gu, X. Zheng, Y. Zhai, S. Chu, X. Zhao, S. Wang, and Q. Gong, *J. Solid State Chem.* **180**, (2007) 240.
44. S.M. Lima, W.F. Falco, E.S. Bannwart, L.H.C. Andrade, R.C. de Oliveira, J.C.S. Moraes, K. Yukimitu, E.B. Araújo, E.A. Falcão, A. Steimacher, N.G.C. Astrath, A.C. Bento, A.N. Medina, and M.L. Baesso, *J. Non-Cryst. Solids* **352**, (2006) 3603.
45. D. H. Zhang, Z. Y. Xue, and Q. P. Wang, *J. Phys. D: Appl. Phys.* **35**, (2002) 2837.
46. J. W. P Hsu, D. R. Tallant, R. L. Simpson, N. A. Missert, and R. G. Copeland, *Appl. Phys. Lett.* **88**, 252103 (2006).
47. S. A. Studenikin, N. Golego, and M. Cocivera, *J. Appl. Phys.* **84**, 2287 (1998).
48. R. P. Sreekanth Chakradhar, G. Sivaramaiah, J. Lakshmana Rao, and N. O. Gopal, *Mod. Phys. Lett. B* **19**, 643 (2005).
49. A. Berthereau, Y. Le Luyer, R. Olazcuaga, G. Le Flem, M. Couzi, L. Canioni, P. Segonds, L. Sarger, and A. Ducasse, *Mater. Res. Bull.* **29**, 933 (1994).

CHAPTER IV

IV. 1 GENERAL CONCLUSIONS

In this dissertation, significant results on the NL optical properties based on the structure–property of organic and inorganic compounds were presented. We carried out the NL optical studies through eight different NL optical techniques that allowed us to visualize the magnitude and with some methods, the signs of their nonlinearities. We conducted our studies through Z–scan, TM Z–scan, TM Z–scan with flow, OPEF, TPEF, THG, EFISH and Pump–probe experiments. My best contribution respect all these NL optical techniques, was in the implementation of the Z–scan technique and variations of this one in our laboratories. With these techniques we could discriminate between electronic and thermo–optical nonlinearities. Although, TM Z–scan is a technique implemented in early 2000, it has not yet been thoroughly analyzed. For instance, through all the obtained results we found a special case where the technique fails in the discrimination of both contributions; in the study of solutions where thermo–optical effects were so pronounced this technique could not resolved its electronic contribution. In order to figure out, in this dissertation was presented a new implementation of the TM Z–scan technique, which allows the solution to flow while the analysis in Z unfolds. Under this new TM Z–scan “with flow” we had the opportunity to resolve better the electronic contribution of samples, where its thermo–optical responses prevailed. Due to these techniques were for the first time implemented in our laboratories, we corroborated that our results were correct by measuring the NL optical contribution of a third–order reference material such as CS₂. Furthermore, taking into account the great importance of these results, we decided to carry out the NL optical study of the most common organic solvents used to dissolve organic compounds. In the literature there are not reported that show in a single analysis the electronic and thermo–optical NL optical contributions presented in the solvents by Z–scan, the NL optical responses are overestimated due to the responses of the solvents are not taking into account.

Once the techniques were implemented and considering all the experimental conditions for the study of the novel organic compounds and photonic glasses, the results were as follows: large NL properties of hb-Polyyne were reported. Under fs excitation around 800 nm, hb-Polyyne exhibited exceptionally high σ^{TPA} of 9068 GM. On the other hand, under pulsed ns excitation at the telecommunication wavelengths, hb-Polyyne films exhibited $\chi^{(3)} \sim 10^{-11}$ esu. Additionally, because the hb-Polyyne was principally formed by repeated units of octupolar compounds and in order to know more about its structure-property, single-octupolar-molecule (crystal violet) was studied to correlate its NL optical behavior in a well defined macroscopic structure as our hb-Polyyne. The NL optical responses of the hb-Polyyne were much higher than those for CV, for instance, CV presented values of $\chi^{(3)} \sim 10^{-12}$ esu and σ^{TPA} of 1980 GM, which means one order of magnitude and 5 times lower than the hb-Polyyne, respectively. It reflects an important feature in the comprehension of the structure-property of our hb-Polyyne, for instance, repeated building blocks of octupolar compounds forming a highly conjugated polymer increase its NL optical behavior and its NL optical responses and contributions can be explained by the cooperative principle. Furthermore, all these reported data should point that the hb-Polyyne could be a promising NL optical material. Its large third-order NL optical responses were within the range of materials with possible photonic and biophotonic applications, i.e., optical power limiting and biomarkers.

We were also interested in the NL optical behavior of highly conjugated dipolar systems where the insertion of a metal unit was present. We studied the second and third-order NL optical properties of tetracoordinated organoboron compounds. We compared the linear and NL optical responses of the ligands with respect their boronates and specially, we focused our attention in the N→B coordinative bond presented in the organoboron compounds. In addition, because our compounds had different donor/acceptor substituents, we could associate their NL optical behavior with the strength of these ones, an important feature that allowed us also to have better understanding of their structure-property relations.

In summary, the results suggest that the N→B bond allowed more effective delocalization of the π -systems and that the boron atom stabilizes the negative charge more efficiently than the nitrogen in the ligand. In particular, under fs excitation at 800 nm the process of TPA was presented in the organoboron while such effect was practically absent for the ligands. We study also the process of NL absorption under ns excitation at 532 nm and found that, the compounds exhibited ESA: SA for the boronates and RSA for the ligands. On the other hand, second-order NL optical studies showed that, the presence of the N→B coordinative bond increases their NL optical contributions up to 5 times with respect to those for their ligands. The higher NL result was of $\mu\beta = 26.1 \times 10^{-46} esu$. This result is important because in previous studies reported in our group, a series of boronates with values of the same order were reported, but the importance in that research work was that their organoboron compounds exhibited SHG efficiencies 26 times larger than in KDP (inorganic crystal for NL applications). In addition, we found that the diethylamine and the Nitro groups were the strongest donor and acceptor substituents in the ligands and organoboron compounds. Unlike the combination of dimethylamine and phenyl substituents that were the electronic groups with the lowest NL optical contributions. Finally, based on the concept of hybrid materials, we decide to study the NL optical properties of four tellurite glasses to correlate their responses through different network modifiers and intermediates. We found three significant results; the photonic glasses showed high resistance at high peak intensities of laser excitation, after excitations at 355 and 437 nm, they exhibited two emission bands that were associated to defects produced during the glass fabrication and to the presence of their modifiers and the third one, these photonic glasses had great possibilities to dissipate heat; They presented only NL electronic contributions, which differed by their different networks modifiers and intermediates. Negligible thermo-optical contributions are fundamental in photonic applications; for instance, in optical signal processing and optical power limiting only electronic responses are significant. For different modifiers and intermediates, the electronic NLR indices n_{2elec} of these glasses varied in the range 1.31–2.81 ($\times 10^{-15}$

cm²/W). It was found that n_{2elec} increases as the ionic radius of both, network modifiers and intermediates decreases.

To conclude, all these significant results of organic, organometallic and photonic glasses could be combined in one material in order to improve and increase its mechanical and NL optical properties in view of photonic applications. In our group are being designed novel hybrid materials, which are grown from aerogel process, that offers extraordinary possibilities to be used as photonic devices due two significant facts: they are in solid state and particularly, they could combine several of the best novel organic groups and those for of the photonic glasses.

IV.2 SCIENTIFIC PRODUCTION

The research work presented in this dissertation allowed the publication of four scientific articles and two more manuscripts are in preparation, as follows:

1. **R. Castro-Beltran**, G. Ramos-Ortiz, C. K. W. Jim, J. L. Maldonado, M. Häußler, D. Peralta-Dominguez, M. A. Meneses-Nava, O. Barbosa-Garcia and B. Z. Tang, "*Optical nonlinearities in hyperbranched polyynes studied by two-photon excited fluorescence and third-harmonic generation spectroscopy*", Applied Physics B: Lasers and Optics, **97** (2009) 489.
2. M. Rodríguez, **R. Castro-Beltrán**, G. Ramos-Ortiz, J. L. Maldonado, N. Farfán, O. Domínguez, J. Rodríguez, R. Santillan, M. A. Meneses-Nava, O. Barbosa-García, J. Peón, "*Synthesis and third-order nonlinear optical studies of a novel four-coordinated organoboron derivative and a bidentate ligand: The effect of the N→B coordinative bond*" , Synthetic Metals, **159** (2009) 1281.
3. **R. Castro-Beltrán**, H. Desirena, G. Ramos-Ortiz, E. De la Rosa, G. Lanty, J. S. Lauret, S. Romero-Servin, Axel Schülzgen, "*Third-order nonlinear optical response and photoluminescence characterization of tellurite glasses with different alkali metal oxides as network modifiers*", Journal of Applied Physics, **110**, (2011) 083110.
4. V. M. Herrera, J. L. Maldonado, M. Rodríguez, **R. Castro-Beltrán**, N.E. Magaña G. Ramos-Ortiz, M. A. Meneses-Nava, O. Barbosa-García, R. Santillán, N. Farfán, F. X. Dang, P. G. Lacroix, and I. Ledoux-Rak, "*Highly efficient photorefractive organic polymers based on aryl-cyano non-linear chromophores*", The Journal of Physical Chemistry C - Published on line 2011. DOI: [dx.doi.org/10.1021/jp206204p](https://doi.org/10.1021/jp206204p).

5. **R. Castro-Beltrán**, M. Rodríguez, Anu Singh, G. Ramos-Ortiz, I. Ledoux-Rak, *“Synthesis, structure and nonlinear optical properties of bidentate ligands and borinates. The effect of the NO₂ and the N→B coordinative bond”*, **(in preparation)**.
6. **R. Castro-Beltrán**, G. Ramos-Ortiz, J. L. Maldonado, M. A. Meneses-Nava, O. Barbosa-Garcia, Jorge Peon, *“Measurement of Electronic and Thermo-optical nonlinearities in static and dynamic solvents and solutions using thermally managed Z-scan technique”*, **(in preparation)**.

CHAPTER V

GENERAL VIEWS

The study of the NL optical properties of the most common solvents (used to dissolve organic materials), an octupolar compound, a hyperbranched polymer, organometallic compounds and tellurite glasses throughout this dissertation allowed a better understanding about the structure–property of them. Furthermore, the results obtained from this dissertation, motivated the GPOM to create two new lines of research focus mainly on the development materials used as biomarkers and hybrid materials.

This final chapter aims to give a general outline about these two lines and relate them with the results derived from this dissertation.

V.1 The design of biomarkers in the GPOM: beginnings.

From the study of $\chi^{(3)}$ out of resonance of our hb–Polyyne it was observed that the imaginary part of such tensor element persisted so that we decided to perform TPA to evaluate such imaginary component.

Our hb–Polyyne is a very special compound because this is conformed in such a way that its NL properties can be understood as a cooperative effect from its individual octupolar units, in our particular case triphenylamine moieties. Our hb–Polyyne had a TPA cross section σ^{TPA} in the order of 10^4 GM: this range has been reported in the literature for the strongest TPA compounds.

On the other hand, we presented also studies about the NL optical absorption activity in organoboron compounds in order to know the importance of a metal atom in a π –conjugated system. Our four–coordinated organoboron compound had a σ^{TPA} of 152 GM, although this value is somewhat moderate (in comparison with standard dyes, but very weak compared with the hb–Polyyne), we demonstrated that the presence of a N→B coordinative bond enhance the NL absorption of dipolar π –conjugated system. We

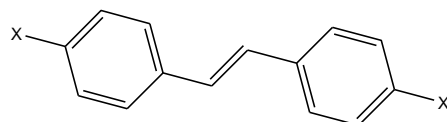
associated also this NL optical behavior with the strength of the electron donor and electron acceptor substituents. The compounds here studied also exhibited excited state absorptions (ESA) at the visible wavelength of 532nm with ns excitation: saturable absorption for the boronate and reversible saturable absorption for the ligand.

The results of NL absorption obtained from both molecules give rise to two immediate conclusions:

- a) The high density of extended π -conjugated systems in hyperbranched polymers is advantageous for producing large NL optical effects.
- b) The insertion of a metal unit in a conjugated structure significantly influences the π -electron behavior that can have essential manifestations in optical nonlinearity.

From these two immediate conclusions we can establish possible trends in the molecular design, in order to improve the Structure-Property of the NL materials:

In 1997, Marder, Perry, and co-workers reported a comparison of trans-stilbenes **a** and



a, X=H, σ^{TPA} = 12 GM at 514 nm (fs-TPEF)

b, X=NBu₂, σ^{TPA} = 110 GM at 620 nm (fs-TPEF)

c, X=NPh₂, σ^{TPA} = 340 GM at 514 nm (fs-TPEF)

its derivative **b** with terminal donor substituents¹. The σ^{TPA} of **b** is almost ten times higher than that of the unsubstituted stilbene (**a**; a further increase was observed for **c** with diphenylamine substituents)^{2,3}. The discovery that centrosymmetric CT results in high σ^{TPA} led to a general approach for the design of TPA materials, with two electro donors **D** or electro acceptors **A** terminals linked by a π -conjugated bridge². Variation of the donor

and acceptor substituents has now become a popular approach to creating new two-photon dyes^{1,4,5-8}.

While Marder, Perry, and co-workers were exploring centrosymmetric chromophores, Reinhardt, Prasad, and co-workers developed dipolar dyes with polarizable bridges¹. These D – π – A dyes exhibited strong apparent TPA from ns Z-scan measurements, but subsequent fs measurements gave significantly lower values in most cases (<100 GM)⁴. On the other hand, several groups have been investigated that nondipolar structures as quadrupolar systems **D – π – A – π – D** and **A – π – D – π – A** are generally more effective structures than D – π – A, A – π – A and D – π – D⁹ systems.

Under this scenario, and taking into account the results obtained along this dissertation, in the GPOM have been developed novel organic and organometallic quadrupole compounds as above mentioned. The originality in this synthesis of organometallic compounds is that, they will be based on the design of four-coordinative organoboron compounds and under this assumption, these novel syntheses will have in addition to the above properties, the properties of the N→B coordinative-bond.

V.2 Feasible application: the contrast cells through TPA excitation and hybrid materials for optical power limiting

Although our TPA materials presented σ^{TPA} values in the order of 100 - 10⁴ GM, their poor solubility in water prevent them from being used in biological applications based in the use of efficient NL effects, i.e., two-photon activity. On the other hand, most of the commonly used water soluble TPA materials only exhibit σ^{TPA} values that are less than 100 GM¹⁰.

In general, three approaches have been utilized to enable their applications in biological fields. The first approach is a chemical modification of compounds/polymers with water soluble segments or moieties¹¹⁻¹⁴; the second approach is the preparation of organic/polymer nanoparticles through a polymer precipitation approach¹⁵⁻¹⁷; the third way utilizes micelles formed from amphiphilic block copolymers to encapsulate

hydrophobic organic molecules and polymers to enable their applications in biological environments¹⁸.

Particularly, the group has interests in the third method, which uses micelles formed from silica in water to deliver hydrophobic conjugated polymers. Using this approach, conjugated polymers can be hydrophobic, endowing their easy preparation and purification. We are very interested in encapsulating polymers by the main reason of its high nonlinearity. Polymer as hb-Polyyne (Unlike traditional dyes) could present cooperative effect which makes that its NL properties increases.

Micelles are biocompatible and, at the same time these remain high σ^{TPA} values in polar aqueous media, which make them ideal materials to be use as markers of biological specimens. In addition, their surfaces can be modified with suitable targeting moieties for targeted delivery and imaging.

Taking into account both properties (biocompatibility and high σ^{TPA} values), the group (through one of our collaborators) uses the two-photon microscopy technique to obtain biological imaging. This technique enables noninvasive study of biological specimens. This excitation process has a number of unique advantages, such as reduced specimen photodamage and enhanced penetration depth. It also produces higher-contrast images and is a novel method to trigger localized photochemical reactions. Furthermore, two-photon microscopy can effectively exploit the tissue “optical window” at 700–1000 nm. Tissue absorbance in this window is orders of magnitude less than the absorbance in the UV or blue-green region.

On the other hand, focus in the great possibility of having a photonic or optoelectronic device, and referring to the most important results derived from this dissertation about organic and inorganic samples, the group is developing new materials that combine the advantages of both in order to apply them as optical power limiting devices. The main idea of using the properties of each material (separately) in a single material was because: inorganic glasses are not universally suited for optical and optoelectronic devices since they have low flexibility, high brittleness and need to be processed at high temperatures.

On the other hand, polymer-based optical materials can overcome some of the disadvantages of inorganic glasses. They exhibit a low heat resistance (~ 50 °C) but can be processed at fairly low temperatures.

Silicate-based inorganic-organic hybrid polymers have attracted considerable attention of the group due to their outstanding properties resulting from their inorganic and organic units.

Initially, the group started with the idea of design glasses doped with organic compounds through the sol-gel process. The sol-gel process replace the high-temperature technique for the production of vitreous bodies, by a low temperature process (lower than 100 °C - ideal for handling organic compounds without them suffer degradation) based on the formation of a glassy network (Si – O – Si) by the polymerization of appropriate precursor. In this way is possible to produce glassy matrices containing organic molecules scattered with high NL optical properties. However, in order to consolidate the glassy network, the sol-gel process needs to be subjected to sintering. The sintering process implies temperature in the order of 700 – 1100 °C. Nevertheless, to these temperatures the organic molecules are degraded. Therefore, our samples were not well consolidated; this state is known as Xerogel. Therefore, the samples were presented in a soft and porous consistency. Besides that, in the hydrolysis process to form the gel are added water, methane and ethanol, and most of the organic compounds are not soluble in them.

At that time, the group was very interested in measuring the NL refractive index through Z-scan measurements, but its characterization was not easy for the following reasons:

1. The final quality of most of the samples was not ideal to make Z-scan measurements; i.e., the samples showed no flat surfaces on their faces.
2. By the final state in which the samples were presented, they absorbed water (in the environment) constantly. This resulted in distortion of the beam in many of the samples.

3. We were limited with respect to the molecule used. This had to be soluble in the above solvents.

Taking into account all these disadvantages, we saw in silicate-based inorganic–organic hybrid materials the possibility to find a material with great expectation to be used as a photonic device. In the group these novel materials are prepared from the aerogel process. This method consists in the introduction of organic molecules in inorganic porous materials. We used porous silicon as the inorganic material and with the new class of organic materials, we will have a tremendous flexibility in the in the selection of the molecule, i.e., dipolar compounds, octupolar compounds, conjugated polymers, organometallic compounds, macrocycles, porphyrins, etc.

The main interest is to apply these hybrid materials as optical power limiters. The term “optical power limiter” is used to describe a material that exhibits intensity–dependent absorption, such that it is transparent to light at low intensities but opaque to intense light. Such a material behaves like a shutter, responding on an ultrafast (ps to ns) timescale. Optical limiters are “smart materials” in the sense that their function originates from the intrinsic properties of the material, rather than requiring any external control mechanism. There is a strong demand for optical power limiters that can protect delicate sensors from lasers. They also have applications in optical telecommunications for removing intensity spikes. There is a particular demand for optical limiters which operate over a broad range of wavelengths to give “frequency–agile” protection.

The main mechanism for optical–power limiting is the excited saturable absorption (ESA). In section II.3.2. of the chapter II, we presented a brief explanation of ESA because was the mechanism that best described the NLA response of our organoboron compound under 532 nm of excitation. Briefly, absorption by excited singlet states ($S_1 \rightarrow S_n$) gives an immediate, but short–lived, effect. Absorption from excited triplet states ($T_1 \rightarrow T_n$) grows on a slower timescale (ps to ns), because of intersystem crossing (ISC), and typically decays over a few microseconds. The longer lifetimes of triplet states lead to greater

populations of the excited states, for a given light intensity, and lead to a more sensitive optical power limiter.

On the other hand, TPA would appear to be an ideal mechanism for optical–power limiting because (unlike ESA) it requires NLA, so should give excellent transparency at low intensity light. However, TPA cross-sections of current materials are not large enough to form effective optical limiters purely by TPA. A more practical strategy is to use a combination of TPA and ESA. Precisely one of our organoboron compounds showed both behaviors.

Effective optical limiting requires the following combination of properties at the excitation wavelength: large TPA cross–section, small 1PA cross–section (that is, low $S_0 \rightarrow S_1$ extinction coefficient), high triplet quantum yield ($S_1 \rightarrow T_1$ ISC faster than $S_1 \rightarrow S_0$ IC), strong ESA, and long triplet lifetime (slow $T_1 \rightarrow S_0$ ISC). Under these conditions phase–separation can occur, which leads to problems of scattering, and aggregation can broaden the linear absorption bands, which leads to a loss of transparency. It can be difficult to synthesize an organic molecule with the right combination of solubility properties and optical characteristics; under these problems, a hybrid material may be preferable to use a mixture of organic and inorganic such that one captures light by TPA and transfers this energy to a second exhibiting ESA.

Finally, we intend to characterize these novel compounds through the TM Z-scan technique since this technique will be useful discriminating between electronic and thermal contributions. It is important to note that the NL optical contributions of these compounds will be a mixture of the contributions of organic compounds with inorganic material. Through this dissertation we had the opposite, firstly we studied the NL optical contributions of organic solvents and organic solutions and secondly we studied the contribution of inorganic materials (tellurite glasses).

V.3 References

1. J. E. Ehrlich, X. L. Wu, I.-Y. S. Lee, Z.-Y. Hu, H. Röckel, S. R. Marder, J.W. Perry, *Opt. Lett.* **22**, (1997) 1843.
2. M. Albota, D. Beljonne, J.-L. Brédas, J. E. Ehrlich, J.-Y. Fu, A. A. Heikal, S. E. Hess, T. Kogej, M. D. Levin, S. R. Marder, D. McCord-Maughon, J. W. Perry, H. Röckel, M. Rumi, G. Subramaniam, W. W. Webb, X.-L. Wu, C. Xu, *Science* **281**, (1998) 1653.
3. N. S. Makarov, M. Drobizhev, A. Rebane, *Opt. Express* **16**, (2008) 4029.
1845
4. B. A. Reinhardt, L. L. Brott, S. J. Clarson, A. G. Dillard, J. C. Bhatt, R. Kannan, L. Yuan, G. S. He, P. N. Prasad, *Chem. Mater.* **10**, (1998) 1863.
5. L. Beverina, J. Fu, A. Leclercq, E. Zojer, P. Pacher, S. Barlow, E. W. Van Stryland, D. J. Hagan, J.-L. Brédas, S. R. Marder, *J. Am. Chem. Soc.* **127**, (2005) 7282.
6. S.-J. Chung, S. Zheng, T. Odani, L. Beverina, J. Fu, L. A. Padilha, A. Biesso, J. M. Hales, X. Zhan, K. Schmidt, A. Ye, E. Zojer, S. Barlow, D. J. Hagan, E.W. Van Stryland, Y. Yi, Z. Shuai, G. A. Pagani, J.-L. Brédas, J.W. Perry, S. R. Marder, *J. Am. Chem. Soc.* **128**, (2006) 14444.
7. S.-J. Chung, K.-S. Kim, T.-C. Lin, G. S. He, J. Swiatkiewicz, P. N. Prasad, *J. Phys. Chem. B*, **103**, (1999) 10741.
8. R. Kannan, G. S. He, T.-C. Lin, P. N. Prasad, R. A. Vaia, L.-S. Tan, *Chem. Mater.* **16**, (2004) 185.
9. **a)** B. Strehmel, V. Strehmel, *Adv. Photochem.* **29**, (2007) 111; **b)** M. Rumi, S. Barlow, J. Wang, J. W. Perry, S. R. Marder, *Adv. Polym. Sci.* **213**, (2008) 1; **c)** G. S. He, L.-S. Tan, Q. Zheng, P. N. Prasad, *Chem. Rev.* **108**, (2008) 1245; **d)** F. Terenziani, C. Katan, E. Badaeva, S. Tretiak, M. Blanchard-Desce, *Adv. Mater.* **20**, (2008) 4641; **e)** H. M. Kim, B. R. Cho, *Chem. Commun.* (2009) 153.
10. By Yanqing, Ching-Yi Chen, Yen-Ju Cheng, A. Cody Young, Neil M. Tucker, and Alex K. -Y. Jen, *Adv. Funct. Mater.*, DOI: 10.1002/adfm.200600916.
11. Wang Y, Liu B, Mikhailovsky A, Bazan GC, *Adv Mater.* **22**, (2010) 656.
12. Pu KY, Li K, Liu B, *Adv Funct. Mater* **20**, (2010) 2770.
13. Pu KY, Li K, Shi J, Liu B, *Chem Mater* **21**, (2009) 3816.
14. Feng X, Tang Y, Duan X, Liu L, Wang S., *J Mater Chem* **20**, (2009) 1312.
15. Kaeser A, Schenning APHJ, *Adv Mater.* **22**, (2010) 2985.
16. Wu C, Bull B, Christensen K, McNeill J, *Ratiometric. Angew Chem Int Ed* **48**, (2009) 2741.
17. Wu C, Szymanski C, Cain Z, McNeill J, *J Am Chem Soc* **129**, (2007) 12904.
18. **a)** H. Y. Woo, B. Liu, B. Kohler, D. Korystov, A. Mikhailovsky, G. C. Bazan, *J. Am. Chem. Soc.* **127**, (2005) 14; **b)** H. Y. Woo, J. W. Hong, B. Liu, A. Mikhailovsky, D. Korystov, G. C. Bazan, *J. Am. Chem. Soc.* **127**, (2005) 820; **c)** H. Y. Woo, D. Korystov, A. Mikhailovsky, T. Q. Nguyen, G. C. Bazan, *J. Am. Chem. Soc.* **127**, (2005) 794.